Neutrino cosmology and large scale structure

Christiane Stefanie Lorenz
Pembroke College and Sub-Department of Astrophysics
University of Oxford

A thesis submitted for the degree of
Doctor of Philosophy

Trinity 2019

Neutrino cosmology and large scale structure

Christiane Stefanie Lorenz

Pembroke College and Sub-Department of Astrophysics
University of Oxford

A thesis submitted for the degree of
Doctor of Philosophy

Trinity 2019

The topic of this thesis is neutrino cosmology and large scale structure. First, we introduce the concepts needed for the presentation in the following chapters.

We describe the role that neutrinos play in particle physics and cosmology, and the current status of the field. We also explain the cosmological observations that are commonly used to measure properties of neutrino particles.

Next, we present studies of the model-dependence of cosmological neutrino mass constraints. In particular, we focus on two phenomenological parameterisations of time-varying dark energy (early dark energy and barotropic dark energy) that can exhibit degeneracies with the cosmic neutrino background over extended periods of cosmic time. We show how the combination of multiple probes across cosmic time can help to distinguish between the two components.

Moreover, we discuss how neutrino mass constraints can change when neutrino masses are generated late in the Universe, and how current tensions between low- and high-redshift cosmological data might be affected from this.

Then we discuss whether lensing magnification and other relativistic effects that affect the galaxy distribution contain additional information about dark energy and neutrino parameters, and how much parameter constraints can be biased when these effects are neglected.

We conclude by describing current fields of active research in cosmology, and how the work presented in this thesis contributes to them.

Declaration

I declare that no part of this thesis has been accepted, or is currently being submitted, for any degree or diploma or certificate or any other qualification in this University or elsewhere. Except where explicit reference is made to the work of others, the work contained in this thesis is my own.

Chapter 2 and parts of Chapter 1 are based on work I led that was published in Physical Review D: "*Distinguishing between Neutrinos and time-varying Dark Energy through Cosmic Time* [1]". I led all aspects of this work, except the implementation and running of the Fisher forecasting code which was done by Dr. David Alonso and Dr. Erminia Calabrese. Minor edits reflect comments and suggestions from the co-authors and the referee.

Chapter 3 is based on work I led that was published in Physical Review D: "*Time-varying neutrino mass from a supercooled phase transition: current cosmological constraints and impact on the* Ω_m-σ_8 *plane*" [2]. I led most aspects of this work, apart from the theoretical part, which was led by Dr. Lena Funcke. This chapter has summarized findings from Refs. [3, 4] more briefly compared to the paper [2]. Minor edits reflect comments and suggestions from the co-authors and the referee.

Chapter 4 is based on work I led that was published in Physical Review D: "*Impact of relativistic effects in cosmological parameter estimation*" [5]. Minor edits reflect comments and suggestions from the co-authors and the referee.

Christiane Stefanie Lorenz
October 2019

Acknowledgements

Firstly, I would like to thank my supervisors Pedro Ferreira, Erminia Calabrese and David Alonso. I have learnt very much from each of them, and I am very grateful to them for their support during the last three years.

In addition, I would like to thank the people who made my transfer to astrophysics department possible, especially Erminia Calabrese, Pedro Ferreira, Jo Dunkley, Helen Johnson, Ashling Morris, Garret Cotter and my college advisor Alfons Weber.

I also would like to thank the members of the cosmology group in Oxford, in particular Shahab Joudaki and Elisa Chisari, and my collaborators, Lena Funcke and Steen Hannestad.

I am also grateful to the Clarendon Fund, Oxford University Press and Pembroke College for financial support that allowed me to pursue my course in Oxford.

I would like to thank all the people who have supported me during the past months: most importantly my family, my friends Kilian, Lena, Andreas, Jonas, Hannah, Isa, Lena, Alice, Mariel, Harriet, Gus, Thibaud, Nina, Viki and Sonja. Especially I would like to thank Matthias who is always at my side to share both the happy and the difficult moments with me and who gives me optimism and vitality.

Contents

List of Figures

List of Tables

List of Abbreviations

The following abbreviations are used in this thesis.

ACT	Atacama Cosmology Telescope
BAO	Baryonic acoustic oscillations
BBN	Big bang nucleosynthesis
BOSS	Baryon Oscillation Spectroscopic Survey
CMB	Cosmic microwave background
DES	Dark Energy Survey
DESI	Dark Energy Spectroscopic Instrument
EDE	Early Dark Energy
JLA	Joint Light-curve analysis
KATRIN	Karlsruhe Tritium Neutrino Experiment
KiDS	Kilo Degree Survey
ΛCDM	Lambda Cold Dark Matter
LSST	Large Synoptic Survey Telescope
MCMC	Monte Carlo Markov Chains
PTOLEMY	Princeton Tritium Observatory for Light, Early-Universe, Massive-Neutrino Yield
RSD	Redshift-space distortions
SDSS	Sloan Digital Sky Survey
SN	Supernovae
SO	Simons Observatory
SPT	South Pole Telescope
S4	Stage-4

Chapter 1

Introduction

The work presented in this thesis presents novel results and methodology to study the composition and evolution of our Universe. In this chapter we will describe the Standard Model of Cosmology (Sec. 1.1), cosmological observations that can probe this model (Sec. 1.2), the role of neutrinos in particle physics and cosmology (Sec. 1.3) and finally the statistical tools used in this thesis (Sec. 1.4).

1.1 The Standard Model of Cosmology

Over the last few decades major improvements in theory and observations have established a Standard Model of Cosmology. This model is also called ΛCDM model and is the simplest model currently favoured by a wide range of cosmological observations. In ΛCDM, Λ stands for the *cosmological constant*, which was originally proposed by Albert Einstein back in 1917 to keep the Universe static [6]. Later, observations of supernovae explosions showed that the expansion of the Universe is in fact accelerating [7, 8]. This acceleration might be due to an additional energy component in the Universe ('dark energy') [9] or a modification of the theory of gravity [10]. The most simple model for dark energy is the cosmological constant, and describes a component with a constant energy density through cosmic history.

CDM stands for *cold dark matter*. Dark matter is not constituted of baryons, not visible and interacts with baryons via gravitational effects. One can distinguish between 'cold' DM, 'warm' and 'hot' DM, depending on how long the DM particles are in thermal equilibrium [11]. Cold dark matter is moving slowly compared to the speed of light at all times. Baryons form galaxies and stars and also fill the intergalactic medium, whereas dark matter forms halos around galaxies. This

additional matter component is required to explain the velocity profile of stars in galaxies [12], as well as structure formation in the Universe [13, 14].

Cosmology assumes a homogeneous and isotropic Universe (the *cosmological principle*) [15]. This means that the Universe will look the same independent of the direction of our line of sight (isotropy), and that on large scales it will look the same independent of translations (homogeneity). In addition, the ΛCDM model also assumes *inflation*, a period of rapid acceleration at the beginning of the Universe (see [16] for an overview). Inflation would solve several problems, for example why the Universe is flat ('*flatness problem*'), and why the temperature of the cosmic microwave background is so uniform ('*horizon problem*'). Further details can be found in Refs. [16, 17]. The most distinctive prediction of inflation, a background of primordial gravitational waves, is still undetected, but many future surveys are being designed and optimized for their search (see also Sec. 1.2.6).

In what follows, we will introduce the main theoretical and observational concepts of an expanding Universe. First, we will give a brief overview of the thermal history of the Universe (Sec. 1.1.1), then we introduce the Einstein and Friedmann equations (Sec 1.1.2), describe some common distance measures in the Universe (Sec. 1.1.3), describe the evolution of energy densities of different components in the Universe 1.1.4 and then quickly introduce the concept of cosmological perturbations (Sec. 1.1.5).

1.1.1 An overview of thermal history

The favoured theory for the beginning of the Universe is the Hot Big Bang Theory [18, 19, 20]. In the early Universe, small quantum fluctuations form and get inflated in a period of rapid acceleration to larger cosmological perturbations, which will then grow under gravity to form the objects we see today.

Initially, the Universe is very hot, and photons, electrons and positrons are in thermal equilibrium with each other. Around $T \sim 100$ GeV, massive particles acquire their mass during the electroweak phase transition [21, 22, 23]. During the QCD phase transition, at around $T \sim 100$ MeV, the first baryons and mesons are formed [24]. Later on, neutrinos decouple at $T \sim 0.8$ MeV [16, 25]. Shortly afterwards, electrons and positrons annihilate with each other and transfer their energy to photons. Because neutrinos decoupled beforehand, the neutrino and photon temperature today is different. Three minutes after the big bang, light elements are formed during big bang nucleosynthesis (BBN, see also Sec. 1.3.4).

At a redshift of $z \sim 1100$, or after 300000 years, or a temperature of $T \sim 0.3$ eV, electrons and protons recombine to form hydrogen. Since the electron density drops, photons do not interact effectively with electrons via Thomson scattering anymore, and decouple from them [26, 27]. These photons form the cosmic microwave background radiation that we can observe today (see Sec. 1.2.1).

1.1.2 Einstein and Friedmann equations

In this section, we will introduce some of the basic equations used in this thesis. In an evolving Universe, the Friedmann-Robertson-Walker metric can be described in spherical coordinates by [28, 29]

$$ds^2 = dt^2 - a(t)^2\Big[\frac{dr^2}{1-kr^2} + r^2(d\theta^2 + sin^2\theta d\varphi^2)\Big], \tag{1.1}$$

where $a(t)$ is the *scale factor*, k is the *curvature* constant and the speed of light is $c = 1$. The value of k is $k = 0$ for an Euclidean space, $k = 1$ for a spherical space and $k = -1$ for a hyperbolic space. The scale factor $a(t)$ is normalised so that it is $a(t_0) = 1$ today. Alternatively, the scale factor a can be replaced by the *redshift* z, given by $1 + z = 1/a$. Photons are redshifted because of the Doppler effect due to the expansion of the Universe.

The evolution of the Universe can be described with the Einstein equations. In tensor form they are given by [30, 31]

$$G_{\mu\nu} = R_{\mu\nu} - \frac{1}{2}Rg_{\mu\nu} = 8\pi G T_{\mu\nu}, \tag{1.2}$$

where $G_{\mu\nu}$ is the Einstein tensor, $R_{\mu\nu}$ the Ricci tensor, R the Ricci scalar and $T_{\mu\nu}$ the stress-energy tensor. The left side of the Einstein field equations describe the evolution of spacetime curvature, whereas the right side describes the energy or matter content of the Universe. When a cosmological constant Λ is included, this gives an additional term on the left side, which can also be added to the stress-energy tensor.

We will quickly describe the different parts of the Einstein equations. The non-vanishing components of the Ricci tensor can be expressed as (see e.g. Refs. [29, 32])

$$R_{00} = -3\frac{\ddot{a}}{a} \tag{1.3}$$

$$R_{ij} = -\Big[\frac{\ddot{a}}{a} + 2\Big(\frac{\dot{a}}{a}\Big)^2 + 2\frac{k}{a^2}\Big]g_{ij} \tag{1.4}$$

and the Ricci scalar is the contraction of the Ricci tensor, written as

$$R = R^{\mu}{}_{\mu} = g^{\mu\nu}R_{\mu\nu} = -6\Big[\frac{\ddot{a}}{a} + \Big(\frac{\dot{a}}{a}\Big)^2 + \frac{k}{a^2}\Big]. \tag{1.5}$$

For a perfect fluid, the stress- energy tensor $T_{\mu\nu}$ can be written in matrix form as

$$T^{\mu}{}_{\nu} = g^{\mu\lambda}T_{\lambda\mu} = \begin{pmatrix} \rho & 0 & 0 & 0 \\ 0 & -P & 0 & 0 \\ 0 & 0 & -P & 0 \\ 0 & 0 & 0 & -P \end{pmatrix}. \tag{1.6}$$

The conservation of the stress-energy tensor gives the *continuity equation*

$$\dot{\rho} + 3\frac{\dot{a}}{a}(\rho + P) = 0, \tag{1.7}$$

which will be used in Sec. 2 to describe the evolution of time-varying dark energy.

Using Eqs. 1.3, 1.5 and 1.6, we can derive the Friedmann equations which describe the evolution of the Universe. By evaluating the Einstein tensor and the stress-energy tensor at $\mu = \nu = 0$, we find

$$G_{00} = -3\frac{\ddot{a}}{a} + 3\left[\frac{\ddot{a}}{a} + \left(\frac{\dot{a}}{a}\right)^2 + \frac{k}{a^2}\right] \tag{1.8}$$

$$8\pi G T_{00} = 8\pi G\rho. \tag{1.9}$$

Therefore, we obtain the *First Friedmann equation* [28]

$$H^2 = \left(\frac{\dot{a}}{a}\right)^2 = \frac{8\pi G}{3}\rho - \frac{k}{a^2}, \tag{1.10}$$

where $H(a)$ is the Hubble parameter. Similarly, for $\mu = \nu = i$, where i is a spatial index, we find

$$G_{ii} = \left[\frac{\ddot{a}}{a} + 2\left(\frac{\dot{a}}{a}\right)^2 + 2\frac{k}{a^2}\right] - 3\left[\frac{\ddot{a}}{a} + \left(\frac{\dot{a}}{a}\right)^2 + \frac{k}{a^2}\right]. \tag{1.11}$$

$$8\pi G T_{ii} = 8\pi G P. \tag{1.12}$$

By inserting the first Friedmann equation from Eq. 1.10, we obtain the *Second Friedmann equation* [28]

$$\frac{\ddot{a}}{a} = -\frac{4\pi G}{3}(\rho + 3P). \tag{1.13}$$

The Friedmann equations can be perturbed (see Sec. 1.1.5) in order to describe the development of small fluctuations to larger structures.

1.1.3 Distances

Distances in the Universe can be expressed in different ways. Here we will quickly review some of the most common distance measures (see e.g. Refs. [29, 32]).

- The *comoving radial distance* is given by

$$\chi(z) = \int_{t_1}^{t_0} \frac{dt}{a(t)} = \int_0^z \frac{dz}{H(z)} \tag{1.14}$$

and is a measure of the radial distance between two points in the Universe, if we were to freeze time. In a flat Universe, the comoving distance equals the *metric distance* d_M which is equal to the comoving angular diameter distance. The comoving distances are not directly observable.

- The *luminosity distance* can be used to measure distances to objects with known luminosity L. Since the luminosity is known, these objects are *standard candles*. The energy flux in a telescope depends on the luminosity of the object, the comoving angular diameter distance and the redshift z. This is due to the fact that the Universe expands while the light travels from the object to the telescope, stretching the wavelength of the photon. In addition, the rate of arrival of photons is changed because of time dilation. In total, the flux is given by $F = L/(4\pi d_M^2(1+z)^2)$ and the luminosity distance is defined as

$$d_L = d_M(1+z). \tag{1.15}$$

- The *angular diameter distance* is used to measure distances to objects of known size D. By observing their angular size $\delta\theta$ on the sky, we can infer their observable distance $d_A = D/\delta\theta$. The angular diameter distance is related to d_M and d_L by

$$d_A = \frac{d_M}{1+z} = \frac{d_L}{(1+z)^2}. \tag{1.16}$$

The angular diameter distance can be measured with baryonic acoustic oscillations (see Sec. 1.2.3).

1.1.4 Energy densities

The expansion rate of the Universe can be described in terms of the energy fractions of cold dark matter (CDM), baryons (B), dark energy (DE) and radiation (R) by

$$H^2(a) = H_0^2\Big[\frac{\Omega_\mathrm{R}}{a^4} + \frac{\Omega_\mathrm{CDM}+\Omega_\mathrm{B}}{a^3} + \frac{\Omega_\mathrm{DE}}{a^{3(w+1)}}\Big]. \tag{1.17}$$

Here, w is the *equation of state factor* defined by the pressure divided by the density $w = p/\rho$. In addition, Ω is the density parameter of a given component and is the density of that component divided by the *critical density* of the Universe. The critical density is the energy density required

for a flat Universe, which is given by $\rho_{\rm crit} = 3H^2/(8\pi G)$. For example, Ω_m would be the fraction of the matter density of the total energy density, assuming that the Universe is flat.

At the beginning, the Universe is dominated by radiation. As the temperature drops, the Universe becomes dominated by matter. This matter-radiation equality happens around $z = 3400$ between BBN and recombination [16]. In addition, neutrinos contribute to the radiation density when they are still relativistic, and to the matter density when they are non-relativistic (see Sec. 1.3.3).

In total, the energy densities of the different components are proportional to the scale factor a in different ways (see e.g. [32]):

- *Radiation* describes a gas of relativistic particles or photons, and also neutrinos when they are still relativistic. Their energy density is proportional to $\rho_{\rm R} \propto a^{-4}$, and their equation of state factor is $w_{\rm R} = 1/3$.

- *Matter* (baryons and cold dark matter) describes an energy component with $P_{\rm M} = w_{\rm M} = 0$. Therefore, their energy density is proportional to $\rho_{\rm M} \propto a^{-3}$.

- *Neutrinos* contribute to radiation at early times, and to matter at late times. Their energy density can be described in two regimes with

$$\rho_\nu \propto \begin{cases} a^{-4} & z > z_{\rm NR} \\ a^{-3} & z \leq z_{\rm NR}. \end{cases} \tag{1.18}$$

  Here, $z_{\rm NR}$ is the redshift when neutrinos become non-relativistic (see Sec. 1.3.3).

- Dark energy: For a cosmological constant, the density of dark energy is constant, $\rho_{\rm DE} = \text{const.}$, and $w_{\rm DE} = -1$ at all redshifts. Otherwise, the energy density is described by (see e.g. [33, 34])

$$\rho_{\rm DE}(z) = \rho_{\rm DE,0} \cdot \exp\left[\int_0^z dz' \frac{3(1+w(z'))}{1+z'}\right]. \tag{1.19}$$

1.1.5 Cosmological perturbations

Inital quantum fluctuations expand rapidly during inflation. This creates small perturbations both in the metric g_{ij}, as well as in the stress-energy tensor T_{ij}. Following Ref. [35, 29], the perturbed FRW metric in the conformal Newtonian gauge is then given by

$$ds^2 = a^2(\tau)[(1+2\Psi)d\tau^2 - (1-2\Phi)\delta_{ij}dx^i dx^j], \tag{1.20}$$

where τ is the conformal time, defined by $d\tau = dt/a$, and Ψ and Φ are metric potentials. Together, they can be combined to obtain the linear perturbed Einstein field equations, perturbing the standard Einstein equations from Eq. 1.2. If we assume that there is no anisotropic stress, then the metric potentials are identical, $\Psi = \Phi$. For example, the perturbed First and Second Friedmann equation in first order become [29]

$$\nabla^2\Phi - 3\frac{a'}{a}\left(\Phi' + \frac{a'}{a}\Phi\right) = 4\pi G a^2 \delta\rho \tag{1.21}$$

$$\Phi'' + 3\frac{a'}{a}\Phi' + \left[2\left(\frac{a'}{a}\right)' + \left(\frac{a'}{a}\right)^2\right]\Phi = 4\pi G a^2 \delta P. \tag{1.22}$$

Here, all derivatives are with respect to conformal time τ. The initial conditions are set by inflation. Then the perturbed Einstein equations can be numerically integrated with CAMB [36] or CLASS [37]. This way, we can track the evolution of perturbations to larger structures in the Universe.

1.2 Cosmological observations

In this section, we will briefly introduce the cosmological observables relevant for the following chapters.

1.2.1 The cosmic microwave background

At a redshift of $z = 1100$, electrons and protons recombine and form hydrogen atoms [26, 27]. Because photons can then not easily interact with electrons and protons via Thomson and Compton scattering any more, photons decouple from the primordial plasma. As the Universe expands, the photon wavelengths get stretched and they lose energy. Today the photons are very cold and have a temperature of around 2.7 K. This cosmic microwave background (CMB) radiation can be observed with both ground-based telescopes, such as the Atacama Cosmology Telescope (ACT) [38] and the South Pole Telescope (SPT) [39], as well as with satellites, such as the Planck satellite [40].

Prior to recombination, photons, electrons and protons are tightly coupled to each other. This photon-baryon fluid is oscillating due to the interplay of radiation pressure and gravity. At recombination, these oscillations stop and gravity becomes the dominant force. The CMB photons then propagate on geodesics through the Universe. We can observe the perturbations in the energy density of photons

as angular temperature fluctuations over the sky, $\Theta(\hat{\mathbf{n}}) = \Delta T/T$. The temperature fluctuations Θ can be expanded in terms of spherical harmonic coefficients (see e.g. [41])

$$\Theta_{lm} = \int d\hat{\mathbf{n}} Y^*_{lm}(\hat{\mathbf{n}})\Theta(\hat{\mathbf{n}}), \tag{1.23}$$

where the Y^*_{lm} are spherical harmonics, and $\hat{\mathbf{n}}$ is the unity vector along the line of sight. For Gaussian random fluctuations, all the information is encapsulated in the variance of these coefficients, which we call the power spectrum. The power spectrum multipoles C_ℓ's are defined as

$$\langle \Theta^*_{lm}\Theta_{l'm'}\rangle = \delta_{ll'}\delta_{mm'}C_l. \tag{1.24}$$

The oscillatory behaviour observed in the CMB is the imprint of the acoustic oscillations in the baryon-photon plasma. For example, the first peak corresponds to the mode when the fluid has compressed once and the first trough to the mode when the fluid is in between the first compression and the first rarefaction at the time of recombination. The wavenumber of the first peak is given by $k = 2\pi/\lambda = \pi/r_s$, where r_s is the *sound horizon* at recombination, e.g. the distance sound waves can travel until recombination. The higher-order peaks will have wavenumbers that are multiples of the wavenumber of the first peak, $k_n = n \cdot k_1$. The wavenumbers correspond to the multipoles ℓ in the CMB power spectrum.

The COsmic Background Explorer (COBE) observed the first temperature anisotropies in the cosmic microwave background [13]. Later, the Boomerang and Maxima-1 experiments detected the first peak in the angular CMB temperature anisotropy power spectrum [42, 43], and the Wilkinson Microwave Anisotropy Probe (WMAP) [44] and the Planck satellite [40] measured the CMB spectrum with high precision.

Fig. 1.1 shows several examples for how the different parts of the CMB temperature anisotropy power spectrum can be used to constrain different cosmological parameters (see e.g. [41, 45]).

- **Low multipoles:** On scales much larger than the sound horizon, the perturbations are directly frozen in their initial conditions. The precision with which we can measure the anisotropies on these scales is *cosmic variance* limited, because we can only observe the anisotropies in one Universe. The error due to cosmic variance is given by

$$\Delta C_\ell = \sqrt{\frac{2}{2\ell+1}} C_\ell \tag{1.25}$$

  and therefore is smaller for higher multipoles.

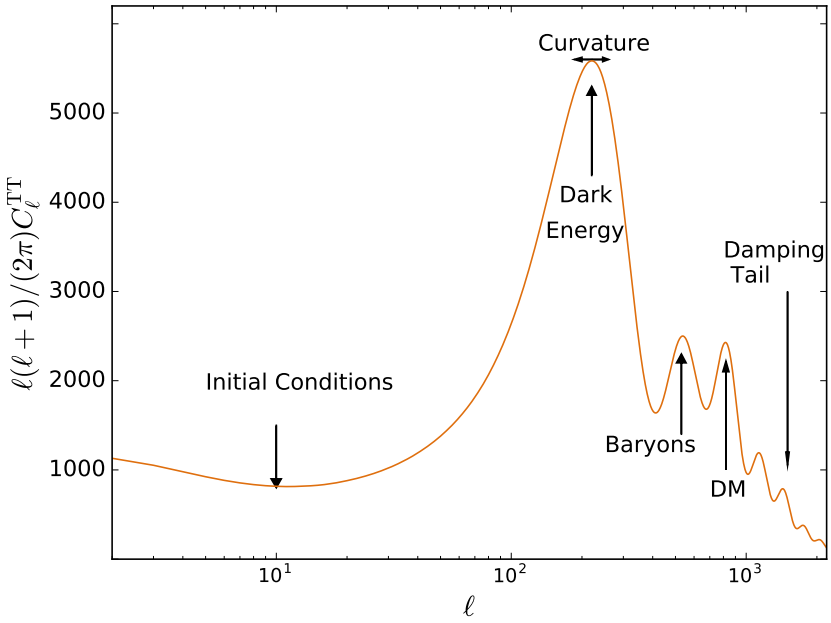

Figure 1.1: The CMB temperature anisotropy power spectrum. Arrows show examples how some cosmological parameters can be constrained with different parts of the power spectrum. The power spectrum has been obtained with the publicly available Boltzmann code CAMB.

- **First peak:** The location of the first peak measures the curvature of the Universe. The localisation of the first peak at $l \sim 200$ with the Boomerang and Maxima-1 experiments suggested that the Universe is (at least almost) flat [42, 43]. In addition, the amplitude of the first peak also contains information about the dark energy equation of state (see e.g. [45]).

- **Second peak:** The amplitude of the second peak is related to the baryon density in the Universe.

- **Higher peaks:** The amplitude of the third peak can be used to determine the dark matter density. Apart from that, the higher peaks depend on the time of matter-radiation equality.

- **Damping tail:** The damping tail of the CMB temperature anisotropy power spectrum depends on the photon diffusion length at recombination. This length also depends on the baryon density, since baryons interact with photons and reduce the mean free path of photons, as well as the dark matter density. Therefore, the damping tail is an additional test of these two quantities.

Besides the CMB temperature anisotropies, the CMB polarisation anisotropies also contain much useful information for constraining cosmological parameters (see e.g. [46] for an overview). Thomson scattering of the quadrupole of CMB photons generates linearised polarisation. The polarisation can be decomposed into E-modes and B-modes [47]. Only E-modes are generated from scalar perturbations [48, 49, 50]. B-modes are generated when CMB radiation is weakly lensed, and can also come from primordial gravitational waves (see also Sec. 1.2.6). These gravitational waves would produce both E-modes as well as B-modes. The analysis of CMB polarisation can be used as a consistency check of the constraints obtained from CMB temperature power spectra, and can also be used to constrain specific parameters more precisely. This has been demonstrated in the most recent Planck data release [51]. In particular, CMB polarisation spectra can be used to obtain a precise constraint of the optical depth to reionization τ, which is particularly relevant for cosmological neutrino mass measurements [51, 52].

1.2.2 Supernovae

Supernovae observations can be used as standard candles to measure cosmological parameters, for example the Hubble constant (see e.g. Ref. [53] for a review). The observation of Type Ia supernovae has established that the expansion of the Universe is accelerating [7, 8]. The Joint-Light-Curve Analysis (JLA) has obtained a catalogue of 740 Type Ia supernovae with light curves and distance measurements [54]. The supernovae were observed among other surveys with SDSS [55] and the Supernova Legacy Survey (SNLS) [56]. The JLA supernovae dataset gives a precise measurement of the Hubble diagram, in which the magnitudes of the supernovae are shown as a function of redshift z between $z = 0.01 - 1.2$. Supernovae can be used as an additional consistency check for ΛCDM, constraining for example the matter density Ω_m and dark energy parameters.

1.2.3 Baryonic acoustic oscillations

Before recombination, baryons and photons are tightly coupled with each other. After photons decouple from the plasma at $z = 1000$, the baryons keep moving due to their momentum until the baryon-drag epoch. The wavelength of these baryonic acoustic oscillations (BAO) is given by the comoving sound horizon at the baryon-drag epoch z_d [57]

$$r_s(z_d) = \int_0^{t(z_d)} c_s(1+z)dt, \tag{1.26}$$

where the sound speed c_s is a function of Ω_b and h. These oscillations are imprinted both in the distribution of radiation as well as matter, and thus can be observed both in the CMB as well as in the galaxy distribution today. Measurements of baryon acoustic oscillations in galaxy distributions can be used to constrain the Hubble parameter and the angular diameter distance. Since the scales corresponding to the acoustic peaks can be described with linear perturbation theory, they can be observed at low redshift in the large scale structure of the Universe [58, 59]. The acoustic scale has been measured among others with the 2-degree Field Galaxy Redshift Survey (2dFGRS) [60], the Baryon Oscillation Spectroscopic Survey (BOSS) DR12 dataset of the Sloan Digital Sky Survey (SDSS) [61] and the WiggleZ Dark Energy Survey [62].

1.2.4 Galaxy surveys

We now turn our attention to galaxy surveys. Galaxy surveys can be divided into spectroscopic and photometric surveys. For spectroscopic surveys, the redshift of an object is determined by analysing frequency shifts of characteristic spectroscopic lines. For photometric surveys, the redshift is inferred from the galaxy's flux in a small set of broad frequency bands. The determination of accurate photometric redshifts remains a challenge and many methods have been developed to obtain better photometric redshifts, including spectral energy distribution fitting [63, 64], Bayesian photometric redshift estimation [65] and machine learning methods [66, 67, 68].

Galaxy clustering

The power spectrum of density fluctuations is defined as

$$\langle \delta(\vec{k})\delta(\vec{k'})\rangle = (2\pi)^3\delta(\vec{k}+\vec{k'})P_\delta(k). \tag{1.27}$$

where δ is the contrast between the observed density and the mean density. In addition to the power spectrum, higher correlation functions, such as the bispectrum and trispectrum, might also yield important information about the underlying cosmology [69]. Initial quantum density fluctuations in the Universe can be evolved with linear perturbation theory through [70, 71, 32]

$$P_{\text{matter}}(k,a,\theta) = G^2(a,\theta)T^2(k,\theta)P_{\text{primordial}}(k). \tag{1.28}$$

Here θ is the background cosmological model, $G(a,\theta)$ is the growth factor, $T(\theta)$ is the transfer function and $P_{\text{primordial}}(k)$ is the primordial power spectrum of density perturbations. We do not

observe directly the matter power spectrum, but instead galaxies or galaxy clusters at different positions in the sky at different redshifts. The auto-correlated power spectrum of a galaxy is related to the matter power spectrum through the galaxy bias b on very large scales (see e.g. [72])

$$P_{gg}(k,a) = b^2 P_{\text{matter}}(k,a) \tag{1.29}$$

The perturbation in the number counts of galaxies is related to the number counts of observed galaxies, which is a function of the true underlying number density of galaxies, and several observational effects, such as redshift space distortions (RSD), and gravitational lensing (see [73, 74] and Chapter 4). Redshift space distortions (RSD) arise because of the peculiar velocities of galaxies (see e.g. [75]). The observed redshift of a galaxy differs from the true redshift due to the Doppler effect. Because of the peculiar velocity of a galaxy in a specific direction, the power spectrum is not isotropic any more. Therefore the observed power spectrum differs from the theoretical power spectrum (see e.g. [76]). For example, a bound galaxy cluster can look elongated in redshift space ('Fingers of God effect') [77]. By contrary, a collapsing cluster will look squashed in redshift space ('Kaiser effect') [78]. RSD need to be accounted for due to this anisotropy, and they can also be used to constrain the logarithmic growth rate f [79, 80], defined by $f = d\ln G/d\ln(a)$, as well as to probe modified gravity theories [81].

Cosmic shear

The large scale structure of the Universe can also be probed with weak gravitational lensing [82, 83], the distortion of light due to foreground structures. Strong lensing creates double images and rings [84], whereas weak lensing amplifies the brightness, changes the number of observed galaxies and changes the galaxy shapes ('shear'). Weak gravitational lensing of the large scale structure was first detected around the year 2000 by several different groups [85, 86, 87, 88].

In general, weak lensing can be described with the lensing equation (see e.g. [83]).

$$\Psi_{ij} = \begin{pmatrix} \kappa+\gamma_1 & \gamma_2 \\ \gamma_2 & \kappa-\gamma_1 \end{pmatrix} = \int_0^{\chi_H} d\chi g(\chi)\partial_i\partial_j\Phi. \tag{1.30}$$

Here Φ is the Newtonian potential and $g(\chi)$ is the radial weight function or lensing probability, defined by

$$g(\chi) = 2\int_\chi^{\chi_H} d\chi' n(\chi')\frac{r(\chi)r(\chi'-\chi)}{r(\chi')}. \tag{1.31}$$

where $r = d_A/a$. The radial distribution of galaxies enters this equation with $n(\chi)$. The shear γ describes the change of the shape of a galaxy, and the convergence κ the change of its size [89]. Both are related to the projected mass of the galaxy. Cosmic shear studies measure the projected mass and therefore directly probe the matter power spectrum. The cosmic shear power spectrum is related to the matter power spectrum through the Limber approximation [90, 83]. This gives the shear power spectrum

$$C_\ell = \frac{9}{16}\Big(\frac{H_0}{c}\Big)^4 \Omega_m^2 \int_0^{\chi_H} d\chi \Big[\frac{g(\chi)}{ar(\chi)}\Big]^2 P\Big(\frac{l}{r}, \chi\Big). \tag{1.32}$$

In order to reach a high precision of parameter constraints, the matter power spectrum needs to be modelled very precisely. Whereas the linear scales of the matter power spectrum can already be accurately described, the non-linear scales are much harder to model, but hold most of the information. On these scales, various systematic effects come into play, for example baryonic effects which further increase the uncertainty in the modelling of the matter power spectrum [91, 92, 93, 94, 95, 96]. In addition, intrinsic alignments of galaxies complicate galaxy shear measurements [97, 98, 99], but can also yield additional information [100].

Currently, the cosmology community is constructing next decade galaxy surveys, for example the Large Synoptic Survey Telescope (LSST) [101], the Dark Energy Spectroscopic Instrument (DESI) [102] and the Euclid satellite [103].

1.2.5 Sunyaev-Zeldovich cluster counts

Galaxy clusters can be detected through the thermal Sunyaev-Zeldovich (SZ) effect [104]. CMB photons scatter off the hot electrons in galaxy clusters, which results in a shift in their frequencies (see [105] for an overview). This signal is independent of redshift, and is therefore a powerful probe of the evolution of matter fluctuations in the Universe. SZ cluster counts are sensitive to the matter density Ω_m, to the amplitude of matter fluctuations on $8\mathrm{h}^{-1}$ Mpc scales, σ_8 and to the Hubble constant [71, 105]. In particular, they are sensitive to the total neutrino mass sum (see the discussions in Refs. [106, 107]). These constraints depend crucially on the determination of the cluster masses. Cluster masses can be approximated with X-ray proxies [108], or with weak lensing [109].

1.2.6 Cosmic microwave background lensing

Similarly to galaxies (see Sec. 1.2.4), the CMB photons are lensed by gravitational potentials along the line of sight (see e.g. [110, 111, 112, 113]). This leads to a deflection of the CMB photons, as well as to a change of the sizes of cold and hot temperature spots. Lensing smoothes out the acoustic peaks in the CMB power spectrum [112]. This effect becomes mostly important for small angular scales (large multipoles), resulting in a damping of the CMB power spectrum on these scales. In addition, a map of the CMB lensing convergence can be generated, which quantifies the the integrated large-scale structure fluctuations over a wide range of redshifts [114, 115]. The CMB angular convergence power spectrum $C_\ell^{\kappa\kappa}$ can be related to the weighted matter power spectrum with the Limber approximation [113].

$$C_\ell^{\kappa\kappa} = \int_0^{\chi_H} d\chi \frac{W^2(\chi)}{d_M^2(\chi)} P\Big(\frac{\ell}{d_M(\chi)}, \chi\Big), \tag{1.33}$$

where W is the lensing window function, χ_H the comoving horizon, $d_M(\chi)$ the comoving angular distance in a flat Universe and P the matter power spectrum. For $\chi < \chi^*$, that means within the comoving distance of the last scattering surface, the window function is given by

$$W(\chi) = \frac{3\Omega_m H_0^2}{2c^2} \frac{d_M(\chi) d_M(\chi^* - \chi)}{a(\chi) d_M(\chi^*)}. \tag{1.34}$$

The lensing of the CMB was detected in 2011 by the Atacama Cosmology Telescope [116] and the South Pole Telescope [117], and in 2013 by the Planck satellite [118]. The combination of CMB temperature and CMB lensing can be used to break degeneracies between cosmological parameters (see also Sec. 2), for example between the amplitude of primordial fluctuations A_s and the optical depth to reionization τ [118].

In addition, the lensing of CMB polarisation E-modes generates a foreground of B-modes [119, 120], which can make the detection of primordial B-modes much harder. This would correspond to an indirect detection of primordial gravitational waves, which would be a powerful probe of different inflation scenarios (see e.g. the discussions in [121, 122]). Many strategies have been developed for delensing the CMB in order to reconstruct the unlensed CMB temperature and polarization spectra [123, 124, 125].

1.3 Neutrinos

Neutrino particles are a key component of the Standard Model of particle physics which includes three flavours of very light active particles. They were first postulated by Wolfgang Pauli to explain the continuous electron energy energy spectrum from β decay [126]. He proposed that these particles should be uncharged, and only weakly interacting with matter. The first antineutrinos were discovered in the 1950s by measuring photons which were produced in nuclear reactions [127]. Later, an additional neutrino type was detected, the ν_μ neutrino [128], and, even later, also the ν_τ neutrino [129]. The existence of three different neutrino types, or neutrino flavours, was also postulated before to explain decays of Z^0 bosons [130], and to explain the abundance of ^{4}He produced during BBN in the early Universe [131].

The detection of neutrino oscillations (see Sec. 1.3.1) has shown that at least two of the three neutrino mass eigenstates must have a non-vanishing mass. However, many questions about neutrinos remain open until today. For example, the exact neutrino mass ordering (neutrino hierarchy) remains unknown, as well as the absolute neutrino masses. Apart from that, it is still not clear if there are only three neutrino species, or any additional "sterile" neutrinos. The interactions of sterile neutrinos with active neutrinos is strongly suppressed. Besides, the Standard Model of Particle Physics does not explain yet how the neutrino masses are generated. Cosmology has helped to come closer to answering some of these questions. In particular, cosmological observations are sensitive to the imprint of neutrinos on structure formation, because neutrinos suppress structure formation on small scales and slow down growth of structure at all scales.

This section is structured as follows: First, we will briefly describe the experimental motivation for neutrino oscillations and the implications of their discovery (Sec. 1.3.1). Then we will introduce some of the most common neutrino mass models (Sec. 1.3.2) and how neutrinos evolve over the cosmic history (Sec. 1.3.3). Finally, we will present current constraints of neutrino properties (Sec. 1.3.5) and open questions about neutrinos (Sec. 1.3.6).

1.3.1 Neutrino oscillations

A source of neutrinos are cosmic ray collisions in the atmosphere. They generate pions which decay to muons and then further to electrons, ν_e and ν_μ neutrinos [132]. Both calorimeter and water Cherenkov detectors have been used to measure the atmospheric neutrino flux. The earlier water

Cherenkov neutrino detectors observed a lower ratio of ν_μ to ν_e neutrinos than expected [133], which implied that there are less ν_μ neutrinos than expected. This phenomenon was called the 'atmospheric neutrino anomaly' and was also sometimes referred to as the 'muon neutrino disappearance' [134]. The disappearance of ν_μ neutrinos was further confirmed by results by the Super-Kamiokande experiment in Japan [135].

The Sun also produces a high amount of neutrinos via proton-proton fusion. A long-standing puzzle had been why neutrino detectors, such as the Homestake mine experiment [136] and the Kamiokande experiment [137], had measured much less solar neutrinos than predicted from the Sun's luminosity and the standard solar model [138]. This 'solar neutrino problem' [139] could not be explained with modifications of the standard solar model [140]. The Sudbury Neutrino Observatory (SNO) independently measured the flux of ν_e and $\nu_\tau + \nu_\mu$ neutrinos coming from the Sun, and confirmed that there are ν_τ and ν_μ neutrinos contained in the solar neutrino flux [141]. This result indicated that some of the ν_e neutrinos produced in the Sun transform to ν_τ and ν_μ neutrinos while propagating to the Earth.

As an explanation for the solar neutrino problem and the atmospheric muon neutrino deficit, neutrino oscillations had been proposed [142, 143]. Flavour eigenstates of the neutrino can be described as linear combinations of the neutrino mass eigenstates and are connected to those through the Pontecorvo-Maki-Nakagawa-Sakata (PMNS) mixing matrix U [144]

$$\begin{pmatrix} \nu_e \\ \nu_\mu \\ \nu_\tau \end{pmatrix} = \begin{pmatrix} U_{e1} & U_{e2} & U_{e3} \\ U_{\mu 1} & U_{\mu 2} & U_{\mu 3} \\ U_{\tau 1} & U_{\tau 2} & U_{\tau 3} \end{pmatrix} \begin{pmatrix} \nu_1 \\ \nu_2 \\ \nu_3 \end{pmatrix} \tag{1.35}$$

where ν_i with $i = 1, 2, 3$ are the neutrino mass eigenstates. The matrix elements U_{lj} depend on the mixing angles of the mass eigenstates θ_{ij}, the Dirac violation phase δ and two Majorana CP violation phases [145, 146, 147]. The latter become only important if neutrinos were to be Majorana particles and therefore their own antiparticles. Until now, only the mixing angles have been precisely measured, whereas the current experimental focus mostly lies on measuring the Dirac violation phase δ [144].

The probability to observe, for instance, a ν_e neutrino depends on the length L between the neutrino source and the detector, the mass differences Δm^2_{12} and Δm^2_{23}, the neutrino energy E, the mixing angles and the flavour composition at the source. For example, if assuming that neutrinos

were only oscillating between ν_e and ν_μ neutrinos, the probability for a ν_e neutrino produced in the Sun to be observed as a ν_e neutrino in the detector is given by [126]

$$P_{ee} = 1 - \sin^2 2\theta \sin^2 \Big(\frac{\Delta m^2 L}{4E}\Big). \tag{1.36}$$

In case that $\Delta m^2 \neq 0$, the probability $P_{e\mu}$ does not vanish. Therefore, the experimental detection of neutrino oscillations at the SNO [148, 141] and Super-Kamiokande experiments [135], and subsequent data from atmospheric, solar and reactor experiments implied that at least two of the three neutrino mass eigenstates must have a non-vanishing mass.

1.3.2 Neutrino mass mechanisms

The Standard Model of Particle Physics does not accommodate massive neutrinos. Numerous neutrino mass mechanisms have been proposed, and most of them can be broadly separated into two groups, depending whether neutrinos are 'Majorana' particles and therefore their own antiparticles, or 'Dirac' particles. We will also present a more recently developed neutrino mass mechanism in Chapter 3.

One of the most common explanations for how neutrinos gain their mass is the seesaw mechanism [146, 149, 150, 151, 152, 153]. This mechanism has been proposed to explain why neutrino masses are so small compared to other fermion masses, and requires the introduction of a Majorana mass term in the Lagrangian in addition to a Dirac mass term. Following Ref. [154], the neutrino masses of one flavour are then given by

$$m_\pm \sim \frac{1}{2}M \pm \frac{1}{2}\Big(M + \frac{2m_D^2}{M}\Big) \tag{1.37}$$

where M is the Majorana mass, m_D is the Dirac mass and m_+ and m_- is the heavy and light neutrino mass. If the Dirac mass is of the order of the other charged fermion masses, and the Majorana mass is assumed to be very large, then the light neutrino masses can be in the meV - eV range and will be almost entirely left-handed. The heavier neutrinos will be almost entirely right-handed. The detection of neutrinoless double-β decay will be only possible if neutrinos are Majorana particles, and would support the hypothesis of the Majorana seesaw mechanism.

For reviews on neutrino mass mechanisms, we refer the reader to Refs. [155, 156].

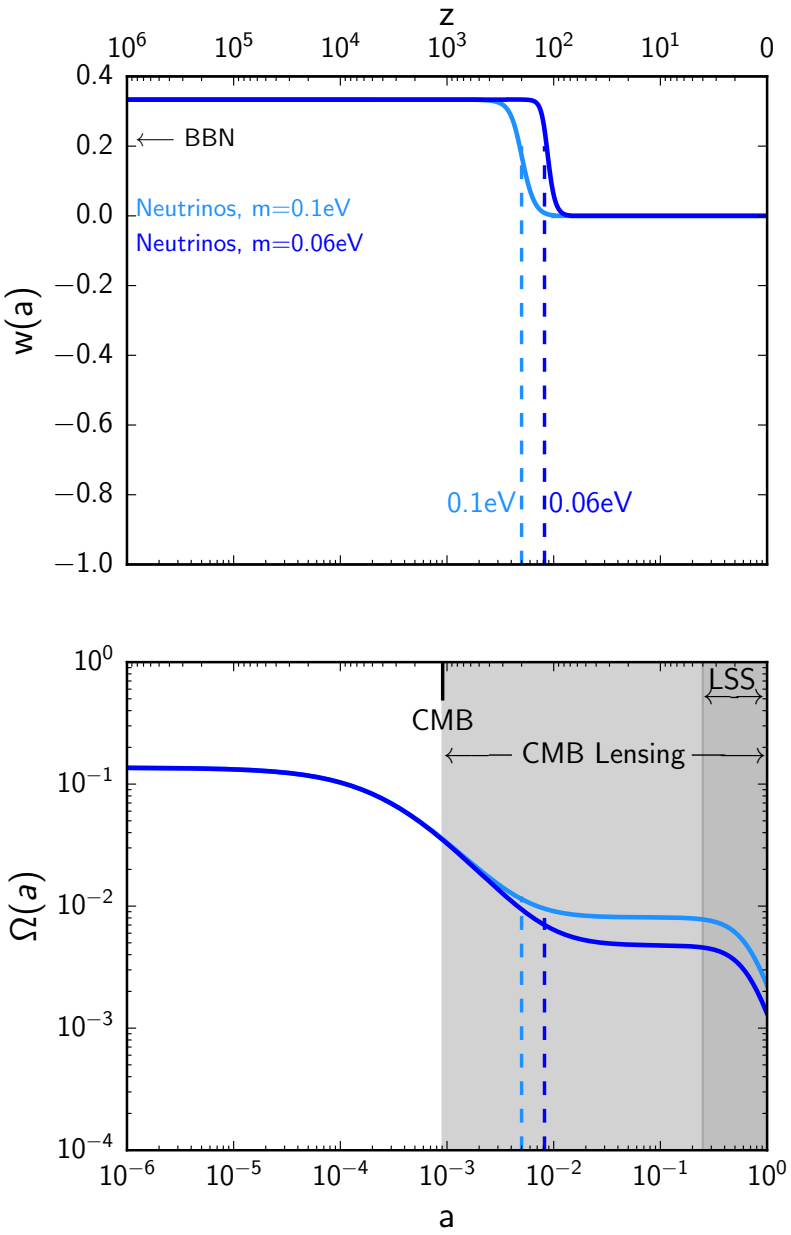

Figure 1.2: The equation of state parameter $w(a)$ (top) and density parameter $\Omega(a)$ (bottom) for neutrinos. The x axis in both panels shows the scale factor at the bottom and the corresponding redshift at the top. To generate these plots we use the standard ΛCDM *Planck* 2015 best-fit cosmological parameters [157] in combination with $N_{\rm eff} = 3.046$ and a single massive neutrino with $\Sigma m_\nu = 0.06$ or 0.1 eV. Dashed vertical lines show the matter-radiation and matter-Λ equalities and the time at which a 0.1 eV and a 0.06 eV neutrino become non relativistic. The plot also highlights the time at which the CMB decouples and which epoch primary CMB anisotropies are probing, and the range probed by CMB lensing and large-scale structure (LSS) data.

1.3.3 The evolution of cosmic neutrinos

During the history of the Universe, neutrinos from the early Universe evolve from a relativistic phase at very early times to a massive-particle behaviour at later times (see Ref. [25] for a review). Initially, the neutrinos' kinetic energy dominates over their rest-mass energy, and as a consequence, neutrinos can be described as massless particles fully characterized by their temperature. As the Universe cools down, the kinetic energy decreases and neutrinos transition to a non-relativistic phase with a non-negligible mass. In terms of the energy budget of the Universe, this means that neutrinos contribute to radiation at early times and to matter after the transition, with an energy density given by

$$\begin{aligned}\rho_\nu(m_\nu \ll T_\nu) &= \frac{7\pi^2}{120}\Big(\frac{4}{11}\Big)^{4/3} N_{\rm eff} T_\gamma^4 \\ &= \frac{7}{8}\Big(\frac{4}{11}\Big)^{4/3} N_{\rm eff}\rho_\gamma\,, \\ \rho_\nu(m_\nu \gg T_\nu) &= \frac{\rho_c}{93.14h^2{\rm eV}}\Sigma m_\nu \end{aligned} \tag{1.38}$$

where T_ν and T_γ are the neutrino and photon temperatures respectively, ρ_γ is the photon density, and h is the dimensionless Hubble constant. The two parameters of this model are the effective number of relativistic species, $N_{\rm eff}$, and the total neutrino mass, Σm_ν.

The transition between the two epochs for the individual neutrino particle happens at a redshift [158]

$$1 + z_{\rm nr} \simeq 120 \times \Big(\frac{m_\nu}{60\ {\rm meV}}\Big)\,. \tag{1.39}$$

In the standard fluid approximation, this can be pictured as a time-evolving equation of state parameter $w_\nu(a) = p_\nu(a)/\rho_\nu(a)$, which starts from $w_\nu = 1/3$ at early times, as for relativistic components, and then subsequently drops to $w_\nu \sim 0$ when neutrinos become non relativistic, and as expected for pressure-less matter. The density parameter will reflect this evolution of the individual neutrino particle and manifest distinctive phases as well. This is shown in Figure 1.2 with blue lines.

The neutrino number

The Standard Model of particle physics predicts $N_{\rm eff} = 3.046$, accounting for the three standard neutrino particles (ν_e, ν_μ, ν_τ) and QED corrections, as well as extra energy transferred between neutrinos and the thermal bath [159, 160, 161]. This extra energy is generated during a non-perfectly-instantaneous decoupling of neutrinos from the primordial plasma, with a small part of the

entropy released through electron-positrons annihilations transferred to neutrinos instead of photons. Deviations from the standard predictions will point towards extra radiation in the early Universe or non-standard neutrino decoupling with the initial plasma.

Until the matter-radiation equality, the expansion of the Universe is completely driven by the amount of radiation, which receives contributions from both photons and neutrinos

$$H^2(a) \approx \frac{8\pi G}{3}\Big(\rho_\gamma(a) + \rho_\nu(a)\Big)\,. \tag{1.40}$$

The effective number of neutrinos will then leave an imprint on observables probing $H(a)$ at early times, including the abundances of light elements predicted from BBN, and the CMB primordial temperature and polarization anisotropies. Indeed, the extra energy stored from free-streaming neutrinos at early times delays the time of the matter-radiation equality, and changes the abundances of Helium and Deuterium during BBN. These in turn modify the amplitude, the position and the damping of the CMB anisotropy power spectrum (see, e.g., Refs. [162, 163, 164, 165, 166, 167, 168, 169, 170, 171] for useful discussions). The effect of varying $N_{\rm eff}$ on the CMB temperature anisotropies when fixing all the other cosmological parameters is shown in Fig. 1.3. Similar features can be seen in the CMB polarisation anisotropies.

The neutrino mass

The neutrino mass plays a role only at later times in the history of the Universe. As such, the CMB primordial anisotropies are only mildly affected, but the interaction of the CMB photons with the low-redshift Universe and the large-scale structure formation and growth will have strong signatures of the neutrino mass.

Since they only interact weakly, neutrinos tend to free-steam out of small-scale density perturbations. As a result, they suppress structure formation on small scales: they do not cluster as a normal matter component would do and they additionally obstacle the cold dark matter and baryon clustering. This can be seen by explicitly comparing the expression of the matter power spectrum, $P(k)$, in the case of massless and massive neutrinos. The power spectrum is suppressed as [172]

$$\frac{P(k,\Sigma m_\nu) - P(k,\Sigma m_\nu = 0)}{P(k,\Sigma m_\nu = 0)} \approx -0.08\Big(\frac{\sum m_\nu}{1\text{eV}}\Big)\frac{1}{\Omega_m h^2} \tag{1.41}$$

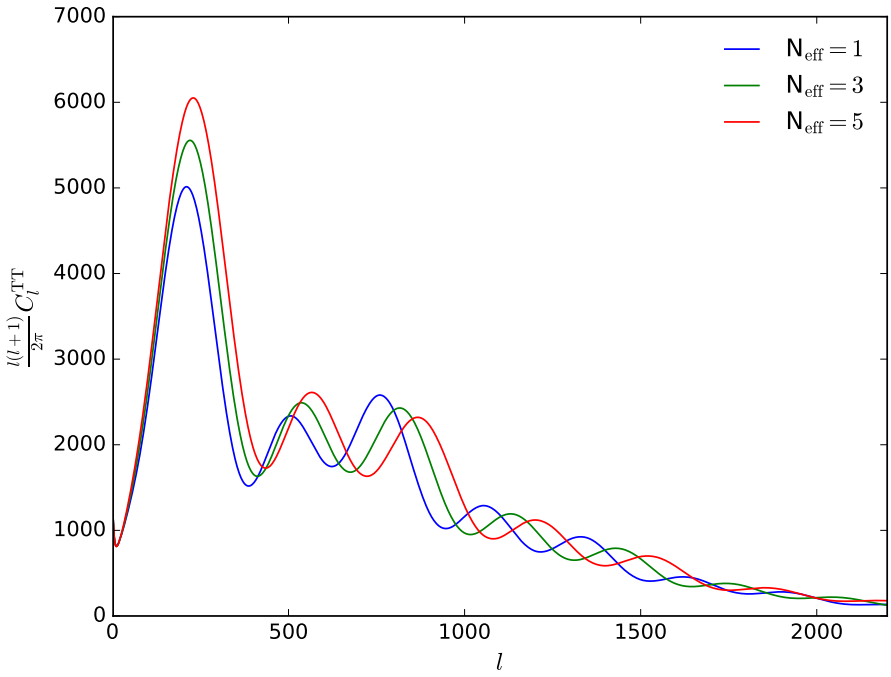

Figure 1.3: The impact of changing N_{eff} on the CMB temperature anisotropy power spectrum. This plot has been obtained with the publicly available Boltzmann code CAMB.

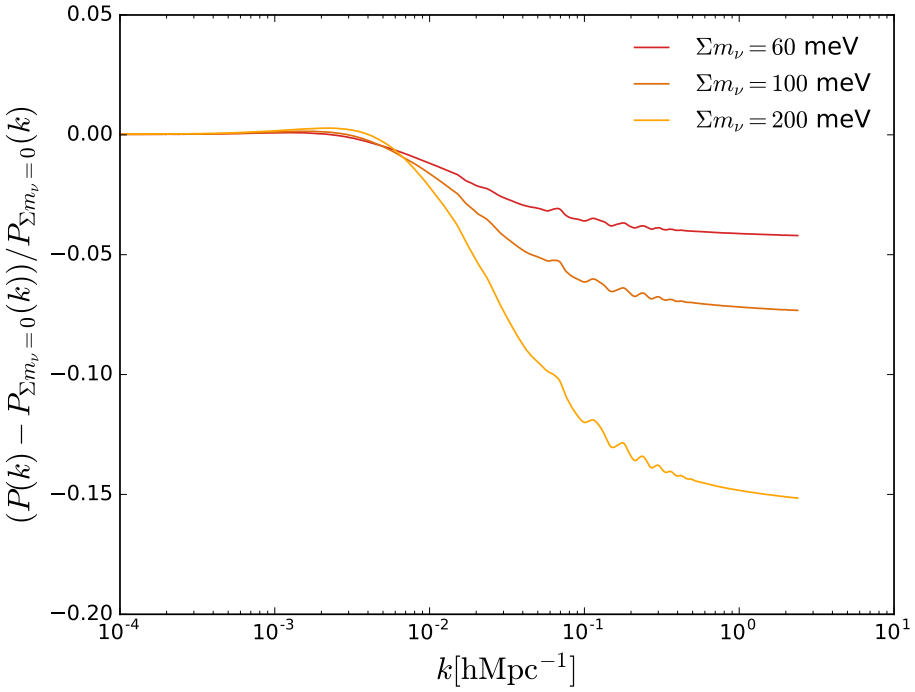

Figure 1.4: The impact of changing Σm_ν on the matter power spectrum $P(k)$. This plot has been obtained with the publicly available Boltzmann code CAMB.

with Ω_m being the matter density, for comoving wavelengths larger than $k_{\rm nr}$

$$k_{\rm nr} \approx 0.026 \Big(\frac{m_\nu}{1\mathrm{eV}}\Big)^{1/2} \Omega_m^{1/2} h\mathrm{Mpc}^{-1}\,. \tag{1.42}$$

Here, $k_{\rm nr}$ is the comoving free-streaming wavenumber when neutrinos become non-relativistic. The suppression of the matter power spectrum at large k is shown for different values of the total neutrino mass in Fig. 1.4.

The matter distribution is observationally probed with e.g., measurements of baryon acoustic oscillations, galaxy lensing, and the clustering of galaxies [173, 174]. The distribution of matter also affects the path of the CMB photons while they travel from the recombination epoch to today: gravitational potential wells along the photons' path will generate small deflections in the CMB temperature and polarization anisotropies and produce a CMB weak-lensing signal [175]. CMB lensing will therefore reflect the matter power spectrum dependence on the neutrino mass (with massive neutrinos suppressing the overall amplitude of the CMB lensing signal) and will be an indirect probe for it (see e.g., Refs. [176, 177, 157, 52, 178]).

1.3.4 Neutrinos and BBN

Neutrinos also play an important role for BBN (see e.g. [131] for a review). The Standard Big Bang Nucleosynthesis (SBBN) Model describes how light elements are formed in the early Universe, and predicts their abundances today [179, 180, 181]. Big bang nucleosynthesis starts when the weak interaction rate Γ_{wi} for protons, neutrons, electrons, positrons and neutrinos interacting with each other falls below the Hubble expansion rate

$$\Gamma_{wi}(T_f) = H(T_f) \tag{1.43}$$

at a freeze-out temperature T_f. At first, neutrons and protons form deuterium and emit photons. As we have seen in Sec. 1.3.3, the Hubble constant depends on the radiation and neutrino energy density, and on the effective number of neutrinos $N_{\rm eff}$. Therefore BBN probes the expansion rate at freeze-out, and indirectly the effective number of neutrinos. The predicted abundances of light elements, for example of ^{4}He, can be compared to those obtained from observations of the corresponding emission lines, for example from ionised gas in low-metallicty dwarf galaxies [182].

1.3.5 Current constraints of neutrino parameters

The discovery of neutrino oscillations [135, 148, 141] implies that at least two of the three neutrino mass eigenstates must have a non-vanishing mass. The squared mass differences between the neutrino mass eigenstates have been measured as $\Delta m^2_{2,1} = 7.37 \times 10^{-5}$ eV, and $\Delta m^2_{3,1} = 2.56 \times 10^{-3}$eV for the normal hierarchy or $\Delta m^2_{3,2} = 2.54 \times 10^{-3}$ eV for the inverted hierarchy [144, 183]. This leads to a lower limit on the total mass of the three active neutrinos, $\sum m_\nu$, of 59 meV for the normal hierarchy and 109 meV for the inverted hierarchy. The absolute value of the neutrino mass eigenstates, as well as whether $\Delta m_{3,1}$ and $\Delta m_{3,2}$ are positive or negative and therefore if the neutrino mass hierarchy is normal (positive sign) or inverted (negative sign), are yet to be determined.

For the high-end tail of the mass distribution, the most stringent upper limit is set by cosmological data. Observations of the CMB from the *Planck* satellite, combined with baryon acoustic oscillations (BAO), give $\sum m_\nu < 0.12$ eV at 95% confidence [51]. The projected sensitivity of future CMB and BAO data is ~ 0.03 eV [184, 185], and future combination of CMB and large-scale structure (LSS) data predict a 4-5σ detection of the total neutrino mass with $\sigma(\sum m_\nu) \sim 0.015$ eV in the next

decade [52, 184, 186, 187, 188]. This is an indirect measurement tracking the effect of the neutrino masses on the matter distribution in the Universe.

In addition to the total neutrino mass, cosmological observations also constrain the effective number of neutrino species, $N_{\rm eff}$, via measurements of the neutrino contribution to radiation density in the early Universe. The current bound on $N_{\rm eff}$ from *Planck* CMB combined with BAO is 3.15±0.23 (at 68% confidence) [157], in agreement with the prediction of the Standard Model of particle physics. An additional constraint on $N_{\rm eff}$ comes from BBN which limits the number of additional relativistic degrees of freedom at early times to $\Delta N_{\rm rel} \leq 1.0$ at 95% confidence level [189]. A 1-2% determination of $N_{\rm eff}$ is expected from future CMB data [184, 170, 186].

Upper limits on the absolute ν_e neutrino mass have also been obtained from direct β-decay searches (see e.g. Refs. [190, 191, 192]), with $m_{\nu_e} \leq 2.2$ eV at 95% confidence. The Karlsruhe Tritium Neutrino Experiment (KATRIN) β-decay experiment will improve these limits by measuring m_{ν_e} down to 0.2 eV at 90% confidence [193]; this is about one order of magnitude higher than future cosmological sensitivity. Recently, the first results from KATRIN were published. They find an upper limit of $m_{\nu_e} \leq 1.1$ eV at 90% confidence [194].

In addition, the proposed Princeton Tritium Observatory for Light, Early-Universe, Massive-Neutrino Yield (PTOLEMY) would aim to detect the relic neutrino background and improve KATRIN's neutrino mass bounds [195].

1.3.6 Open questions about neutrinos

In the following, we will discuss several open questions about neutrinos.

1.3.6.1 How many neutrino types are there?

Experimental results from the Liquid Scintillator Neutrino Detector (LSND) experiment [196] and the MicroBooNE experiment [197] might hint towards neutrino oscillations with additional neutrinos in the eV range. The most common explanation are light sterile neutrinos, which are singlet states and which interact only very rarely with active neutrinos. The most recent analysis from the *Planck* satellite has put stringent bounds on the effective number of neutrinos in the early Universe (see [51] and also Sec. 1.3.5). Since light sterile neutrinos would thermalise in the early Universe, they would, in general, lead to a larger $\Delta N_{\rm eff}$ than allowed by the *Planck* bounds [198, 199, 200].

Heavier sterile neutrinos with energies in the range of keV have also been proposed as a candidate for dark matter [201]. Ref. [202] placed strong limits on the sterile neutrino mass, making them an unlikely dark matter candidate. Recently, the detection of a signal at 3.5 keV might be created by the decay of keV sterile neutrinos [203, 204, 205].

1.3.6.2 Are neutrinos Majorana or Dirac particles?

Neutrinoless double β decay experiments (see e.g. [206] for a review) aim to detect whether neutrinos have a Majorana mass [146]. In the neutrinoless double beta decay, two neutrons decay to two protons and two electrons. If neutrinos are their own antiparticles, they can annihilate with each other. In this case, the double beta decay can take place without the emission of antineutrinos. In this process, the lepton number L would be not conserved.

The detection of Majorana neutrino masses would hint towards how neutrino mass are generated (see Sec. 1.3.2). Moreover, double beta decay experiments indirectly constrain the effective Majorana neutrino mass, a specific combination of neutrino masses [207], and are therefore complementary to direct neutrino mass and cosmological neutrino mass searches. If Majorana neutrinos exist, they could also provide an explanation for the baryon asymmetry in the Universe [208, 209, 20]. The decay of Majorana neutrinos would violate lepton number conservation, and through baryon and lepton number violation this could lead to an excess in baryons. In addition, this explanation would also require CP (charge parity) violation [208]. Hints of CP violation have been observed with the Japanese T2K experiment [210].

The GERmanium Detector Array (GERDA) has not found any evidence for neutrinoless double beta decay of ^{76}Ge, and found that the half life time of the decay is larger than $2.1 \cdot 10^{25}$ years (90% C.L.) [211]. Similarly, the CUORE and KamLAND-Zen experiments have not detected yet any neutrinoless double beta decay in ^{130}Te [212] and ^{136}Xe [213]. Future experiments, including the upgraded SNO+ experiment [214], will continue the search for neutrinoless double beta decay.

1.3.7 What are the absolute neutrino masses?

As discussed in Sec. 1.3.5, current and future cosmology and particle physics experiments have only been able to obtain upper limits for the neutrino mass sum, or the electron neutrino mass respectively. The absolute neutrino masses are yet to be determined, and might shed new light on the nature of the underlying neutrino mass mechanism. Closely related to the question what the absolute neutrino

masses are, is the question whether the neutrino mass is normal, inverted or almost degenerate. Current cosmological experiments cannot distinguish yet between the different hierarchies [215, 216, 217, 218, 219, 220, 221, 222]. A global analysis of neutrino oscillation experiments indicate a preference for the normal neutrino hierarchy [223].

1.4 Statistical methods in cosmology

1.4.1 Fisher forecasts

In the following chapters, we will often make predictions for how well a given experiment will be able to constrain cosmological parameters. For these forecasts, we follow a Fisher information matrix approach. Given the Fisher information matrix of an experiment, it is possible to compute the minimal standard deviation for unbiased estimators of the parameters of interest (see e.g. [224]).

The Fisher information matrix is defined as the expectation value of the derivative of the log-likelihood $L(\theta)$ with respect to parameters θ_i and θ_j by [225]

$$F_{ij} \equiv -\left\langle \frac{\partial^2 L(\theta)}{\partial\theta_i \partial\theta_j} \right\rangle. \tag{1.44}$$

Given the Fisher matrix, we can compute lower limits for the standard deviations for an estimator of a parameter θ_i by marginalising over the other parameters θ_j, for $j \neq i$, with

$$\sigma(\theta_\alpha) = \sqrt{(F^{-1})_{\alpha\alpha}}.$$

The real standard deviations will be at least as large as the calculated standard deviations (Cramer-Rao lower bound [226, 227]). If we assume a specific value of a parameter θ_j, we can also fix this value and compute the standard deviations of the other parameters by removing the corresponding row and column from the Fisher matrix.

1.4.2 Monte Carlo Markov chains

Often, we wish to estimate cosmological parameters by comparing astronomical data with theoretical predictions from an underlying cosmological model.

A widely used method to estimate cosmological parameters, and thus to constrain cosmological models, is to use Bayesian inference. Here, the unknown parameter values are modelled as random variables by putting a prior distribution on them. Using the observed data and Bayes' Theorem, one can obtain a posterior distribution. From the posterior distribution, it is possible to obtain

estimators, such as the posterior mean, and credible intervals. Usually, the posterior distribution is not analytically tractable, since it would involve describing a function in a high-dimensional space [228].

In order to obtain samples from the posterior distribution to perform Bayesian inference, one often uses Monte Carlo Markov Chains (MCMC) [229, 230, 228], for example obtained through the Metropolis-Hastings algorithm. Instead of computing the individual probabilities of all points in the parameter space, one draws samples from the probability distribution. The samples form a chain, and the chain is representative of the underlying probability distribution if it has converged. When using the Metropolis-Hastings algorithm, one chooses a trial or proposal distribution, and then accepts or rejects a new sample based on the relative probability of the new and old sample points. A new point is then found by drawing from the proposal distribution.

Usually, the sampling is stopped when a chain has converged, e.g. when we assume that the chain or multiple chains represent sufficiently well the underlying probability distribution. A converged chain is characterized through a low correlation between successive samples. Different convergence diagnostics have been proposed for use in cosmology, for example the Gelman and Rubin statistics [231], where one computes the variance of means, and the power spectrum of a single finite chain as a measure of convergence [232]. The Gelman and Rubin statistics has also been implemented in the MCMC package COSMOMC [36].

After having obtained the MCMC chains, it is possible to compute the mean and the standard deviations of the individual parameters. When including additional parameters in a model, one can compare the base and the extended model by computing their best fit log likelihoods.

1.5 Overview of this thesis

In the following chapters, we will present results obtained during our studies for the doctorate of Philosophy degree.

In Chapter 2, we will present that cosmological neutrino mass constraints are model-dependent, for example when the dark energy equation of state is allowed to vary. We consider two different phenomenological parameterisations of time-varying dark energy (early dark energy and barotropic dark energy) that can be degenerate with neutrino masses or with the effective number of neutrinos. We will show how the combination of multiple cosmological probes can help to distinguish between

dark energy and neutrinos. This work was published in Physical Reviews D as "*Distinguishing between Neutrinos and time-varying Dark Energy through Cosmic Time*" by Lorenz, C. S., Calabrese, E. and Alonso, D., PR D96 (2017) no. 4, 043510 [1].

Afterwards, in Chapter 3, we investigate how neutrino mass constraints can change when neutrino masses are generated late in the Universe. In addition, we study how current tensions between low- and high-redshift cosmological data might be affected by this. This work was published in Physical Reviews D as "*Time-varying neutrino mass from a supercooled phase transition: current cosmological constraints and impact on the* Ω_m-σ_8 *plane*" by Lorenz, C. S., Funcke, L., Calabrese, E. and Hannestad, S., Phys.Rev. D99 (2019) no.2, 023501 [2].

Then in Chapter 4, we will discuss whether lensing magnification and other relativistic effects that affect the galaxy distribution contain additional information about dark energy and neutrino parameters. We also investigate how much parameter constraints can be biased when these effects are neglected. This work was published in Physical Reviews D as "*Impact of relativistic effects in cosmological parameter estimation*" by Lorenz, C. S., Alonso, D. and Ferreira, P. G., Phys.Rev. D97 (2018) no.2, 023537 [5].

Finally, in Chapter 5, we will give a brief overview of current developments in neutrino and large scale structure cosmology that are related to the findings of this thesis.

Chapter 2

Neutrinos and time-varying dark energy

2.1 Introduction

Observations from Type Ia Supernovae (SN) [7, 8], followed by indirect evidence from the Cosmic Microwave Background (CMB) [233, 177], have shown that the expansion of the Universe is accelerating and hint at the existence of an unknown dark energy (DE) component.

In the standard, concordance cosmological model, dark energy is described in terms of the simplest possible component: a cosmological constant, Λ, with an equation of state parameter $w_{\rm de} = p_{\rm de}/\rho_{\rm de}$ (pressure over density) constant in time and equal to -1. However, because of the numerous theoretical issues of the cosmological constant (see e.g., Ref. [9] and references therein), additional, and more complex, dark energy scenarios have been discussed in the literature, including models in which the dark energy equation of state is varying in time (see e.g., Ref. [234] for a review). While waiting for ongoing and future CMB lensing and galaxy redshift surveys to shed light on the physics of this component, currently available cosmological data are used to constrain all kinds of exotic dark energy models. At present, none of these is a better fit to the data compared to a cosmological constant but they also are not completely ruled out (see e.g., Ref. [235] for recent analyses).

Understanding the nature of dark energy is also particularly relevant for future measurements of parameters characterizing neutrino physics. In particular, Ref. [52] have performed forecasts for upcoming measurements of neutrino parameters in more extended dark energy scenarios, and have

shown that our understanding of neutrinos would be significantly improved if the exact behaviour of dark energy were known.

At the level of precision of future measurements of the total neutrino mass and the effective number of neutrinos (see Sec. 1.3.5), theoretical degeneracies between different cosmological scenarios become important and need to be addressed. In this chapter we investigate in detail the degeneracies between dark energy and neutrino parameters. We show that the main correlations arise if a time-varying dark energy fluid and a neutrino fluid behave very similarly during specific cosmic times and demonstrate that a multi-probe analysis might be able to distinguish between the two. Here, we consider two specific phenomenological dark energy parametrizations (early dark energy and barotropic dark energy) chosen because of their similarity to either the effect of $\sum m_\nu$ or $N_{\rm eff}$, and extend previous analyses presented in Refs. [236, 237]. We use these as a proxy for more general cases and show how to anchor them through cosmic time with a combination of early- and late-time cosmological probes. A multi-probe approach for the specific case of the neutrino mass (without discussing dark energy), and a detailed physical derivation of how to isolate the neutrino mass, has also been presented in Ref. [238].

The chapter is structured as follows. We describe the role of neutrinos in cosmology and the two time-varying dark energy models analysed in this chapter in Section 2.2. We then present constraints on these models obtained with current CMB and BAO data in Section 4.2, and forecasts for upcoming experiments in Section 2.4. We conclude in Section 2.5.

2.2 Theoretical degeneracies

Neutrinos and dark energy both affect the expansion rate of the Universe and the growth of cosmic structures, leading to degeneracies between the parameters of the two components even in the case of simple extensions of the cosmological constant (see e.g., Ref. [240, 176, 173, 241, 242, 243, 244, 245, 246]). These can be alleviated by combining data which provide orthogonal information in parameter space (an example of this is the measurement of the matter and dark energy densities from galaxy statistics or CMB). Here, we show that a more complicated scenario, with extended degeneracies, arises when dark energy evolves in time with some tracking behaviour.

To understand phenomenologically why neutrinos and dark energy might look like each other we consider here a fluid parametrization for both components. For each component we define a density

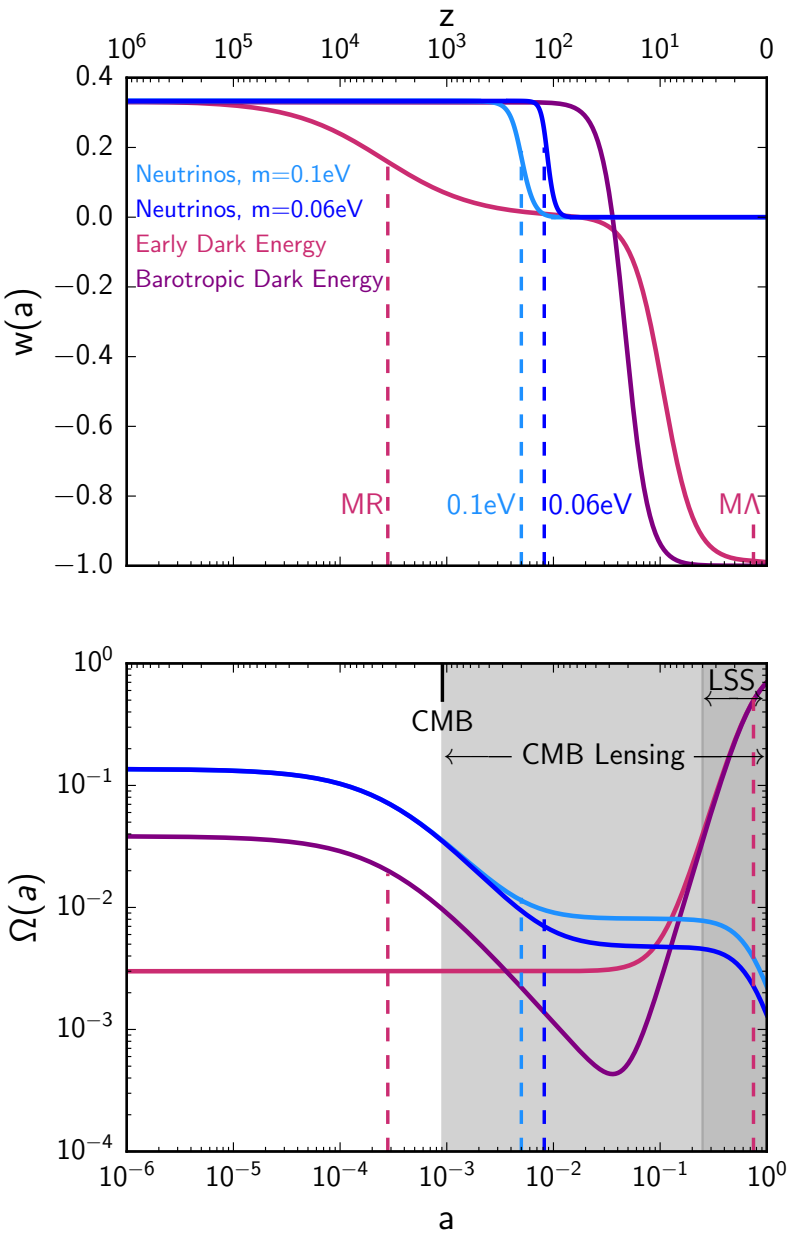

Figure 2.1: Same as Fig. 1.2, but with additionally two specific models of time-varying dark energy [239, 237] (violet) considered in this chapter. To generate these predictions we use the standard ΛCDM *Planck* 2015 best-fit cosmological parameters [157] in combination with $w_0 = -0.99$, $\Omega_e^{\rm EDE} = 0.003$, $\Omega_e^{\rm B} = 0.038$, $N_{\rm eff} = 3.046$ and a single massive neutrino with $\Sigma m_\nu = 0.06$ or 0.1 eV.

parameter, $\Omega(a) \equiv \rho(a)/\rho_{\rm c}(a)$ with $\rho_{\rm c}(a)$ being the critical energy density of the Universe, and an equation of state, $w(a)$, that we evolve with the scale factor, a, to track the behaviour of the fluid at different times. We summarize this discussion in Figure 2.1, which we will gradually populate with models and observational ranges in what follows. For the discussion of the effects of the effective number of neutrinos $N_{\rm eff}$ and the sum of neutrino masses Σm_ν, we refer the reader to Sec. 1.3.3.

2.2.1 Time-varying dark energy

To study the evolution of the Universe in the presence of more complicated dark energy models, we implemented two phenomenological parametrizations described below. The choice of the models is based on their interesting, and at the same time problematic, similarity to the neutrino fluid evolution. For both models we included a full set of perturbation equations with constant sound speed and viscosity parameters equal to 1/3. The viscosity parameter $c^2_{\rm vis}$ accounts for anisotropic stress and parameterises the relationship between velocity and metric shear [236, 237, 247, 248]. The choice of parameters is made to highlight the degeneracies with the neutrino sector and is discussed in detail in Ref. [237].

2.2.1.1 Barotropic dark energy

The barotropic class of dark energy models [249] include all sorts of models in which the physics of the dark energy fluid is fully determined by the pressure as an explicit function of the density. The key feature of these models is the simple extension of the cosmological constant to a theory where DE is varying in time through a non-zero DE term present at early times and then quickly transitioning to Λ today. This alleviates the Λ fine-tuning problem and is still in agreement with current cosmological data.

One such example is the model presented in Ref. [249] where the DE equation of state is given by

$$w_{\rm baro}(a) = [c_s^2 B a^{-3(1+c_s^2)} - 1]/[B a^{-3(1+c_s^2)} + 1]\,, \tag{2.1}$$

where c_s is the dark energy sound speed, $B = (1 + w_0)/(c_s^2 - w_0)$, and w_0 is the present value of the equation of state. We extend this model by introducing perturbations in the DE fluid as in Ref. [237] and in fact continuing the late-time DE term with a dark radiation term at early times.

To discuss the interesting degeneracies with neutrino physics we fix $c_s^2 = 1/3$. Consequently w goes to $1/3$ for $a \to 0$, as in the case of radiation and neutrinos, and approaches $w = -1$ today.

The barotropic dark energy density is now obtained by inserting Eq. 2.1 in the dark energy continuity equation and integrating this latter to obtain

$$\rho_{\rm baro}(a) = \frac{\rho_{\rm baro,0}}{B+1}(1 + Ba^{-4})\,, \tag{2.2}$$

where the subscript 0 stands for today and with $\rho_{\rm baro,0}$ given by

$$\rho_{\rm baro,0} = \left(\frac{3H_0^2}{8\pi G}\right) \times (1 - \Omega_{\rm m,0})\,. \tag{2.3}$$

In this model the dark energy fluid can be approximated as the sum of a late-time cosmological constant and an additional radiation term dominating at early times, $\rho_{\rm baro} \sim \rho_\infty + Aa^{-4}$, where ρ_∞ is the energy density of the cosmological constant.

The fraction of barotropic dark energy contributing to radiation in the early Universe depends on the only free parameter of the model, B, and can be computed through

$$\begin{aligned} \Omega_e^{\rm B} &= \lim_{a\to 0} \frac{\rho_{\rm baro}(a)}{\rho_{\rm c}(a)} \\ &= \frac{B\rho_{\rm baro,0}}{B\rho_{\rm baro,0} + (B+1)\rho_{\rm r,0}} \end{aligned} \tag{2.4}$$

where $\rho_{\rm r,0}$ is the radiation density today (assuming $N_{\rm eff}$ massless neutrinos)[1].

The density and equation of state for this model in the case of $B = 5 \times 10^{-6}$ ($\Omega_e^{\rm B} \sim 0.038$) are shown in Figure 2.1 in dark violet lines. By construction, this model is now degenerate with the neutrino fluid during radiation domination and, because of this, we expect correlations between B (or equivalently $\Omega_e^{\rm B}$) and $N_{\rm eff}$.

2.2.1.2 Early dark energy

The second model that we consider is an early dark energy model (EDE) that has been first suggested by Ref. [239] and extensively explored in the literature [250, 236, 237, 251, 252, 253, 235]. This model falls into the tracking dark energy class of models [254], where the dark energy density is a sub-dominant fraction of the dominant component of each cosmic epoch, i.e., radiation first, matter later and evolving into Λ today.

[1] We note that we have derived here a different parametrization of $\rho_{\rm baro}(a)$ and therefore a new derivation of $\Omega_e^{\rm B}$, which does not directly correspond to the same parameter in Ref. [237].

The dark energy density and the equation of state parameters are given by

$$\Omega_{\rm ede}(a) = \frac{\Omega_{\rm ede,0} - \Omega_e^{\rm EDE}(1-a^{-3w_0})}{\Omega_{\rm ede,0} + \Omega_{\rm m,0}a^{3w_0}} + \Omega_{\rm e}^{\rm EDE}(1-a^{-3w_0})\,, \tag{2.5}$$

$$w_{\rm ede}(a) = -\frac{1}{3[1-\Omega_{\rm ede}(a)]}\frac{d\ln\Omega_{\rm ede}(a)}{d\ln a} + \frac{a_{\rm eq}}{3(a+a_{\rm eq})}\,, \tag{2.6}$$

and shown in Figure 2.1. The two free parameters of the model are the present value of the equation of state parameter, w_0, and $\Omega_{\rm e}^{\rm EDE}$, which is the asymptotic limit of the DE energy density at $a = 0$. $a_{\rm eq}$ is the scale factor at matter-radiation equality. The evolution of w in this case is more complex and can be divided into three regimes: $w \simeq 1/3$ during radiation domination, $w \simeq 0$ during matter radiation and $w = w_0$ today.

In this case, as is clear from Figure 2.1, $w_{\rm ede}$ transitions to a matter-like behaviour before neutrinos become non relativistic and the two fluids are degenerate at early-to-intermediate times. Hence, the early dark energy model parameters will be mostly correlated with the neutrino mass. In particular, in the late Universe, both early dark energy and neutrinos now suppress structure formation: neutrinos through the effect of their mass described before, and dark energy by changing the expansion rate [176].

2.2.2 Observations at different cosmic times

The above discussion and Figure 2.1 stress the need to test cosmological models at different cosmic epochs to distinguish between neutrinos and time-varying dark energy, with observations spanning a wide range of redshifts. This is possible combining measurements of the early Universe via the CMB primary anisotropies with large-scale structure data measuring the late-time evolution (including galaxy weak lensing and clustering, baryonic acoustic oscillations and SN distance measurements), connected at intermediate times via the CMB gravitational lensing. This is schematically shown in Figure 2.1, where we highlight the time of the CMB decoupling (redshift of $z \simeq 1100$), and where CMB lensing (integrated signal from decoupling to today) and LSS ($3 \gtrsim z > 0$) sit relative to the evolution of massive neutrinos and a time-varying dark energy. The blue dashed lines show the time when a 0.1 eV and a 0.06 eV neutrino become non-relativistic, at $a \simeq 5 \times 10^{-3}$ and $a \simeq 8 \times 10^{-3}$, respectively. Magenta dashed lines show the times of the matter-radiation and the matter-Λ equality defining the DE transitions.

In particular, for the models considered here, the pattern of acoustic peaks in the CMB primary power spectra will anchor the relativistic behaviour and so provide information on $N_{\rm eff}$ and $\Omega_e^{\rm B}$, while CMB lensing and LSS will distinguish the fluids in the matter- and Λ-dominated epochs, improving the limits on $N_{\rm eff}$ and $\Omega_e^{\rm B}$, and constraining $\sum m_\nu$, w_0 and $\Omega_e^{\rm EDE}$.

This multi-probe combination has already proven to be very powerful in testing cosmological models [157] and will become a standard approach for future analyses of CMB and LSS data. Anticipating high-precision and high-sensitivity CMB primary and lensing observations from the ground-based CMB Stage IV experiment [184], and their combination with BAO from the Dark Energy Spectroscopic Instrument (DESI) [102], or galaxy lensing and clustering from the Large Synoptic Survey Telescope (LSST) [101], the Euclid satellite [103] and the Wide-Field InfraRed Survey Telescope (WFIRST) mission [255], we investigate in the following current limits and future prospects for these models.

2.3 Constraints from current data

To constrain the dark energy model parameters in conjunction with neutrino physics with current CMB and LSS data, we modified a publicly available version of the CAMB Boltzmann code [256] and interfaced it with CosmoMC [257], a public Monte Carlo Markov chain package that explores cosmological parameters for different theoretical models and data combinations.

We explore an extended ΛCDM model where we vary the standard cosmological parameters (the baryon density today $\Omega_{\rm b}h^2$, the cold dark matter density today $\Omega_{\rm c}h^2$, the scalar spectral index n_s, the Hubble constant H_0, the amplitude of primordial scalar perturbations A_s) and additional DE and neutrino parameters: $N_{\rm eff}$, Σm_ν, $\Omega_e^{\rm EDE}$, w_0 (in the range $w_0 > -1$), and B. For this latter parameter we impose a flat prior in the range [-7,-2] on its logarithmic variation to better explore very small values, and we report results in terms of its derived parameter $\Omega_e^{\rm B}$. When not varied, we follow the standard convention of fixing $N_{\rm eff} = 3.046$, $\Sigma m_\nu = 0.06$ eV, $\Omega_e^{\rm EDE} = 0$, $w_0 = -1$, and $B = 0$. We further impose a Gaussian prior on the reionization optical depth, $\tau = 0.06 \pm 0.01$, in order to incorporate recent CMB large-scale polarization data from the *Planck* satellite [258].

We extract cosmological parameters using CMB primary and lensing data from the *Planck* 2015 data release [259, 260] (retaining only high-multipole temperature for primary anisotropies as recommended by the *Planck* team), and BAO distance ratio r_s/d_V from BOSS DR12 (CMASS

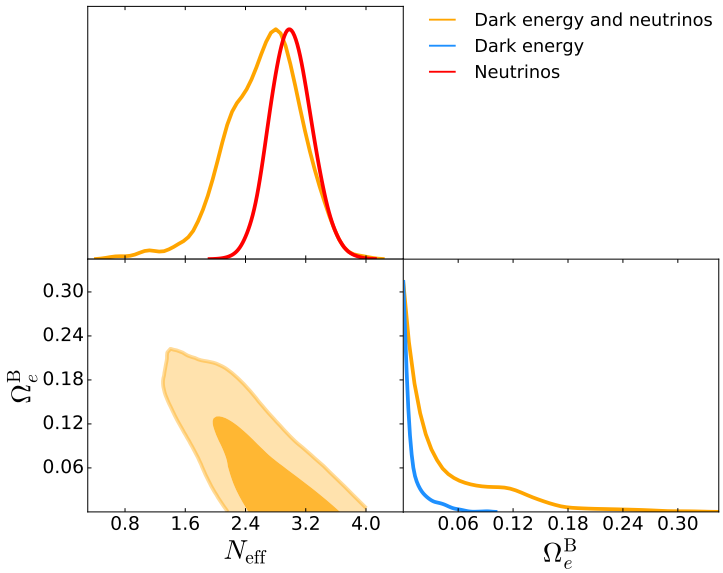

Figure 2.2: 1-dimensional posterior and 2-dimensional contour levels at 68% and 95% confidence for the effective number of neutrinos, $N_{\rm eff}$, and the early barotropic dark energy density, $\Omega_e^{\rm B}$, constrained by *Planck* CMB temperature anisotropies. Different colours distinguish runs with different freedom in parameter space: red for varying only the neutrino parameters, blue for varying only dark energy ones, and orange for parameters of both components varying at the same time.

and LOWZ) [261], SDSS MGS [262], and 6DF [263]. Here, the distance measure d_V is defined by $d_V(z) = [(1+z)^2 d_A^2 cz/H(z)]^{1/3}$ [264]. We further impose the BBN consistency relation between $N_{\rm eff}$ and the baryon density on the primordial Helium abundance [265].

2.3.0.1 Single-probe degeneracies

We first consider the case in which a single probe is used to constrain time-varying DE and neutrinos. For this we retain the most constraining probe of the Universe's content and evolution, the primary CMB anisotropies. Limits from *Planck* CMB temperature data are shown in Figures 2.2, 2.3, where we recover the expected $N_{\rm eff} - \Omega_e^{\rm B}$, $\sum m_\nu - \Omega_e^{\rm EDE} - w_0$ degeneracies.

To show the impact of one component on the other, we run three different cases for each of the time-varying DE models: (i) varying only neutrino parameters, (ii) varying only DE parameters, (iii) varying all DE and neutrino parameters at the same time. We report quantitative results in terms of the correlation coefficient, defined as

$$R = C(P_1, P_2)/\sqrt{(C(P_1, P_1) \times C(P_2, P_2))}\,, \tag{2.7}$$

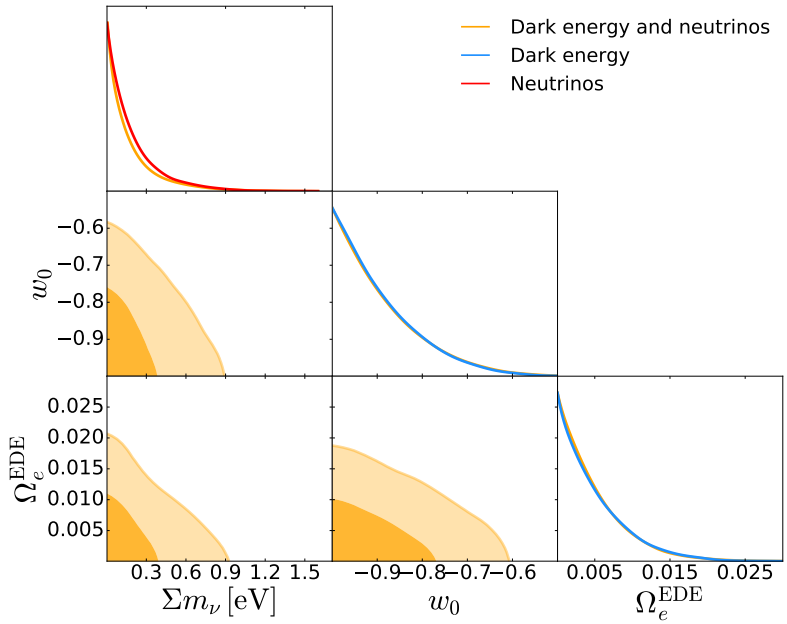

Figure 2.3: 1-dimensional posterior and 2-dimensional contour levels at 68% and 95% confidence in the case of degeneracies between massive neutrinos and the early dark energy model. The parameters varied are the neutrino mass sum, $\sum m_\nu$, the early dark energy density, $\Omega_e^{\rm EDE}$, and the present value of the DE equation of state, w_0. The colour scheme is the same as Figure 2.2.

where C is the covariance matrix of the P parameters.

In the case of (i) we recover the *Planck* limits on $N_{\rm eff}$ and Σm_ν [258], yielding $N_{\rm eff} = 3.00 \pm 0.28$ (68% confidence) and $\sum m_\nu < 0.63$ eV (at 95% confidence).

The individual DE parameters in the case of (ii) are instead constrained to be: $\Omega_e^{\rm B} < 0.045$, $\Omega_e^{\rm EDE} < 0.014$, and $w_0 < -0.72$ (all at 95% confidence), where the latter two are consistent with the *Planck* results in Ref. [235].

When letting both components free to vary we see that the limits on the individual parameter degrade by 77% for $N_{\rm eff}$ and 284% for $\Omega_e^{\rm B}$, and a correlation of −81% is found between the two. To fit the *Planck* high-precision CMB acoustic peaks position, the amount of radiation is split between $N_{\rm eff}$ and $\Omega_e^{\rm B}$ along a tightly constrained anti-correlated region.

The impact on individual constraints is instead less strong in the case of $\Omega_e^{\rm EDE} - w_0 - \sum m_\nu$. This can be understood by noticing that in this case the results are dominated by the sampling and physical priors ($\Omega_e^{\rm EDE} > 0$, $w_0 > -1$, and $\sum m_\nu > 0$) which confines all the parameters into the lower limit region of the samples and hides the anti-correlation (see Figure 2.3). We will show that

Parameters	CMB	CMB +CMBL	CMB +CMBL+BAO
Baro DE			
$\Omega_e^{\rm B}$	≤ 0.164	≤ 0.115	≤ 0.107
$N_{\rm eff}$	2.64 ± 0.49	2.83 ± 0.35	2.87 ± 0.33
EDE			
$\Omega_e^{\rm EDE}$	≤ 0.013	≤ 0.011	≤ 0.007
w_0	≤ -0.71	≤ -0.73	≤ -0.89
$\sum m_\nu$[eV]	≤ 0.64	≤ 0.53	≤ 0.12
Correlations	CMB	CMB +CMBL	CMB +CMBL+BAO
Baro DE			
$N_{\rm eff} - \Omega_e^{\rm B}$	-81%	-66%	-79%
EDE			
$\sum m_\nu - \Omega_e^{\rm EDE}$	-3.7%	-20%	-15%
$\sum m_\nu - w_0$	2.3%	0.3%	-19%

Table 2.1: *Top:* Marginalized constraints on dark energy and neutrino parameters for different data combinations: *Planck* primary CMB and CMB lensing (CMBL), and BAO data probing the large-scale structure. Errors are 68% confidence levels while upper limits are reported at 95% confidence. *Bottom:* Correlation coefficients between the DE and neutrino model parameters for different data combinations.

this will not be the case with future data, when one of the parameters (the neutrino mass sum in this case) will be constrained away from the sampling bounds.

2.3.0.2 Multi-probe analysis

To show how a multi-probe analysis can help confine the two components and hence break the degeneracies, we report the results of gradually adding to the main *Planck* CMB primary spectra late-time probes, including *Planck* CMB lensing, and BOSS/SDSS/6dF BAO. State-of-the-art constraints on these models are reported in Table 2.1 and Figures 2.4, 2.5.

In the case of the barotropic dark energy model, low-redshift data only marginally improve individual parameters constraints and do not help in reducing the correlations. This can be understood considering that both B and $N_{\rm eff}$ are mainly constrained via the expansion rate at very early times. Primary CMB is then dominating the constraints, with CMB lensing providing some additional contribution at intermediate redshifts and no extra information coming from BAO.

For the second scenario (early dark energy), low-redshift data have a stronger impact by providing tight bounds on the matter component. Because of this, the sum of the neutrino masses and the

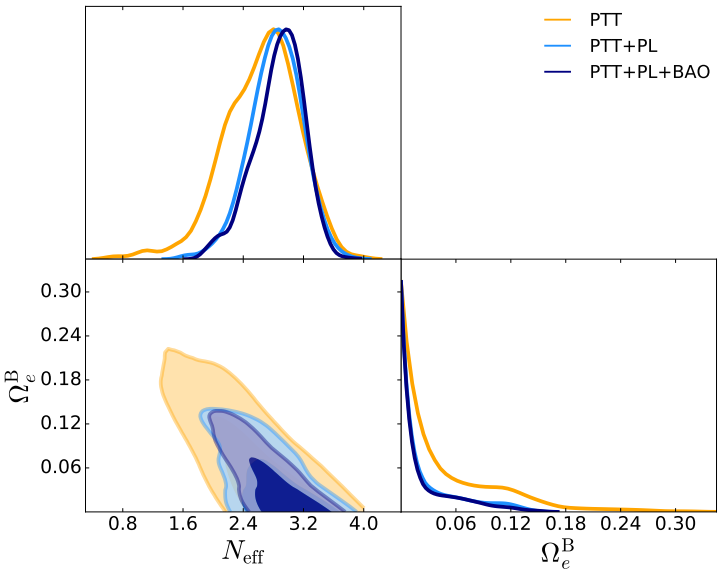

Figure 2.4: 1-dimensional posterior and 2-dimensional contour levels at 68% and 95% confidence for the effective number of neutrinos, $N_{\rm eff}$, and the early barotropic dark energy density, $\Omega_e^{\rm B}$, from different data combinations: *Planck* CMB primary anisotropies (PTT) only in orange, combined with *Planck* CMB lensing spectra (PL) in light blue, and with also BAO in dark blue. The inclusion of low-redshift data helps only marginally to reduce the degeneracies between $N_{\rm eff}$ and $\Omega_e^{\rm B}$.

amount of $\Omega_e^{\rm EDE}$ are better constrained. They also provide a much tighter constraint on w_0, helping to better limit the 3-dimensional degeneracy $\sum m_\nu - \Omega_e^{\rm EDE} - w_0$. We have also tested whether the inclusion of the Type Ia Supernovae compilation of the Joint Light-curve analysis (JLA) team [54] helps to better constrain the early dark energy model, but found no significant improvement.

Table 2.1 also reports the values of the correlation coefficient for both scenarios and all data combinations. While the combination of CMB and BAO (as a LSS probe) improves the individual parameters' constraints, the current level of sensitivity is not able to isolate and then break the correlations in two dimensions.

2.4 Future predictions

To estimate the power of future cosmological data in distinguishing between neutrinos and these time-varying dark energy models, we present here predictions of future limits using the CMB Stage-4 experiment (S4) in combination with BAO measurements from DESI as a tracer of the large-scale

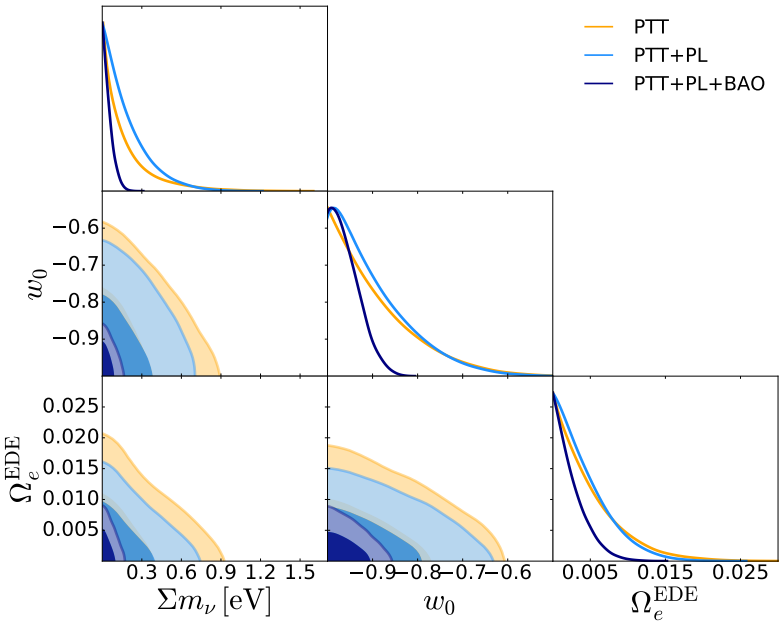

Figure 2.5: 1-dimensional posterior and 2-dimensional contour levels at 68% and 95% confidence for the sum of the neutrino masses, Σm_ν, the early dark energy density, $\Omega_e^{\rm EDE}$, and the present value of the dark energy equation of state, w_0, from different data combinations: *Planck* CMB primary anisotropies (PTT) only in orange, combined with *Planck* CMB lensing spectra (PL) in light blue, and with also BAO in dark blue. The inclusion of low-redshift data helps to reduce the degeneracies between $\sum m_\nu$ and $\Omega_e^{\rm EDE} - w_0$.

structure[2]. From mid-2020s we anticipate access to arcminute-resolution CMB temperature and polarization data with a 1μK-arcmin noise level from CMB-S4 [184], and percent-level determination of the Hubble constant and angular diameter distance from DESI [173], tracing the history of the Universe with unprecedented sensitivity.

We run Fisher matrix analyses using the code presented in Ref. [266] and following the methodology described in Ref. [186] for the data combination (see Table I in there). Our reference datasets are:

- PL+S4

  CMB-S4 temperature and E-modes of polarization anisotropies over $30 < \ell < 3000/5000$ on 40% of the sky measured with a 3-arcmin resolution and 1μK-arcmin noise level in temperature; combined with expected full-mission *Planck* data (as implemented in Refs. [52, 186]) to complement the multipole range and extend the sky fraction;

- PL+S4+S4L

  same as above but including also CMB-S4 measurements of the CMB lensing power spectrum over $30 < \ell < 3000$ on 40% of the sky;

- PL+S4+S4L+BAO

  same as above plus BAO distance ratio as measured by DESI in the range $0.15 < z < 1.85$.

The results are shown in Figures 2.6, 2.7 for barotropic and early dark energy, respectively.

In the case of barotropic dark energy, future CMB data will significantly improve the constraints on the individual parameters, reaching the current level of sensitivity for $N_{\rm eff}$ in the case of no varying dark energy ($\sigma(N_{\rm eff}) \sim 0.2$ from *Planck*+BAO) and limiting the fraction of barotropic dark energy at early times with percent-level accuracy. The high correlation between $N_{\rm eff}$ and $\Omega_e^{\rm B}$, however, persists even with higher-resolution data

$$\begin{aligned} R(N_{\rm eff}, \Omega_e^{\rm B}) &= -97\% \quad (\text{PL+S4})\,, \\ &= -97\% \quad (\text{PL+S4+S4L})\,, \\ &= -99\% \quad (\text{PL+S4+S4L+BAO})\,. \end{aligned} \tag{2.8}$$

[2]We note that a different LSS tracer would lead to the same qualitative conclusions.

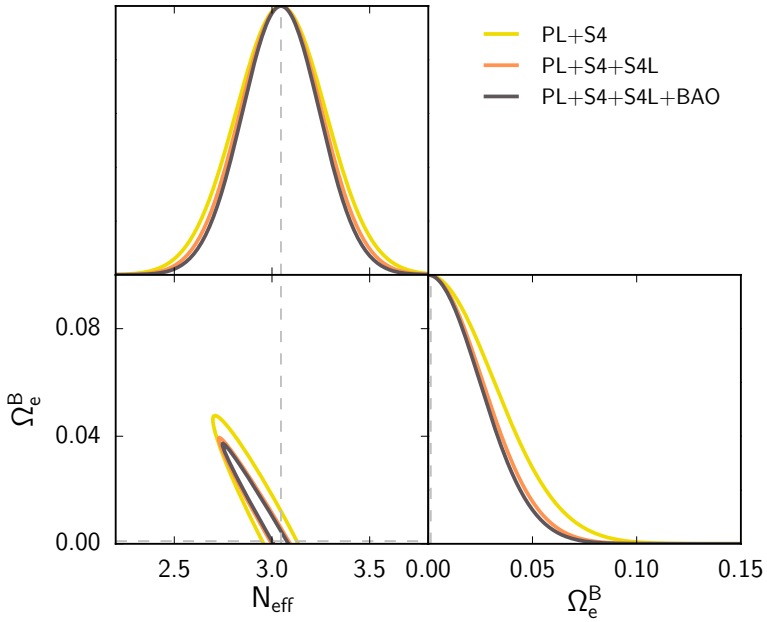

Figure 2.6: Predictions for the constraints on the barotropic dark energy density, $\Omega_e^{\rm B}$, and the effective number of neutrinos, $N_{\rm eff}$, from future CMB-S4 primary anisotropies (S4) and lensing (S4L) data, complemented by *Planck* (PL), and in combination with BAO distance ratio from DESI. The 2-dimensional contours report the 68% confidence levels. The dashed lines show the fiducial values of the parameters used in the Fisher calculations.

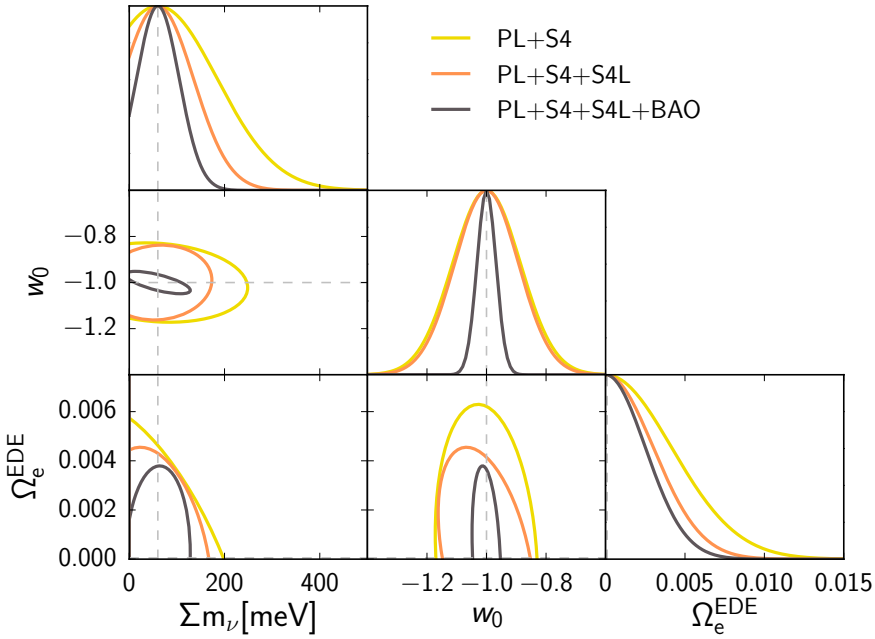

Figure 2.7: Same as Figure 2.6 in the case of early dark energy; showing future constraints on the dark energy density, $\Omega_e^{\rm EDE}$, the present value of the equation of state parameter, w_0, and the neutrino mass sum, Σm_ν, obtained from different early- and late-time data combinations.

Ref. [170] have shown a $\sim 20\%$ improvement on the determination of $N_{\rm eff}$ when BBN information are added to CMB-S4 by, e.g., imposing BBN consistency relations. We choose not to include BBN information here because it would not change our conclusions. In the presence of barotropic dark energy, the addition of BBN would be less effective in constraining $N_{\rm eff}$ and not useful to break the degeneracies with DE. Barotropic DE would in fact affect the BBN just as extra relativistic degrees of freedom (an effective $\Delta N_{\rm eff}$) and therefore will continue to mimic neutrino particles all the way to the BBN epoch. We note that this is due to our way of defining the two fluids with the same sound speed $c_s^2 = 1/3$ and viscosity parameter $c_{\rm vis}^2 = 1/3$, which therefore cannot be isolated with higher-order velocity/viscosity propagation. In the case of non free-streaming extra radiation, a measurement of the phase shift in the CMB anisotropies will break these correlations (see, e.g., Refs. [163, 169, 267]).

The multi-probe approach is instead very successful for the early dark energy scenario. Figure 2.7 shows a decreasing correlation between the parameters (visually appreciated in the rotation of the 2-dimensional contours) with the addition of lower-redshift data. The correlation coefficient is found to be

$$
\begin{aligned}
R(\Sigma m_\nu, \Omega_e^{\rm EDE}) &= -68\% \quad (\text{PL+S4})\,, \\
&= -33\% \quad (\text{PL+S4+S4L})\,, \\
&= +6.0\% \quad (\text{PL+S4+S4L+BAO})\,,
\end{aligned} \tag{2.9}
$$

$$
\begin{aligned}
R(\Sigma m_\nu, w_0) &= -13\% \quad (\text{PL+S4})\,, \\
&= -7.0\% \quad (\text{PL+S4+S4L})\,, \\
&= -7.5\% \quad (\text{PL+S4+S4L+BAO})\,.
\end{aligned} \tag{2.10}
$$

In the presence of time-varying dark energy, the estimate of the neutrino mass is therefore significantly aided by combining multi-epoch datasets. We find for PL+S4+S4L+BAO $\sigma(\Sigma m_\nu) \sim 0.04$ eV, which is a ~ 1.5 factor worse than CMB-S4 predictions in a ΛCDM scenario when combined with DESI. This will improve even more when Supernovae, galaxy shear and clustering, galaxy cluster counts and redshift space distortions are optimally combined with the probes we considered here.

2.5 Conclusion

In this chapter we have investigated the correlations arising between time-varying dark energy models and cosmological neutrinos. We have demonstrated how some dark energy models tracking other cosmic components during specific epochs can look like neutrinos over extended periods of the Universe history. This will affect our ability to constrain the number and sum of the masses of the neutrino particles and the physics of dark energy.

We have considered two phenomenological dark energy models: barotropic dark energy and early dark energy, particularly interesting due to their similarity to the effects on cosmological probes of either $N_{\rm eff}$ or Σm_ν. We have presented state-of-the-art limits on these models but found that current CMB and large-scale structure data are not able to clearly distinguish between the two components. In addition, we have investigated the reach of future experiments and forecast estimates from the CMB Stage-4 experiment in combination with BAO from DESI. We have shown that future data will be able, via a multi-probe combination, to break some of the degeneracies and better limit these extended scenarios.

Chapter 3

Time-varying neutrino masses

3.1 Introduction

The absolute value and the origin of the neutrino masses are two of the main open questions in particle physics and cosmology. Cosmology and laboratory searches are sensitive to different linear combinations of the neutrino mass eigenstates and therefore confine the neutrino parameter space in a complementary way.

As an alternative to standard neutrino mass mechanisms (see Sec. 1.3.2), Ref. [3] proposed a low-energy solution to the neutrino mass problem at a new infrared gravitational scale ($\Lambda_G \lesssim$ eV), which is numerically similar to the scale of dark energy. As reviewed below, this model alters late-Universe cosmology after photon decoupling.

In the Standard Model of cosmology, and/or in the presence of these relic neutrinos with time-varying mass, the neutrino mass affects the growth of cosmic structures in several ways (see e.g. Ref. [268] for a review and Ref. [1] for a summary of the effects relevant here). In particular, non-zero masses suppress the amplitude of matter fluctuations in the late-time Universe compared to those present at early times, i.e. at the time of the CMB decoupling. Therefore, the total sum of the neutrino masses is strongly correlated with the inferred values of the matter density, Ω_m, and matter clustering, for example measured by the amplitude of matter fluctuations on 8 h^{-1} Mpc scales, σ_8. These quantities can be constrained with the CMB, the CMB lensing signal (that is the deflection of the CMB photon paths due to gravitational potential wells along their trajectories), and different probes of the matter distribution in the local Universe, e.g. the galaxy weak lensing signal, galaxy clustering, and the abundance of galaxy clusters.

Over the past few years, measurements of Ω_m-σ_8 from early- and late-time surveys have shown some mild tensions. In particular, taking the parameter combination $S_8 \equiv \sigma_8\sqrt{\Omega_m/0.3}$, the tension exists when comparing *Planck* CMB constraints [51] with galaxy weak lensing data from the Canada France Hawaii Lensing Survey (CFHTLenS) at the 1.7σ level [269] (see also Ref. [270]), from the Kilo Degree Survey (KiDS) at the 2.2σ level [271, 272] (2.6σ in combination with 2dFLenS [273]), and from the first-year release of the Dark Energy Survey (DES) at the 1.7σ level [274]. Similar levels of inconsistency are found between Ω_m-σ_8 inferred from the abundance of galaxy clusters detected with the Sunyaev–Zel'dovich (SZ) effect and *Planck* CMB values [275, 276]. This has generated a lot of interest in the cosmological community with efforts split between investigation of residual systematics in the data or analysis assumptions in KiDS, DES, and *Planck* (e.g. [277, 278, 279, 280, 281, 282]), and the possibility of having seen signatures of new physics beyond the standard ΛCDM cosmological model (e.g. [283, 284, 272, 285, 286, 287, 288, 289, 290, 291]). For example, Refs. [272, 292, 293] explored whether time-varying dark energy or neutrino masses might solve the tensions. Although the significance of the discrepancy changes slightly in more extended models, there is, at present, no clear preference for a beyond-ΛCDM cosmology.

However, a general trend of these results is that low-redshift data prefer less matter fluctuations compared to early-time estimates which, when allowing neutrino masses to vary, translates into higher preferred values of the neutrino mass compared to the constraints coming from the CMB alone. Motivated by this, and taking at face value the analysis assumptions and the likelihood packages of each experiment (i.e. assuming this is not data/analysis systematics driven), we explore here a time-varying neutrino mass model, where the neutrino mass increases with time. Time-varying neutrino mass models were first introduced by Ref. [294] as a way to explain the similar energy scales of massive neutrinos and dark energy, and suggested that mass-varying neutrinos could be the cause of cosmic acceleration. However, Ref. [295] showed that these models would not be stable, and not distinguishable from a cosmological constant. Time-varying neutrino mass models and their cosmological implications were also studied in Refs. [296, 297, 298, 299, 300, 301].

A new time-varying neutrino mass model was recently proposed in Ref. [3], where neutrino masses are generated through a gravitational θ-term in a late cosmic phase transition. This transition can either take place instantaneously at a temperature $T \sim m_\nu$ or become apparent later at temperatures $T \lesssim m_\nu$, for example in the case of substantial supercooling. In both cases, the minimal version of the

gravitational mass model predicts almost complete relic neutrino annihilation after the transition, so that all cosmological mass constraints are entirely evaded. However, a substantial relic neutrino density can survive in the non-minimal presence of neutral lepton asymmetries, which was not considered in Ref. [3]. In this case, impact on neutrino mass constraints from cosmological data would be expected. For example, cosmological constraints on a simplified version of this non-minimal case of the model were presented in Ref. [302], finding that in some cases the cosmological neutrino mass bounds are significantly weakened compared to the standard constant-mass case, with $\sum m_\nu \lesssim 0.6 - 0.8$ eV.

In this chapter, we extend the analysis of Ref. [302] in three ways. 1) We focus on the supercooled phase transition and include a substantial amount of false vacuum energy, which is required in particular when generating relatively large neutrino masses at late times corresponding to low temperatures (see Section 3.2), this was neglected in Ref. [302]. For simplicity, we neglect the neutrino self-interactions and (partial) annihilation, as predicted by the model in Ref. [3], which will be treated in future studies. 2) We add *Planck* polarization data. 3) We examine whether time-varying neutrino masses can ease the tensions between cosmological parameters inferred from high- and low-redshift data, looking at the constraints from different probes in the Ω_m-σ_8 plane. The analysis assumptions are reported in Section 3.3 and results in Section 3.4.2. We summarize our findings and discuss the implications of our analysis both for the KATRIN experiment and for relic neutrino detection experiments, such as PTOLEMY [303], in Section 3.5.

3.2 Time-varying neutrino mass model

3.2.1 Theoretical Foundations

The gravitational neutrino mass model in Ref. [3] predicts the relic neutrinos to be massless until a late cosmic phase transition after photon decoupling. As described in Refs. [3, 4], a neutrino vacuum condensate forms in the transition. This generates small effective neutrino masses $m_\nu \sim \Lambda_G \sim |\langle \bar{\nu}\nu \rangle| \equiv v$, where Λ_G is the neutrino flavor symmetry breaking scale and v is the scale of the vacuum condensate[1]. According to Refs. [3, 4], the massive relic neutrinos quickly decay into the

[1]Ref. [304] showed that this scenario could also solve the strong CP problem if the condensate generates the up-quark mass as well.

lightest neutrino mass eigenstate, become strongly coupled, and (partially) bind up or annihilate into almost massless Goldstone bosons through the process $\nu+\bar{\nu} \to \phi+\phi$. Naively, one might expect this modification of the relic neutrino sector to be ruled out by cosmological observations; for example, the similar idea of a neutrinoless Universe [305] was ruled out by neutrino free-streaming in the early Universe [306, 307], an induced phase shift in the CMB peaks [308], and precision measurements of the effective number of neutrino species from the CMB (more recently from Ref. [51]). This is not the case because, crucially, the temperature T_{Λ_G} of the neutrino phase transition is a free parameter of the model in Ref. [3], fixed to $T_{\rm today} \lesssim T_{\Lambda_G} \lesssim T_{\rm CMB}$ by the above-mentioned cosmological constraints[2]. Thus, Ref. [3] predicts neutrino self-interactions and (partial) annihilation only in the late Universe after photon decoupling, making the model predictions cosmologically viable.

Additionally, an important point to stress here is that, although an almost complete relic neutrino annihilation is a key prediction of the minimal case in Ref. [3], this does not necessarily need to happen if there are neutrino asymmetries. Big Bang Nucleosynthesis (BBN) and CMB data weakly constrain the muon- and tau-neutrino asymmetries [157], while BBN data strongly constrain the electron-neutrino asymmetry [189]. If standard neutrino oscillations in the early Universe mix the neutrino flavors, the strong BBN bounds would apply to all neutrino flavors [310]. However, the model in Ref. [3] predicts massless relic neutrinos in the early Universe. The flavor-violating couplings only turn on at the time of the late-time phase transition [4] (similar to, e.g. axion couplings [311]). Following Ref. [4], we derive that the latest *Planck* CMB limit of $\Delta N_{\rm eff} < 0.33$ at 95% confidence provides a weak bound on the $\nu_{\mu,\tau}$ asymmetries of

$$\left| \frac{n_{\nu_{\mu,\tau}} - n_{\bar{\nu}_{\mu,\tau}}}{n_{\nu_{\mu,\tau}}} \right| \lesssim 0.16 \times \frac{11}{3} \sim 0.58\,. \tag{3.1}$$

Therefore up to $\sim 58\%$ of the ν_μ and ν_τ flavors could still be present after the annihilation, that means $\sim 39\%$ of all relic neutrinos. Such an asymmetry could only survive in the Dirac neutrino case [312], which implies that the Majorana case of Ref. [3] would always yield a neutrinoless Universe.

[2]We note that the upper bound on T_{Λ_G} still applies if neutrinos get small masses through other mechanisms beyond gravity, making this constraint model-independent. A generic lower bound on the scale Λ_G stems from experimental tests of Newtonian gravity down to $\sim {\rm meV}^{-1}$ distances [309], which is similar to the model-dependent lower bound on v from the observed neutrino mass splitting [3].

Consequently, in this work we consider a modified version of the minimal case in Ref. [3], exclusively studying late neutrino mass generation and neglecting the self-interactions and (partial) annihilation which we leave for future studies.

Ref. [3] assumed the phase transition to take place instantaneously, i.e. at a temperature $T_{\Lambda_G} \sim \Lambda_G \sim v \sim m_\nu$. As described in Ref. [4], the phase transition can also be delayed because of supercooling (see e.g. Refs. [313, 314, 315]), which can significantly increase the energy density in an expanding Universe. As discussed in Refs. [4], this mechanism could generate large neutrino masses.

The relevant factors characterizing the potential delay of the phase transition are the possible neutrino asymmetries (see analogous discussions in Refs. [316, 317]) and unknown order-one coefficients in the effective potential $V(\Phi, T)$ of the neutrino-bilinear order parameters $\Phi \equiv \bar{\nu}\nu$. In the case of a strongly supercooled transition, the false metastable vacuum can be stabilized at $\langle\Phi\rangle = 0$ over long cosmological times until the false vacuum tunnels into the true one [318]. This vacuum decay releases positive potential energy density associated with the false vacuum and thus increases the energy density in the late relic neutrino sector relative to the other diluting energy densities in the Universe, e.g. of the photons. Consequently, the model in Refs. [3, 4] includes the possibility that the energy density in the current neutrino component can be larger than expected in ΛCDM.

Since a delayed neutrino phase transition would have a greater impact on cosmological observables than a non-delayed transition, the numerical analysis in this chapter only focuses on the former case. In particular, Ref. [302] found that in the case of neutrino mass generation at $T_{\Lambda_G} \sim \Lambda_G \sim v \sim m_\nu$, the cosmological limits are very similar to the constant-mass neutrino case if relic neutrino annihilation [3] is neglected. The neutrino masses will only slowly rise in this case, while the local minimum of the free energy will slowly decrease, with less impact on cosmological observations. In case of a supercooled phase transition, the neutrino masses and transition temperature are two independent parameters.

We note that generating relatively large masses at a low temperature seems to violate energy conservation at first sight. Therefore, differently from what was done in Ref. [302], we here take into account the false vacuum energy from the supercooled phase transition, which converts into neutrino masses at the low apparent transition temperature. Due to the unknown order-one coefficients in the effective potential mentioned above, the exact amount of false vacuum energy is an unpredictable free parameter of the theory. For simplicity, we assume that the false vacuum energy entirely converts

into neutrino masses, and we neglect the additional conversion into excitations of the Φ field, i.e. dark radiation.

We choose the same step-function parametrization for the late neutrino mass generation as Ref. [302]

$$m_\nu(a) = \begin{cases} 0 & \text{if } a \leq a_s \\ m_\nu \tanh\left(B_s\left[\frac{a}{a_s} - 1\right]\right) & \text{if } a > a_s \end{cases} \tag{3.2}$$

where m_ν is today's individual neutrino rest mass, a is the scale factor, a_s is the scale factor at the apparent phase transition time when the neutrino gains its mass, and B_s is a parameter that determines the speed of the mass generation. We can fix the parameter B_s to 10^{10}, since the timescale of neutrino mass generation is of order m_ν^{-1}, which corresponds to approximately femto/picoseconds.

We note that here we assume a degenerate neutrino mass spectrum, i.e. $m_{\nu_i} \equiv m_\nu$. Degenerate neutrino masses are still allowed in the mass model of Ref. [3] because the standard cosmological mass limits are evaded, the bounds from β-decay experiments are relatively weak, and constraints from neutrinoless double-β experiments only apply to Majorana neutrinos. Moreover, current cosmological data constrains only the sum of neutrino masses and cannot resolve yet whether the neutrino mass ordering is normal or inverted [215, 216, 217, 218, 219, 220, 221]. Therefore, we assume degenerate masses that are generated at almost equal times for each mass eigenstate, i.e. within timescales much smaller than the Hubble timescale. Since the relic neutrinos rapidly decay into the lightest neutrino mass eigenstate, ν_l, after the transition, the cosmologically constrained sum of the relic neutrino masses reduces to $\sum m_\nu = 3 \times m_l$.

To model the time evolution of the false vacuum energy density, we can use a similar parametrization as for the neutrino mass above

$$\rho_{V_0}(a) = \begin{cases} V_0\left[1 - \tanh\left(B_s\left(1 - \frac{a}{a_s}\right)\right)\right] & \text{if } a > a_s \\ V_0 & \text{if } a \leq a_s \end{cases} \tag{3.3}$$

where $V_0 = (\sqrt{p_\nu^2 + m_\nu^2} - p_\nu)\, n_\nu$ is the difference in energy density of massive and massless neutrinos at $a = a_s$, and n_ν is the neutrino number density at that time. We assume here that the equation of state parameter of the false vacuum energy is constant, $w = -1$, and that only the amplitude of the energy density rapidly changes within timescales of femto/picoseconds, as discussed above. Therefore, the false vacuum energy effectively behaves as an additional vacuum energy contribution on top of dark energy, until the vacuum decays into the true minimum. Crucially, this scenario does not enhance the dark energy perturbations as in other mass-varying neutrino models [296], and

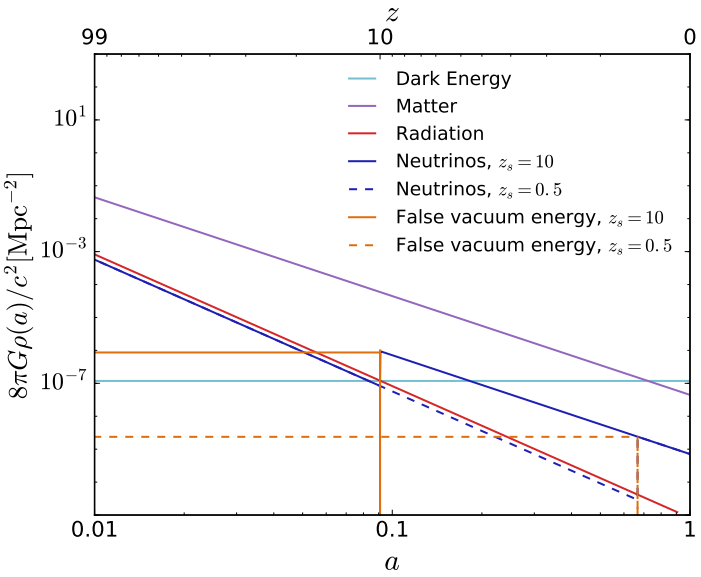

Figure 3.1: Energy densities for different components present in our analysis: neutrinos with a time-varying mass generated at $z_s = 10$ ($z_s = 0.5$) and corresponding to $\sum m_\nu = 0.2$ eV today with solid (dashed) curves, false vacuum energy, standard dark energy, matter (baryons and cold dark matter), and radiation.

hence is not affected by model instabilities. We notice here that we assume a standard cosmological constant for dark energy in our study and do not attempt to link it to the false vacuum energy. We will briefly comment on this in Sec. 3.5.

The energy densities of massive neutrinos and the false vacuum energy component are shown in Fig. 3.1 for $\sum m_\nu = 0.2$ eV and a late phase transition at a redshift of $z_s = 10$ (or equivalently $a_s \sim 0.091$, solid lines). In this case, the false vacuum energy dominates over the dark energy density until the phase transition and is then transferred into the energy required for the generation of the neutrino masses. We also show with dashed lines the case of a very late phase transition happening at $z_s = 0.5$, we note that in this case the false vacuum energy is more subtle and always subdominant compared to dark energy.

3.2.2 Cosmological Observables

The impact of this model on cosmological observables is shown in Figs. 3.2, 3.3: features in the CMB temperature (C_l^{TT}) and polarization (C_l^{EE}) power spectra, the CMB lensing convergence ($C_l^{\phi\phi}$) and matter power spectra ($P(k)$) are shown for $\sum m_\nu = 0.2$ eV and three different values of

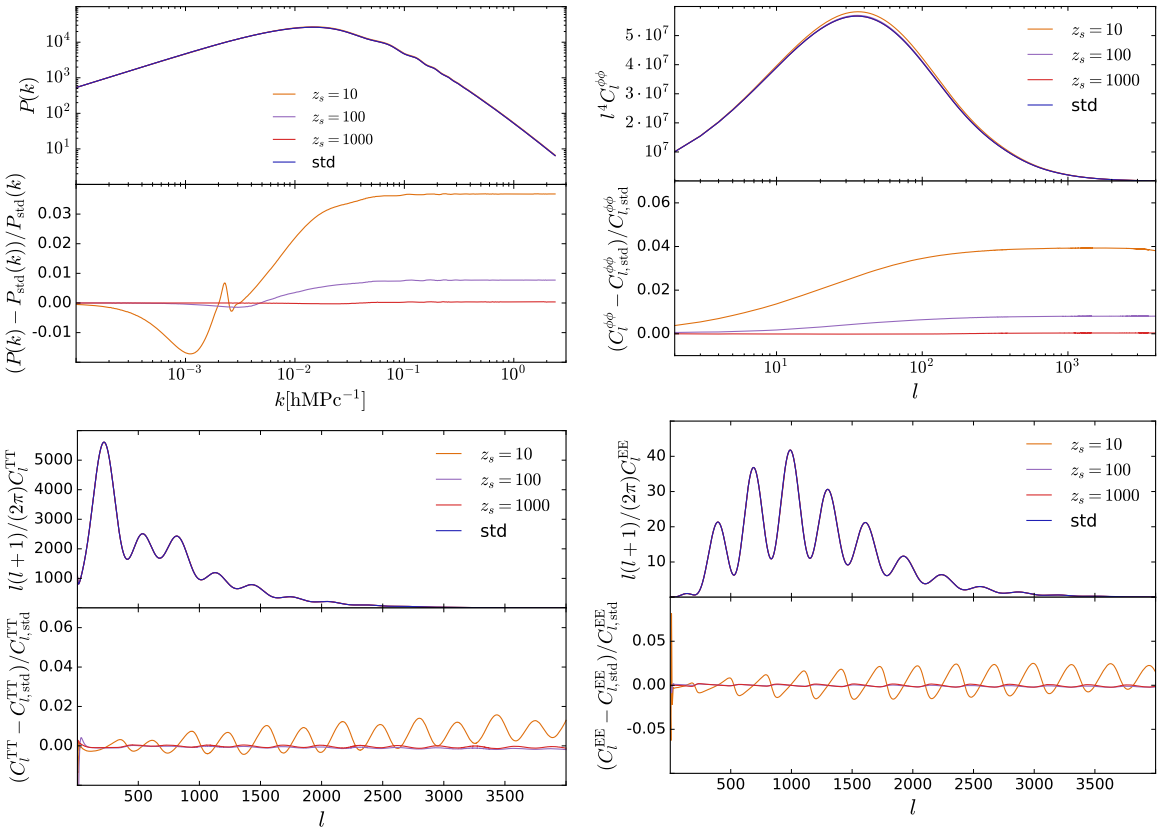

Figure 3.2: Effect on cosmological observables from the time-varying neutrino mass model considered here, shown for $\sum m_\nu = 0.2$ eV and for three different values of the phase transition redshift ($z_s = 1000$ or $a_s = 0.001$, $z_s = 100$ or $a_s = 0.01$ and $z_s = 10$ or a_s=0.09), compared to the standard massive neutrinos case with $\sum m_\nu = 0.2$ eV used as a reference. Different panels report the matter power spectrum (top left), the CMB lensing convergence power spectrum (top right), and CMB temperature and polarization anisotropy power spectra (bottom left and right, respectively). The effects of this model are subtle, with percent level features, but within the reach of future experiments.

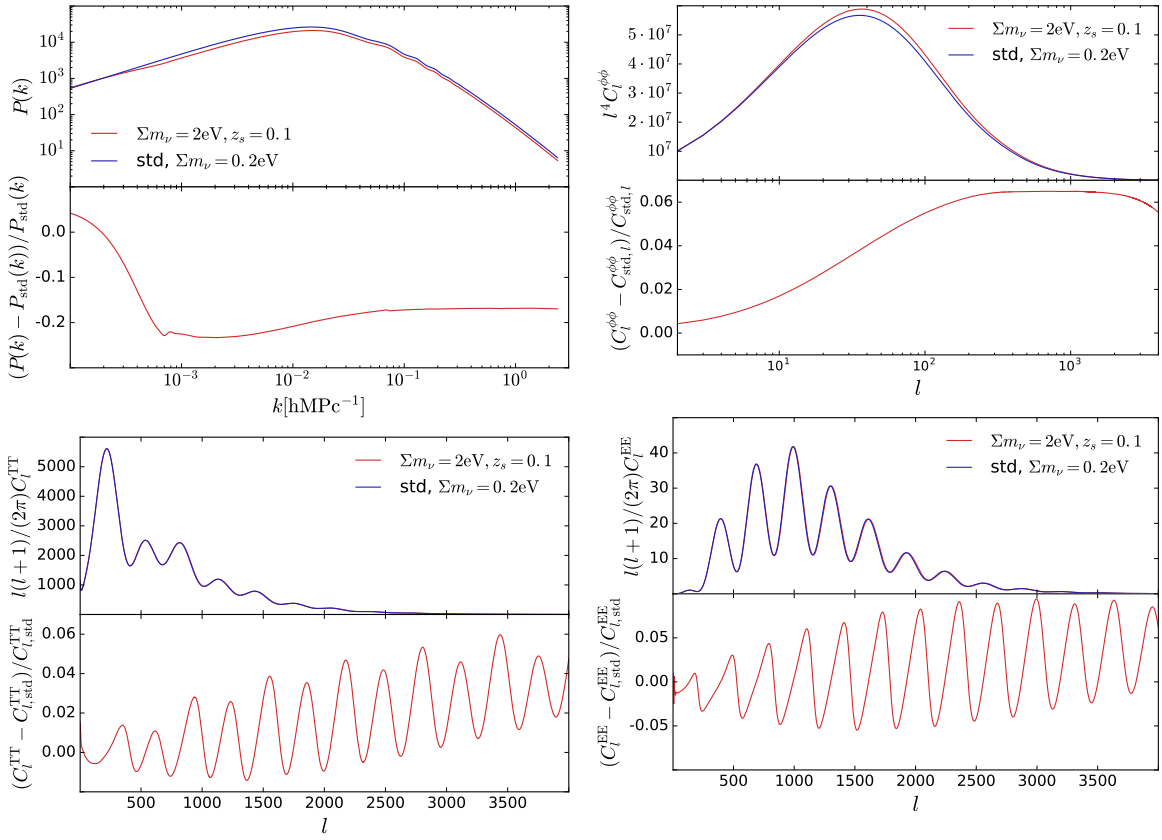

Figure 3.3: Same as Fig. 3.2 in the case of a late phase transition ($z_s = 0.1$ or $a_s = 0.91$) and a large neutrino mass with $\sum m_\nu = 2$ eV, compared to the standard massive neutrinos case with $\sum m_\nu = 0.2$ eV.

z_s (Fig. 3.2), and for a late phase transition and high neutrino masses (Fig. 3.3), with the standard massive neutrino case as the reference model in both cases.

When the phase transition happens late (small values of z_s and large values of a_s), the model becomes more similar to massless neutrinos. On the contrary, for large values of z_s, the model is very similar to the standard constant mass neutrino case. Therefore, for $z_s = 1000$ ($a_s = 0.001$), the effect of the time-varying neutrino mass for all four power spectra is only marginal compared to the reference case.

We start our explanation with the matter power spectrum on the top left corner of Fig. 3.2. For standard massive neutrinos, the matter power spectrum is suppressed on small scales, in the case of $\sum m_\nu = 0.2$ eV this corresponds to $k \geq k_{\rm nr} = 0.0027$. This suppression is more or less pronounced in our case depending on the time of the phase transition. As mentioned above, for a small value of z_s the neutrinos are massless for most of their evolution and as a result the matter power spectrum is less suppressed and more similar to the power spectrum of massless neutrinos. As described in Ref. [302], the turn-over-scale of the matter power spectrum is also affected, depending on the exact time at which the neutrinos gain their mass. As the time of the phase transition moves towards smaller redshifts, the enhancement of the matter power spectrum for large values of k translates into an overall enhancement of the lensing convergence power spectrum (top right panel of Fig. 3.2). The CMB temperature and polarization anisotropy power spectra (bottom left and right panel, respectively) are affected at all multipoles, encoding the impact of extra vacuum energy and neutrino free-streaming in the case of a late phase transition.

Anticipating larger values of $\sum m_\nu$ allowed by a supercooled phase transition, in Fig. 3.3 we compare cosmological observables in the case of mass-varying neutrinos with $\sum m_\nu = 2$ eV with respect to the standard massive neutrino case with $\sum m_\nu = 0.2$ eV. We notice that even in the case of these very different mass scenarios the impact on the observables is subtle. For this comparison, we have not renormalized the values of the different matter density components (i.e. we kept the amount of cold dark matter and baryons fixed) to reproduce the process where neutrinos exchange some energy only with the false vacuum energy component (i.e. moving along the dark energy degeneracy line seen in Sec. 3.4.1). A higher impact is now seen on $P(k)$, showing a suppression on all scales out to the horizon at the phase transition scale, caused by the substantial amount of false

vacuum energy before the transition. The features in the CMB spectra are also enhanced due to the different energy budget of the Universe.

We note that the differences between the models are only of the order of a few percent. We anticipate that this might be hard to uncover with current data but is within the reach of future CMB and galaxy surveys. The CMB SO [185] and Stage-4 projects [184] will have the sensitivity to distinguish the small-scale CMB features, while Euclid [103] and LSST [101] will provide better measurements of $P(k)$.

3.3 Analysis methodology

To constrain the parameters of our model, we use modified versions of the publicly available Boltzmann solver CAMB [319] and the Monte-Carlo Markov chain package CosmoMC [36]. We compare this model where neutrino masses are generated through a supercooled phase transition, named hereafter `Supercool-`ν, to the standard ΛCDM case with fixed neutrino masses $\sum m_\nu = 0.06$ eV, and to the case in which the total mass is varied but constant in time (i.e. the standard massive neutrino case), ΛCDM+$\sum m_\nu$.

When reporting ΛCDM results, we vary the standard six cosmological parameters (the baryon and cold dark matter densities, Ω_b and Ω_c, the scalar spectral index n_s, the amplitude of primordial fluctuations, A_s, the Hubble constant, H_0, and the optical depth to reionization, τ) and fix the total sum of neutrino masses to $\sum m_\nu = 0.06$ eV, corresponding approximately to the lower limit obtained from neutrino oscillation experiments [144]. In the extended analyses for i) ΛCDM+$\sum m_\nu$ we additionally vary $\sum m_\nu$ as a constant parameter; and for ii) the `Supercool-`ν model we additionally consider the full time evolution of the neutrino mass and vary the scale factor of the phase transition, a_s. The false vacuum energy amplitude is set by the value of $\sum m_\nu$ and a_s via Eq. (3.3).

Unless otherwise stated (for example in Section 3.4.2), we assume standard flat priors on the ΛCDM basic parameters (following Ref. [157]). We vary $\sum m_\nu$ between 0.06 and 6.6 eV to incorporate current limits from laboratory searches (i.e. above the minimum threshold set by oscillation experiments and converting $m_{\nu_e} < 2.2$ eV into $\sum m_\nu < 6.6$ eV). We will extend this range in Sec. 3.4.2 to ease the comparison with other published results. The logarithm of the time of the phase transition, $\log(a_s)$, is varied between -5 and 0. This allows the exploration of neutrino mass generation across a large range of cosmic time. We fix the speed of the transition with $B_s = 10^{10}$, corresponding to

Parameters	ΛCDM+$\sum m_\nu$	`Supercool-`ν
$\sum m_\nu$[eV]	≤ 0.20	≤ 4.8 (≤ 1.6)
Ω_Λ	0.69 ± 0.01	$0.66^{+0.02}_{-0.04}$
$\log(a_s)$	—	≥ -3.6 (≥ -2.8)

Table 3.1: Marginalized constraints on the sum of neutrino masses and dark energy content today, and on the scale factor of the neutrino mass generation using *Planck* CMB temperature, polarization and lensing, BAO and SN data. Errors are given at 68% confidence, and upper/lower limits are reported at 95% confidence (and also at 68% confidence in parentheses for very non-Gaussian bounds).

an almost instantaneous phase transition. This parameter was very unconstrained in the analysis of Ref. [302], so we do not expect its exact value to affect our results.

We separate our analysis in two parts: in Sec. 3.4.1 we report state-of-the-art constraints for the parameters of the time-varying neutrino mass model considered here; in Sec. 3.4.2 we study the constraints in the Ω_m-σ_8 plane from different cosmological probes.

3.4 Results

3.4.1 Cosmological Mass Limits

To obtain constraints from current data, we combine *Planck* CMB temperature, polarization, and lensing spectra from the 2015 release [320, 321][3] with BAO distance ratio from BOSS DR12 (CMASS and LOWZ) [322], SDSS MGS [262] and 6DF [263], and Type Ia supernovae redshift-magnitude diagram from the Joint Light-curve analysis (JLA) compilation [323]. This is the baseline data combination of the *Planck* analyses that we follow here. The results are shown in Fig. 3.4 and reported in Table 3.1.

We find that much larger values for $\sum m_\nu$ are allowed in the case of a supercooled phase transition compared to the case of standard constant-mass neutrinos and that the data prefer a large value of the phase transition scale factor, i.e. a late relic neutrino mass generation (peaking at today's scale

[3]The final 2018 *Planck* release occurred during the final stages of this work. We, however, note that the 2018 likelihood software needed to analyse the data is not yet public, and we anticipate that our results will not change with the new data products.

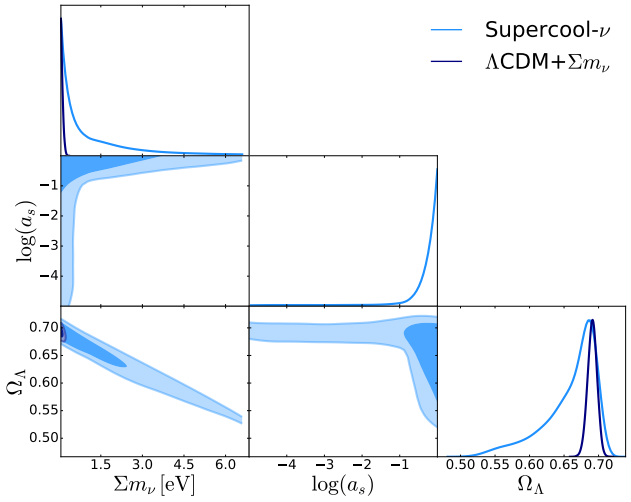

Figure 3.4: Constraints for $\sum m_\nu$, a_s and Ω_Λ (with contours at 68% and 95% confidence) in the case of standard massive neutrino (ΛCDM+$\sum m_\nu$, dark blue) or for relic neutrinos with mass generated in a supercooled phase transition (`Supercool`-ν, light blue). The results are obtained using *Planck* TTTEEE+lensing, BAO and SN.

factor)

$$\left.\begin{array}{ll} \sum m_\nu & \leq 4.8 \text{ eV} \\ \log(\mathrm{a_s}) & \geq -3.6 \end{array}\right\} \text{ at } 95\% \text{ confidence}\,. \tag{3.4}$$

This is a significantly weakened limit for the neutrino mass, to be compared to $\sum m_\nu \leq 0.2$ eV for standard massive neutrinos with the same data combination – we note though that the 68% limit, $\sum m_\nu \leq 1.6$ eV, is much tighter due to the non-Gaussian distribution recovered in this fit. This is expected in this model and the reason for this is illustrated in Fig. 3.1: the inclusion of the false vacuum energy generates a condition where the amplitude of the dark energy density and the combination of the neutrino and false vacuum energy components are very similar over most of the cosmic history. Especially in the case when the transition happens very late ($z_s \leq 10$) and the sum of neutrino masses is large, the neutrino energy density will be of the same order of magnitude as the dark energy density until almost today. Therefore, a strong anti-correlation between $\sum m_\nu$ and Ω_Λ arises (at the level of 98%). This can also be seen in Fig. 3.4. A similar degeneracy has also been observed for early dark energy (EDE) models [1, 237], however in these models the degeneracy is caused by the time-varying evolution of the dark energy component. We also note that the correction that we added to keep energy conserved in the model, i.e. the inclusion of the false vacuum energy, is the main reason why our constraints are broader than those reported in Ref. [302]. The preference

for a late transition captures the trend that has emerged fitting for neutrino masses with early- and late-time cosmological probes: we confirm that the data require lighter neutrinos at CMB decoupling and more significant masses can be generated only in the late Universe.

The goodness of the fit obtained with this time-varying neutrino mass model is only marginally better than that obtained in the standard massive neutrino case, with a difference in best-fit likelihoods of only 1.57 ($\Delta\chi^2 = 3.14$). Therefore, the `Supercool-`ν model is slightly but not significantly favoured, yielding a p-value of 0.08 with one additional degree of freedom for the `Supercool-`ν model compared to ΛCDM+$\sum m_\nu$.

3.4.2 The Ω_m-σ_8 plane

We now compare cosmological constraints in the Ω_m-σ_8 plane. We use *Planck* CMB temperature and polarization data, *Planck* lensing and *Planck* SZ cluster counts data [276], and galaxy weak lensing data from KiDS [271][4]. We take each dataset singularly, except for the SZ case where, following the *Planck* analysis, we further add BBN constraints on $\Omega_b h^2$ to break parameter degeneracies. This choice is made to explore the impact of time-varying neutrino masses on the existing tensions, and whether the inclusion of massive neutrinos generated late in the Universe might ease the discrepancies. *Planck* CMB lensing is also included in our analysis as a dataset on its own, not because of tension with other data but rather to look at the effect of this model at intermediate-to-low redshifts.

To easily compare with the KiDS weak lensing, *Planck* lensing, and *Planck* SZ cluster results, we use now the same flat priors for the unconstrained parameters assumed by the individual experiments. For KiDS we use the priors assumed in Ref. [272]; for *Planck* CMB lensing we use the priors for n_s and Ω_b as stated in Ref. [321]; and for the *Planck* SZ cluster counts we use the priors for n_s and Ω_b reported in Ref. [276]. For these latter data we further assume a Gaussian prior on the bias parameter picking the CCCP baseline case [324] used as reference cluster mass calibration in the *Planck* analyses. For the galaxy weak lensing, *Planck* lensing and SZ cases τ is not varying. We

[4]We work with KiDS weak lensing data because this is the most discrepant data and because it was the only publicly available likelihood at the time this work started.

note that the neutrino mass parameter is now varied between 0.06 and 10 eV consistently with other published analyses and therefore allowing for a simpler comparison.

The results for the three models compared here are shown in Fig. 3.5 (transition from top to bottom) and discussed below.

ΛCDM: The top panel of Fig. 3.5 shows the constraints for Ω_m and σ_8 in the case of $\sum m_\nu$ fixed to 0.06 eV for the four different datasets considered here. These results reproduce the published KiDS [272], *Planck* CMB and CMB lensing [157, 321], and *Planck* SZ+BBN [276][5] results, and are shown here only for reference[6].

ΛCDM+$\sum m_\nu$: When varying $\sum m_\nu$ as a parameter, correlations in the matter components generate a broadening of the constraints. In particular, the middle panel of Fig. 3.5 shows the impact of the standard massive-neutrinos-driven suppression of density fluctuations below their free-streaming length. Larger allowed values for the neutrino mass enlarge the *Planck* CMB primary and lensing constraints towards lower values of σ_8 and higher values of Ω_m. Similar effects are seen for the KiDS and SZ analysis. This has been extensively demonstrated in the literature (e.g. [272, 292, 293, 107]).

`Supercool-`ν: The bottom panel in Fig. 3.5 shows our results for the supercooled phase transition. The largest impact compared to the other two cases is seen on the *Planck* CMB contours: they now extend to much lower values of σ_8 and higher values of Ω_m. CMB lensing contours are slightly affected, while the KiDS and SZ cluster results are almost unchanged. This is explained by the data preferring a late-time mass generation, so that the `Supercool-`ν case only differs significantly from the ΛCDM or ΛCDM+$\sum m_\nu$ cases at CMB and CMB lensing epochs. The contours however broaden along the degeneracy line, bringing data in slightly better agreement but with no substantial model

[5] We have cross-checked our *Planck* SZ+BBN results by additionally including BAO and comparing with the *Planck* SZ+BBN+BAO constraints in Ref. [276].

[6] We note that these contours will shift if using different τ values compared to the *Planck* 2015 one used here. However, we do not expect this to change significantly any conclusion drawn in this chapter. We decided to keep the 2015 value to compare more easily with other published results.

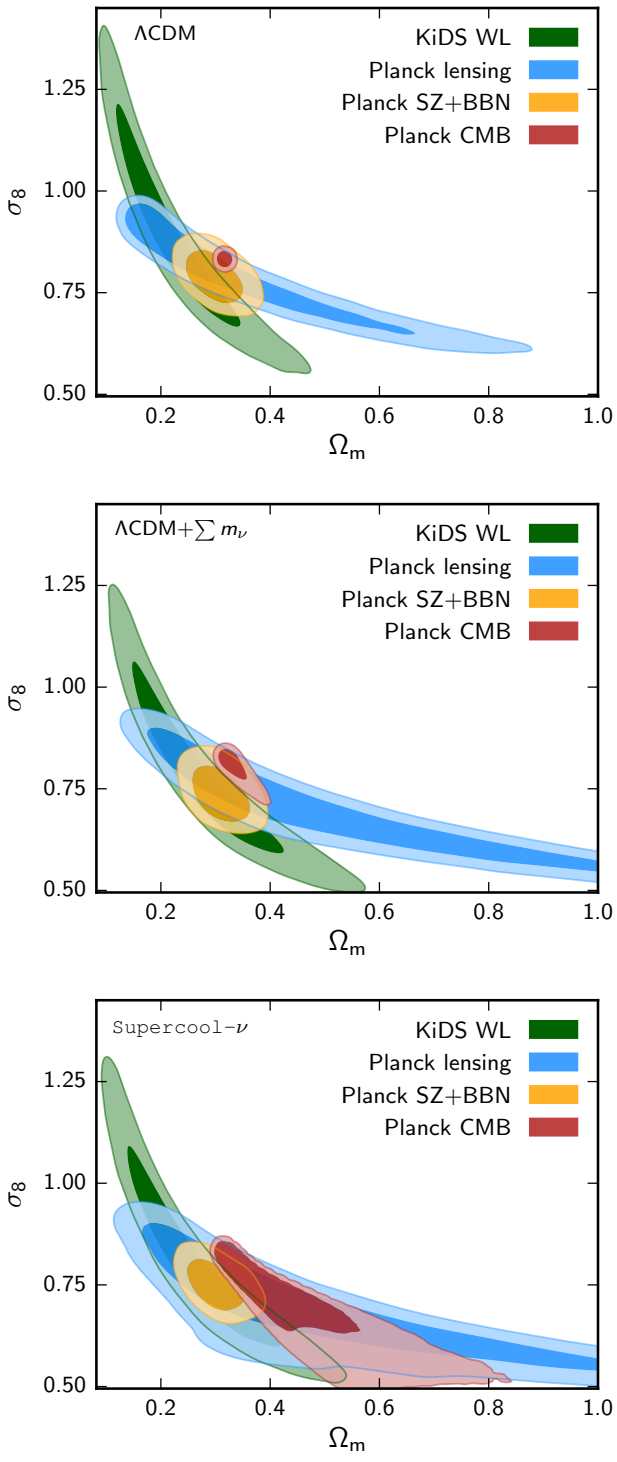

Figure 3.5: Constraints on σ_8 and Ω_m inferred from *Planck* CMB, *Planck* lensing, *Planck* SZ cluster counts and KiDS weak lensing. *Top:* for ΛCDM with fixed neutrino mass $\sum m_\nu = 0.06$ eV. *Middle:* ΛCDM with neutrino mass $\sum m_\nu$ as a constant free parameter. *Bottom:* late neutrino mass generation with $\sum m_\nu$ and a_s as a free parameter.

preference (when considering the broadening due to the extra parameters present in the model). We also note that the derived value of the Hubble constant in this model is not significantly different from the one obtained in the ΛCDM+$\sum m_\nu$ case.

3.5 Summary and concluding remarks

In this chapter, we have presented state-of-the-art constraints from cosmology on a time-varying neutrino mass model motivated by Ref. [3]. We assume that relic neutrino masses are generated from a form of false vacuum energy in a supercooled neutrino phase transition and neglect neutrino annihilation in the late Universe. This is a modified version of the minimal model in Ref. [3] which allows for either a supercooled or a non-supercooled transition but, predicting almost complete neutrino annihilation, implies that all cosmological mass constraints would be entirely evaded. We find that current data prefer a phase transition very late in time (peaking at today) and that the constraint on the total mass of neutrinos is significantly weakened compared to the standard massive neutrinos case, with $\sum m_\nu \leq 4.8$ eV at 95% confidence (≤ 1.6 eV at 68% confidence). This larger bound is mostly due to large correlations with the dark energy component, affected by the presence of the false vacuum energy term. To summarize, we find that the standard constant-mass neutrino case with low masses and the `Supercool-`ν model studied here with high masses are both successful with current data.

The proposed PTOLEMY experiment [303] aims to detect relic neutrinos, and would have an energy resolution of ~ 0.15 eV per neutrino [325]. As also discussed in Ref. [4], the results found here would allow for a detection of relic neutrinos if the neutrino background is strongly asymmetric. The KATRIN β-decay experiment [193] also aims to discover the neutrino mass scale. Since the model considered here allows for larger neutrino masses, a detection of an unexpectedly large absolute neutrino mass scale at KATRIN could provide a strong hint towards this model, at least if the standard cosmological ΛCDM model is valid in other respects. As explained in Ref. [4], the weakened neutrino mass bounds gain even further importance in the hypothetical presence of sterile neutrinos motivated by experimental short-baseline anomalies [326], since the model [3, 4] evades the usual conflicts between light sterile neutrinos and cosmological neutrino mass bounds.

We further looked at the possibility of solving current early- and late-time tensions in the measurements of matter fluctuations with this model. Larger values allowed for the neutrino mass

also weaken constraints on the matter density and clustering. These, however, broaden along the degeneracy direction already present in the standard constant mass case and do not provide a convincing explanation to the tensions.

We made several simplifications to the original neutrino mass model in Ref. [3].

- The model predicts that the relic neutrinos rapidly decay into the lightest neutrino mass eigenstate after the late cosmic transition. Therefore, any cosmological neutrino mass bound derived with this model only applies to the smallest neutrino mass and not to the sum of all masses. Considering that, at present, we do not have further information on the neutrino mass eigenstates ordering and relative weight, we argue that making this simplification is not impacting our conclusion. Moreover, the decay becomes less relevant for larger masses, since then the neutrino mass eigenstates have similar masses and are cosmologically not distinguishable.

- The model in Ref. [3] also predicts that the relic neutrinos become strongly coupled after the phase transition and substantially annihilate into almost massless Goldstone bosons, i.e. dark radiation. In the case of almost complete annihilation, this would not be tracked by neutrino masses from cosmological data. We relax this prediction by Ref. [3] for two reasons: i) first, an evidence of time-varying neutrino masses from cosmology could still inform model building in general. Our study confirms the general trend that low-redshift data prefer heavier neutrinos and showed that large masses can be generated only in the late Universe. We note here that the latter result is expected to also hold true in case of complete neutrino annihilation, due to the larger amount of false vacuum energy required for an earlier phase transition. ii) An almost complete annihilation could in fact be evaded in the presence of large neutrino asymmetries. In case of a neutrino mass detection, the complete neutrino annihilation would be ruled out. We showed that non-complete annihilation is still a viable possibility considering the current bounds on these asymmetries.

- Another aspect we neglected in our study is the formation and evolution of topological defects, as well as out-of-equilibrium effects like bubble nucleation and collision. Related cosmological studies of the resulting inhomogeneities in supercooled late-time phase transitions have been

presented in Ref. [327], which finds that kinetic-SZ data constrain bubble nucleation from false vacuum decay to happen very recently. We defer the studies of such inhomogeneities as well as the cosmological effects of neutrino self-interactions, (partial) annihilation, and dark radiation to future investigations.

- Finally, we note that for simplicity we fixed the false vacuum energy density V_0 to the energy density required to generate the relic neutrino masses. However, a substantial amount of the false vacuum energy could also convert into dark radiation. In general, V_0 is a free parameter of the model [3], which opens up the possibility that V_0 could be identified with the observed dark energy density.[7] In such a "decaying dark energy" scenario, our Universe recently became dark-radiation dominated, will soon enter a matter-dominated era, and will continue to expand at a decelerating rate (see e.g. Refs. [328, 329, 330, 331, 327, 332, 333, 334] for similar considerations). The redshift of dark energy decay is constrained by Type IA supernovae data to $z_s \lesssim 0.1$ at the 2σ level [331]. The dark radiation bosons would not yield directly observable cosmological effects, despite their huge abundance, due to strongly suppressed interactions with Standard Model particles. However, they might yield observable signatures in non-cosmological contexts (see Refs. [3, 304]).

[7] Ref. [3] already noticed a potential connection between the neutrino vacuum condensate and dark energy, due to the surprising numerical coincidence of the dark energy and neutrino mass scales, and because the neutrino condensate is inherently connected to a new low-energy gravitational scale, Λ_G. However, the model does not solve the cosmological constant problem since it cannot explain why other Standard Model vacuum contributions, such as the Higgs condensate, do not contribute to the cosmological constant.

Chapter 4

The impact of relativistic effects in Large Scale Structure

In the next decade, we expect to map out the large scale structure of the Universe with exquisite precision. In doing so it will be possible, for the first time, to access information on the largest possible scales – the scale of the cosmological horizon. It has been shown that, on those scales, a number of general relativistic effects come into play [335, 74, 336, 73]. Such effects might, conceivably, lead to additional and complementary information to that obtained on the usual scales probed by current surveys ($\lesssim 100\,h^{-1}$ Mpc).

General-relativistic effects are more significant on large scales; unfortunately there are fewer modes to sample and cosmic variance severely limits our ability to detect these effects in the standard way. Indeed, it has been shown that from auto-correlations alone (i.e. from the power spectra of individual tracers) it is impossible to detect these effects with any statistical significance [337], and the only way to measure them is via cross-correlations of data sets, through what has been dubbed the multi-tracer technique [338]. It has been shown that a judicious choice of future surveys can be combined to obtain a moderate to high significance detection of general relativistic effects [339, 340].

Common sense would dictate that the various, novel, effects that have been identified need to be taken into account if we are to constrain cosmological parameters from future surveys. Indeed, it has been shown that some of these effects can play a significant role and bias the outcomes of cosmological parameter estimation. We highlight two cases: constraints on primordial non-Gaussianity and the impact of lensing magnification on galaxy number counts.

If primordial fluctuations were non-Gaussian, it has been shown that one should expect corrections in the small k (large wavelength) part of the galaxy power-spectrum through scale-dependent biasing

[341, 342]. This effect, in which the bias parameter gets a correction $\Delta b \propto 1/k^2$, can be confused with some of the general relativistic effects [343]. Thus a correct accounting of both scale dependent biasing and general relativistic effects must be adopted in any analysis of long wavelength modes.

Alternatively, it has been well established that lensing will affect measurements of the galaxy distribution through, for example, magnification bias [344]. Lensing may have a significant effect on all scales and it has been shown that if it is not correctly included, it may lead to significant biases in estimates of cosmological parameters such as the neutrino mass scale [345] or the dark energy equation of state [346].

In this chapter we will systematically explore the role that general-relativistic effects (and large scale modes) play on cosmological parameter constraints. Our focus will be on the importance of lensing correction (following up on the work of [346, 345]) and on the combined general relativistic corrections to galaxy number counts. We will use a Fisher matrix analysis to quantify the importance of these effects on the forecast errors and on the potential measurement bias of cosmological parameters from a selection of Stage IV experiments. We will be comprehensive in our analysis of cosmological parameters in that we will include the standard set of ΛCDM parameters but also encompass a time-varying equation of state for dark energy, the mass of neutrinos, primordial non-Gaussianity and scalar-tensor extensions to the theory of gravity.

We structure this chapter as follows. In Section 4.1 we briefly recap the effects that we will be studying and discuss the methodology that we will use. In Section 4.2 we explain the various parts that go into the Fisher matrix formalism for forecasting and how it can be used to quantify potential biases in the analysis. We then, in Section 4.3, systematically work through the different combination of data sets and cosmological parameters to build up a comprehensive analysis of the role these effects will play in future surveys. In Section 4.4 we discuss the results of our analysis.

4.1 Observables and Large Scale Effects

The goal of modern cosmology is to map out the large-scale structure of the Universe. To do so, observers try to quantify the statistical properties of the distribution of matter by either studying the spatial distribution of bright objects (such as galaxies) or diffuse gas, or by measuring the effect of gravitational potentials on the propagation of light emitted by distant sources. Key to such observations is to accurately characterize the redshifts and directions of photons that propagate from

cosmological distances to observing instruments. From these properties, one can infer the density perturbations, observable volume distortions and perturbed photon paths.

A key quantity is the fluctuation in the number density of galaxies at a particular solid angle and at a particular redshift. The corresponding observable, $\Delta_N(z, \hat{\mathbf{n}})$, consists of a number of terms which can be schematically written as [73, 74]

$$\Delta_N \equiv \Delta^D + \Delta^{RSD} + \Delta^L + \Delta^{GR} \tag{4.1}$$

where "D" stands for density perturbations, "RSD" stands for redshift space distortions, "L" stands for lensing magnification and "GR" stands for general-relativistic corrections. The first three terms are dominant and play a role on all scales. The general-relativistic corrections include large-scale velocity terms and terms involving the gravitational potentials and their derivatives (akin to the integrated Sachs-Wolfe [347] effect and the Shapiro time delay [348], found in other settings). The exact expressions for all these terms can be found in Appendix A.

Redshift space distortions, or the "Kaiser effect" (see [349] and also Sec. 1.2.4) are currently the method *par excellence* for measuring the growth rate of structure, $f = d\ln\delta_M/d\ln a$ (where δ_M is the matter density contrast and a is the scale factor) [350]. These distortions arise from the peculiar velocity sourced by the local gravitational potential which induce shifts in the relationship between the distance and redshift of any particular galaxy. The interplay between the RSD term and the density contrast involves the clustering bias, b, which relates the number density with fluctuations in the comoving-gauge matter perturbations. As such, measuring the growth rate will involve assumptions about the tracer being considered and can, potentially, be amenable to multi-tracer techniques [338].

We will pay particular attention to the magnification term, the most significant effect after RSDs and already well measured by multiple analyses [351, 352, 353, 354, 355, 356]. This magnification bias depends on the slope of the physical number density of sources, $\bar{\mathcal{N}}(\eta, L > L_*)$, as a function of conformal time η and intrinsic luminosity L_*, as:

$$s \equiv \frac{5}{2}\frac{\partial \ln \bar{\mathcal{N}}}{\partial \ln L_*}. \tag{4.2}$$

This correction arises because of the presence of matter overdensities along the photon path, on the one hand stretching the observed separation between galaxies (and therefore supressing the observed

number density) and on the other hand boosting the observability of faint galaxies which otherwise would have fallen below the detection threshold [357]. As we shall see (and as was pointed out in [346, 345]), this term can play a significant role in biasing the estimates of cosmological parameters.

The GR effects are subdominant and only really emerge on the largest scales (as can be seen in Appendix A). There are a few main things to note which will become important when discussing the methodology and results. First of all, some of the GR terms come in with a similar scale dependence as the scale dependent bias arising from primordial non-Gaussianity. Second, some of the terms depend on the slope of the background number density of sources as a function of time, the *evolution bias*:

$$f_{\rm evo} \equiv \frac{\partial \ln(a^3 \bar{\mathcal{N}})}{\partial \ln a} \tag{4.3}$$

Given this, it has been shown [339, 340] that GR effects are amenable to the use of multitracer techniques for mitigating cosmic variance and that, with the appropriate choice of future data sets, it may be possible to detect them at the $\sim 10\sigma$ level.

4.2 Methodology

4.2.1 The space of parameters

In this work, we will consider a number of different cosmological models in order to make a broad and general statement about the impact of the lensing and general-relativistic effects on the estimation of cosmological parameters.

As a first model we choose the standard extension to ΛCDM including non-zero neutrino masses $\sum m_\nu$ and a time-varying equation of state for dark energy. The latter is parametrized by w_0 and w_a [358] as $w(a) = w_0 + (1-a)w_a$. This model also includes the standard cosmological parameters (fractional density of dark matter $\Omega_{\rm cdm}h^2$ and baryons $\Omega_{\rm b}h^2$, the local normalized expansion rate h, the amplitude of primordial scalar perturbations $A_{\rm s}$, the scalar spectral index $n_{\rm s}$ and the optical depth to reionization τ). For these parameters, apart from τ, we will take the best-fit values from the *Planck* 2015 analysis [157] as our fiducial cosmology. We will also take a fiducial $\tau = 0.06$ from the latest measurement from *Planck* [359]. So far, only lower and upper limits for $\sum m_\nu$ are known. Whereas the currently best upper limits on $\sum m_\nu$ come from cosmology [360, 157, 218], the mass differences between the neutrino mass eigenstates have been measured in neutrino oscillation

experiments. Here we will conservatively use $\sum m_\nu = 0.06$ eV as a fiducial value for the total neutrino mass, corresponding approximately to the current lower bound on the total neutrino mass sum from summing the mass differences [361]. Finally, our fiducial dark energy equation of state will correspond to a cosmological constant with $w_0 = -1$ and $w_a = 0$.

Our second model will extend the previous one with the dimensionless parameter $f_{\rm NL}$ that describes the amount of non-Gaussianity in the primordial density field produced in many inflation scenarios. Specifically we will focus on the case of local non-Gaussianity [362], in which $f_{\rm NL}$ is defined through

$$\Phi(\mathbf{x}) = \Phi_G(\mathbf{x}) + f_{\rm NL}(\Phi_G^2(\mathbf{x}) - \langle\Phi_G^2\rangle), \tag{4.4}$$

where Φ is the primordial gravitational potential and Φ_G is a Gaussian random field. Thus, the primordial gravitational potential can be described as the sum of a linear term and a non-linear one. The current constraint on the local value of $f_{\rm NL}$ from the *Planck* satellite is 2.5 ± 5.7 [363]. Although measurements of the cosmic microwave background anisotropies will be most helpful in determining the value of $f_{\rm NL}$ [364], its effects on large-scale structure [341, 342] are one of the most promising ways to improve current constraints. More specifically, primordial non-Gaussianity induces a correction in the Gaussian bias b_X^G of each tracer X [341, 342]

$$\Delta b_X(z,k) = 3 f_{\rm NL} \frac{[b_X^G(z) - 1]\Omega_m H_0^2 \delta_{\rm c}}{(T(k)D(z)k^2)} \tag{4.5}$$

where Ω_m is the fraction of the matter density of the total energy density in the Universe, $\delta_{\rm c} \simeq 1.686$ is the critical density contrast of matter from the spherical collapse model, $D(z)$ is the linear growth factor, H_0 the value of the Hubble constant today and $T(k)$ the matter transfer function. As fiducial value for $f_{\rm NL}$ we choose $f_{\rm NL} = 0$.

In these two models General Relativity is still the underlying theory of gravity. For our third model, and in order to explore the role of relativistic effects in constraining deviations from GR, we will consider scalar-tensor theories within the Horndeski class of models [365, 366]. As proposed by [367], these models can be described through a number of general time-dependent functions α_M, α_K, α_B, α_T and M_* in addition to the standard ΛCDM parameters (we refer the reader to the reference above for further details). These functions parametrize the time variation of Newton's constant (M_* and α_M), the form of the scalar kinetic term α_K, the mixing between the scalar field and the scalar perturbations α_B and the speed of propagation of tensor modes α_T. In order to curb the freedom

allowed by this parametrization we constrained the time-dependence of the α functions to be of the form:

$$\alpha_X(z) = c_X \frac{\Omega_{\rm DE}(z)}{\Omega_{\rm DE}(z=0)}, \tag{4.6}$$

where $\Omega_{\rm DE}(z)$ is the fractional energy density of the dark energy component. Furthermore, as in [368, 369] we will only consider c_M, c_B and c_T as free parameters, since c_K and M_* cannot be constrained by current [368] or future data[1]. As fiducial values we chose $c_{\rm B} = 0.05$, $c_{\rm M} = -0.05$ and $c_{\rm T} = -0.05$, in order to stay close to ΛCDM as a fiducial cosmology while avoiding the singularity at $c_X \equiv 0$.

4.2.2 Fisher matrix forecasting formalism

We produce our forecasts using a Fisher matrix approach (see also Sec. 1.4). We follow the formalism of [337], which incorporates the joint constraining power of multiple experiments and tracers of the matter distribution[2]. Each tracer contains a set of sky maps corresponding to e.g. different redshift bins or the different Stokes polarization parameters in a CMB experiment. In total, the combination of all tracers will observe a number of $N_{\rm maps}$ maps that can be described by their harmonic coefficients $a^{a,i}_{\ell m}$, where a and i label the tracer and map number respectively. We group these harmonic coefficients into a vector $\mathbf{a}_{\ell \rm m}$ and define the power spectrum C_ℓ as the covariance of this vector:

$$\langle \mathbf{a}_{\ell m} \mathbf{a}^*_{\ell' m'} \rangle = \delta_{\ell\ell'}\delta_{mm'}\mathsf{C}_\ell \tag{4.7}$$

We assume that the $a^{a,i}_{\ell m}$ are Gaussian-distributed and that thus their likelihood is given by

$$-2\ln\mathcal{L} = \sum_\ell f_{\rm sky}\frac{2\ell+1}{2}\left[\sum_{m=-\ell}^{\ell}\frac{\mathbf{a}^\dagger_{\ell m}\mathsf{C}_\ell^{-1}\mathbf{a}_{\ell m}}{2\ell+1} + \ln(\det[2\pi\mathsf{C}_\ell])\right] \tag{4.8}$$

By expanding this likelihood around the maximum we find that the covariance of the maximum-likelihood estimate of a set of parameters θ_α can be approximated by the inverse of the Fisher matrix $\mathsf{F}_{\alpha\beta}$. This matrix can be computed as:

$$\mathsf{F}_{\alpha\beta} = \sum_{l=2}^{l_{\rm max}} f_{\rm sky}\frac{2\ell+1}{2}\,{\rm Tr}\left[(\partial_\alpha \mathsf{C}_\ell)\mathsf{C}_\ell^{-1}(\partial_\beta \mathsf{C}_\ell)\mathsf{C}_\ell^{-1}\right] \tag{4.9}$$

[1] Fortunately these parameters are not significantly degenerate with the rest, and therefore can be safely kept fixed without affecting the forecast constraints [369].

[2] The software used to produce these forecasts can be found at https://github.com/damonge/GoFish.

where $f_{\rm sky}$ is the fraction of the sky observed.

The power spectra were computed with a modified version of CLASS [370, 37, 371], and the derivatives in Eq. 4.9 were estimated via central finite differences:

$$\partial_\alpha f = \frac{f(\theta_\alpha + \delta\theta_\alpha) - f(\theta_\alpha - \delta\theta_\alpha)}{2\delta\theta_\alpha} + \mathcal{O}(\delta\theta_\alpha^3). \tag{4.10}$$

The final parameter uncertainties are computed from the inverse of F.

Besides the parameter uncertainties for a given setup, we also estimate the bias on those parameters arising from neglecting to account for a given relativistic effect in the theoretical calculation of the power spectra. In order to do so, we follow a similar method based on expanding the likelihood around the maximum. The approach is similar to that of [372, 373, 374]. As in [345], we compute an "observed" power spectrum $\mathsf{C}_\ell^{\rm obs}$, where all relevant effects are included in the calculation, and a "theoretical" power spectrum $\mathsf{C}_\ell^{\rm th}$, where a given effect (e.g. lensing magnification or the contribution of large-scale GR effects) is not incorporated. Likewise, we define $\theta_{{\rm inf},\alpha}$ as the "inferred" values of the cosmological parameters from the incorrect likelihood, and $\theta_{{\rm true},\alpha}$ as the true underlying parameters. The maximum-likelihood value for θ_α is derived by maximising the likelihood in Eq. 4.8, and therefore we obtain:

$$\begin{aligned}\langle\partial_\alpha\chi^2(\theta_{\rm true})\rangle \approx &\langle\partial_\alpha\chi^2(\theta_{\rm inf})\rangle \\ &+ \langle\partial_\alpha\partial_\beta\chi^2(\theta_{\rm inf})\rangle(\theta_{\rm true} - \theta_{\rm inf}) = 0\end{aligned} \tag{4.11}$$

Taking $v_\alpha = -\langle\partial_\alpha\chi^2(\theta_{\rm inf})\rangle$ and approximating

$$\langle\partial_\alpha\partial_\beta\chi^2(\theta_{\rm inf})\rangle \approx \mathsf{F}_{\alpha\beta}\,, \tag{4.12}$$

we obtain the bias on each cosmological parameter θ_α:

$$\Delta\theta_\alpha = (\mathsf{F}^{-1}\cdot\mathbf{v})_\alpha, \tag{4.13}$$

where the entries of $\mathbf{v}$ are given by

$$v_\alpha = \sum_{\ell=2}^{\ell_{\rm max}} f_{\rm sky}\frac{2\ell+1}{2}{\rm Tr}\left[(\partial_\alpha\mathsf{C}_\ell)\mathsf{C}_\ell^{-1}\Delta\mathsf{C}_\ell\mathsf{C}_\ell^{-1}\right]\,, \tag{4.14}$$

and $\Delta \mathsf{C}_\ell = \mathsf{C}_\ell^{\rm obs} - \mathsf{C}_\ell^{\rm th}$. We show here why the approximation 4.12 is valid at the linear level. Differentiating equation 4.8, we find

$$\partial_\alpha \chi^2 = \sum_\ell f_{\rm sky} \frac{2\ell+1}{2} \left[{\rm Tr}(\mathsf{C}_\ell^{-1} \partial_\alpha \mathsf{C}_\ell) - \sum_m \frac{\mathbf{a}_{\ell m}^\dagger \, \mathsf{C}_\ell^{-1} \partial_\alpha \mathsf{C}_\ell \mathsf{C}_l^{-1} \mathbf{a}_{\ell m}}{2\ell+1} \right] \tag{4.15}$$

$$\begin{aligned} \partial_\alpha \partial_\beta \chi^2 = \sum_\ell f_{\rm sky} \frac{2\ell+1}{2} \Bigg[& {\rm Tr}(\mathsf{C}_\ell^{-1} \partial_\alpha \partial_\beta \mathsf{C}_\ell) - {\rm Tr}(\partial_\alpha \mathsf{C}_\ell \mathsf{C}_\ell^{-1} \partial_\beta \mathsf{C}_\ell \mathsf{C}_\ell^{-1}) - \sum_m \frac{\mathbf{a}_{\ell m}^\dagger \, \mathsf{C}_\ell^{-1} \partial_\alpha \partial_\beta \mathsf{C}_\ell \mathsf{C}_l^{-1} \mathbf{a}_{\ell m}}{2\ell+1} \\ & + \sum_m \frac{\mathbf{a}_{\ell m}^\dagger \, \mathsf{C}_\ell^{-1} \partial_\alpha \mathsf{C}_\ell \mathsf{C}_l^{-1} \partial_\beta \mathsf{C}_\ell \mathsf{C}_l^{-1} \mathbf{a}_{\ell m}}{2\ell+1} + \sum_m \frac{\mathbf{a}_{\ell m}^\dagger \, \mathsf{C}_\ell^{-1} \partial_\beta \mathsf{C}_\ell \mathsf{C}_l^{-1} \partial_\alpha \mathsf{C}_\ell \mathsf{C}_l^{-1} \mathbf{a}_{\ell m}}{2\ell+1} \Bigg] \end{aligned} \tag{4.16}$$

Since $\langle \mathbf{a}^\dagger \, \mathbf{a} \rangle = \mathsf{C}_\ell^{\rm obs}$, we find the expectation value

$$\langle \partial_\alpha \chi^2 \rangle = - \sum_\ell f_{\rm sky} \frac{2\ell+1}{2} {\rm Tr}(\mathsf{C}_\ell^{-1} \partial_\alpha \mathsf{C}_\ell \mathsf{C}_\ell^{-1} \Delta \mathsf{C}_\ell), \tag{4.17}$$

where we have defined $\mathsf{C}_\ell^{\rm obs} \equiv \mathsf{C}_\ell + \Delta C_\ell$. This yields the expression for the vector $\mathbf{v}$ given in equation 4.14. For the second derivatives we find

$$\langle \partial_\alpha \partial_\beta \chi^2(\theta_{\rm obs}) \rangle = \sum_\ell f_{\rm sky} \frac{2\ell+1}{2} \Big[{\rm Tr}(\mathsf{C}_\ell^{-1} \partial_\alpha \mathsf{C}_\ell \mathsf{C}_\ell^{-1} \partial_\beta \mathsf{C}_\ell) + {\rm Tr}(\mathsf{K}_{\alpha\beta,\ell} \, \Delta \mathsf{C}_\ell) \Big] \tag{4.18}$$

where $\mathsf{K}_{\alpha\beta,\ell}$ is given by

$$\mathsf{K}_{\alpha\beta,\ell} \equiv \mathsf{C}_\ell^{-1} \partial_\alpha \mathsf{C}_\ell \mathsf{C}_\ell^{-1} \partial_\beta \mathsf{C}_\ell \mathsf{C}_\ell^{-1} + \mathsf{C}_\ell^{-1} \partial_\beta \mathsf{C}_\ell \mathsf{C}_\ell^{-1} \partial_\alpha \mathsf{C}_\ell \mathsf{C}_\ell^{-1} - \mathsf{C}_\ell^{-1} \partial_\alpha \partial_\beta \mathsf{C}_\ell \mathsf{C}_\ell^{-1}. \tag{4.19}$$

Therefore, if $\Delta \mathsf{C}_\ell \approx \partial_\alpha \mathsf{C}_l \cdot (\theta_\alpha^{\rm obs} - \theta_\alpha^{\rm th})$, the second term in Eq. 4.18 is of second order and we can approximate $\langle \partial_\alpha \partial_\beta \chi^2(\theta_{\rm obs}) \rangle$ as $\mathsf{F}_{\alpha\beta}$.

4.2.3 Upcoming surveys

We will perform our forecasts for two complementary Stage-IV experiments with optimal area overlap: CMB S4 and LSST. Together, they will offer at least four different cosmological tracers: CMB primary and lensing, cosmic shear and galaxy clustering, the latter two encompassing several redshift bins. The assumptions used to model these experiments are described here. In all cases we correctly account for all correlations between different tracers.

4.2.3.1 CMB Stage 4

In the mid 2020s, the current ground-based CMB facilities such as Advanced ACTPol [375], SPT-3G [376], BICEP2/Keck [377] or the Simons Array [378] will be superseded by a CMB Stage 4 (S4) experiment [184], combining the efforts of multiple ground-based instruments. S4 will be able to

derive cosmological constraints from a number of probes, including the primary CMB anisotropies in temperature and polarization, the CMB lensing convergence, Sunyaev-Zel'dovich cluster number counts and other secondary anisotropies. Of these, our forecasts will include the first two, given their relative robustness to astrophysical systematics. Following [186] we model S4 as an experiment mapping 40% of the sky with an rms noise sensitivity of 1μK-arcmin in temperature and a 3 arcmin full width at half maximum beam. Given the important systematic uncertainties on large scales faced by ground-based experiments (associated for instance to atmospheric noise or ground pickup), we further assume that S4 will only be able to effectively cover the multipole range $30 < \ell < 3000$ in temperature and $30 < \ell < 5000$ in polarization (with the lower small-scale cut in temperature motivated by the effect of astrophysical foregrounds). On $\ell < 30$ we supplement S4 with large-scale data from *Planck* [177] with the corresponding noise level. Although we model the noise contribution to the CMB power spectrum as white, the atmosphere generates a non-trivial noise structure on large scales, especially in temperature. The cosmological parameters considered here are however mostly constrained from the high-ℓ CMB power spectrum, and therefore our forecasts should not be strongly affected by this.

It is worth noting that the validity of the Fisher matrix approach can be particularly sensitive to the degeneracies between different parameters (both in terms of predicted uncertainties and biases). Of particular interest are the existing degeneracies between A_s, τ, Ω_M and $\sum m_\nu$, one of the main obstacles to measuring neutrino masses given the currently large uncertainties on τ from *Planck* [359, 186]. In order to verify that our results are not significantly affected by numerical instabilities associated to these degeneracies, we have recalculated our forecasts supplementing S4 on $\ell < 30$ with an optimal future satellite mission with a sensitivity of 4μK-arcmin in temperature. This setup is able to reach a cosmic-variance-limited error on τ, and therefore significantly reduce these parameter correlations. Doing this we verified that the results shown in Section 4.3 are stable with respect to parameter degeneracies.

4.2.3.2 Large Synoptic Survey Telescope

The Large Synoptic Survey Telescope [101] will carry out a 10-year deep and wide imaging survey of the southern sky, reaching a limiting magnitude of $r \sim 27$ over $\sim 20,000\,\mathrm{deg}^2$. The use of photometric redshifts (photo-z) to obtain approximate radial coordinates will allow LSST to obtain

cosmological constraints from a number of probes. These will include tomographic galaxy clustering and cosmic shear, galaxy cluster counts, type Ia supernovae and strong lensing. In particular the complementarity between clustering and lensing make the joint analysis of these two probes the most promising source of cosmological information for LSST, and therefore our forecasts are based on these. We base our modelling of both tracers on the treatment of [337], which we describe briefly below.

Galaxy clustering. In this case the most relevant observable is the shape of the angular power spectrum or correlation function of the galaxy distribution. The standard way to analyze it will be in terms of tomographic redshift bins, including all auto- and cross-correlations between them. We further separate the clustering sample into two disjoint populations of "red" (early-type, ellipticals, high-bias) and "blue" (late-type, disks, low-bias) galaxies. The specific models used for the signal and noise power spectra, redshift distributions and nuisance parameters are described in detail in [337].

The relation between the galaxy and matter power spectra is expected to be well-approximated by a linear "clustering bias", scale-independent, factor $b(z)$ on large scales. Our forecasts therefore marginalize over the value of this quantity defined, for each galaxy sample, at a discrete set of nodes in redshift (with the full $b(z)$ function reconstructed by interpolating between these nodes, see [337] for details). This approximation is, however, bound to fail on small scales, where non-linear, scale-dependent corrections, as well as stochastic contributions, should be taken into account. This makes the analysis of galaxy clustering on small scales very unreliable and often unusable for cosmology. In order to avoid these complications we define, for each redshift bin, angular scale cuts within which the corresponding map is used. At the median redshift of the i-th redshift bin z_i we compute a threshold comoving scale $k^i_{\rm max}$ defined as the cutoff scale for which the variance of the linear matter density contrast on larger scales is below a given threshold $\sigma^2_{\rm thr}$, i.e:

$$\sigma^2_{\rm thr} = \frac{1}{2\pi^2}\int_0^{k^i_{\rm max}} dk\, k^2\, P(k, z_i). \tag{4.20}$$

This comoving scale is then translated into an angular multipole $\ell^i_{\rm max} = \chi(z_i)\, k^i_{\rm max}$. For our fiducial forecasts we used a threshold variance of $\sigma_{\rm thr} = 0.75$.

Cosmic shear. The effect of weak gravitational lensing observed through the projected shapes of galaxies is a direct, unbiased probe of the intervening matter distribution. As such, cosmic shear observations are a potentially strong cosmological probe. The constraining power of this probe is contained in the power spectrum of the traceless part of the cosmic shear tensor for galaxies lying in a set of photo-z bins. As described in [379], we model the galaxy sample used for cosmic shear after the so-called "gold sample" [101], corresponding to galaxies with magnitude $i < 25.3$. We refer the reader to [379] for further details on this sample definition as well as the form of the lensing power spectrum assumed in this analysis. We use a constant minimum scale $\ell_{\rm max} = 2000$ for cosmic shear in our forecasts.

Both galaxy clustering and cosmic shear suffer from a number of sources of systematic uncertainties beyond those described above, such as photo-z uncertainties, the effect of intrinsic alignments or baryonic uncertainties in the matter power spectrum. In order to simplify the analysis we have neglected these systematics[3]. The final constraints on cosmological parameters depend critically on these uncertainties, as well as on the range of angular scales included in the analysis. The absolute forecast constraints on cosmological parameters reported in the next section should therefore not be taken at face value, but rather interpreted in terms of the relative information gain associated to the magnification and relativistic effects, as well as the associated relative biases.

4.3 Results

This section explores the relevance of the magnification bias and the other sub-dominant relativistic corrections to the number counts power spectrum. Here "relevance" will be evaluated in terms of both the information content (i.e. constraining power on particular cosmological parameters) and the associated systematic (i.e. possible bias on the same parameters) of these effects. The results will be presented for three different families of parameter spaces. These results are summarized in Table 4.1, which we describe below. It is worth noting that, even though we only report the bias associated with the parameters listed in this table, neglecting lensing magnification and GR effects

[3]The conservative scale cuts used here have been shown in [369] to be robust against the impact of baryonic uncertainties.

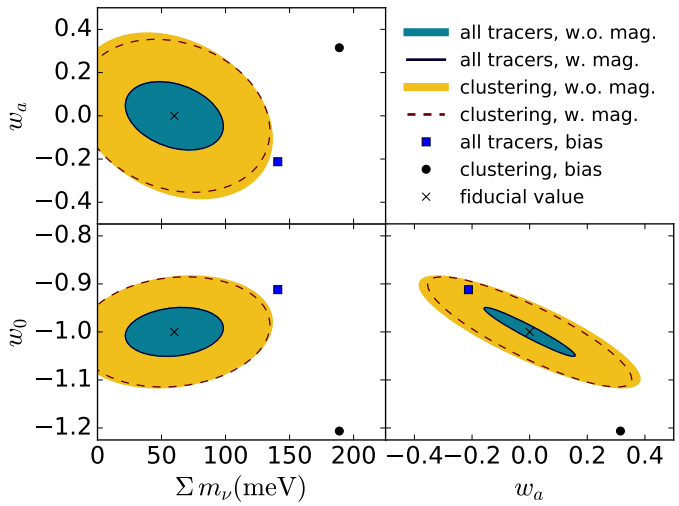

Figure 4.1: Forecast 1σ contours for Σm_ν, w_0 and w_a from LSST clustering only (orange ellipses) and LSST clustering + LSST shear + S4 (cyan ellipses) in the fiducial case without lensing magnification or GR effects. The thin solid and dashed ellipses correspond to the 1σ contours after including the lensing contribution to the clustering power spectrum in the same two cases respectively. The black circle and square show the bias associated with ignoring the presence of lensing magnification (again in the same two cases). In all cases the impact of GR effects is negligible, and therefore we have not included the corresponding ellipses in this figure.

also leads to biases in other standard ΛCDM parameters. We do not report these here, and rather concentrate on the parameter spaces that future large-scale structure facilities will target specifically.

4.3.1 Impact on dark energy and neutrino mass

As has been previously shown by [345], neglecting the lensing magnification effect can significantly bias the estimation of the total sum of neutrino masses $\sum m_\nu$. Our analysis here extends this study to the dark energy equation of state parameters, w_0 and w_a, since they have been shown to be degenerate with $\sum m_\nu$ [52] (see also [346], where w_0 and w_a were studied independently of $\sum m_\nu$).

In addition to this, the combined analysis of galaxy clustering and cosmic shear data is known to be of great use in breaking degeneracies to constrain these parameters [380]. This is relevant for two reasons: on the one hand, it is worth exploring to what extent the lensing information contained within the magnification bias contribution to galaxy clustering can also be used to break these same degeneracies *in lieu* of cosmic shear [346]. On the other hand, since cosmic shear is a direct probe

of gravitational lensing, it is interesting to study whether any biases associated with neglecting the magnification bias term could be mitigated by including cosmic shear information.

Finally, although the large-scale relativistic effects are known to be barely measurable, our treatment will allow us to explore their impact on constraints and systematic biases.

The results are shown in Figure 4.1, where the orange ellipses show the 1σ contours using only clustering information from LSST and the cyan ellipses correspond to the full constraining power of LSST clustering, LSST shear and S4 (including primary CMB and lensing). The thin solid and dashed ellipses correspond to the constraints after accounting for the contribution of magnification to clustering in the same two cases respectively. Although using only clustering information the magnification term does improve constraints slightly (up to 8% in the marginalized uncertainties), the improvement is absolutely negligible when including all other cosmological probes.

In the same plots, the filled circles and squares show the forecast bias on the same parameters, both for clustering alone and including all probes respectively. Although the inclusion of CMB and shear data reduces the size of the bias, the faster improvement in the constraints makes the significance of this bias worse. It is worth pointing out that the direction of the bias changes after including new probes, due to the change in direction of the different degeneracies.

We have also evaluated the information content (i.e. improvement in constraints) of the GR terms as well as the parameter bias they induce. The information content is completely negligible, with an improvement in the 1σ uncertainties well below 1% in all cases. The bias associated with the omission of these terms is equally negligible, with a maximum fractional bias of 6% with respect to the standard deviation in the case of w_0 when only galaxy clustering data are taken into account. These biases are further suppressed when including other probes.

4.3.2 Impact on scalar-tensor theories

As shown in the previous section, the secondary clustering anisotropies (lensing and GR effects) do not contain significant extra information in terms of final constraints on cosmological parameters for standard departures from vanilla ΛCDM. One could however argue that the true constraining power of these relativistic terms would be realized on actual modifications of GR [381], and therefore it is relevant to explore this possibility. To that end we have repeated the same Fisher analysis on the Horndeski parametrization of scalar-tensor gravity theories described in Section 4.2.1.

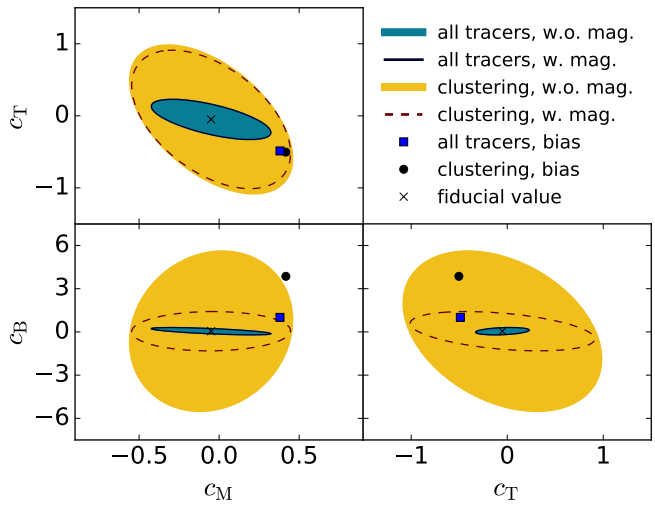

Figure 4.2: Same as Figure 4.1 for the Horndeski parameters c_B, c_M and c_T.

The results are shown in Figure 4.2 using the same color coding as Fig. 4.1. Interestingly, when including only clustering information we observe a large improvement in the constraint on c_B, and no real improvement on c_T and c_M. An inspection of the correlation coefficients between different parameters reveals that the inclusion of magnification is able to break strong degeneracies between c_B and the nuisance galaxy bias parameters, as could have been expected given that lensing effects trace the dark matter perturbations directly, and therefore marginally help constraint $b(z)$. In all cases, the bias associated with the lensing term is of the same order as the 1σ uncertainty when using only clustering information, smaller than the case explored in the previous section. These results change, however, when all probes are included simultaneously: the relative constraining power of the magnification term becomes negligible in the presence of cosmic shear and CMB, while the improvement in the final constraints brought about by these probes makes the bias associated to the lensing term significant at the 5σ level for c_B.

Regarding the relevance of the other GR effects, we find the same results obtained in the previous sections: these terms do not significantly improve the final constraints on the Horndeski parameters ($< 1\%$), and do not induce a significant bias ($\sim 8\%$ of σ at worst).

4.3.3 Impact on primordial non-Gaussianity

Except for the magnification lensing term, all other relativistic corrections to the number counts power spectrum dominate on horizon-sized scales. Therefore, although these effects seem to be

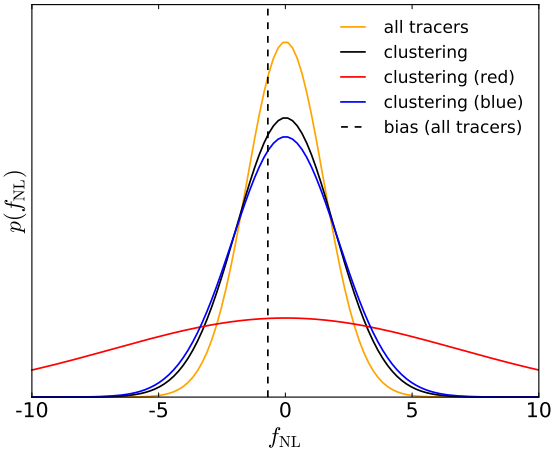

Figure 4.3: Forecast distribution for $f_{\rm NL}$ for LSST red galaxies (red), blue galaxies (blue), the combination of both in a multi-tracer sense (black) and the combination of LSST galaxy clustering, LSST cosmic shear and CMB S4 (orange). The bias on $f_{\rm NL}$ associated with the GR effects, corresponding to $f_{\rm NL}^{\rm GR} \simeq -0.7$ is shown as a vertical dashed line

irrelevant on the standard cosmological parameters explored in the previous sections, any parameter sensitive to the clustering pattern on large scales may be more affected by them. This is the case for the effects of primordial non-Gaussianity on the clustering pattern of biased tracers, as discussed in Section 4.2.1. We have therefore carried out the same Fisher analysis done in Section 4.3.1 including $f_{\rm NL}$ as a free parameter.

The results are shown in Figure 4.3 as 1D posterior distributions for $f_{\rm NL}$ marginalized over all other parameters (including w_0, w_a and Σm_ν). Before discussing the relevance of the lensing and GR effects it is worth inspecting the improvement on $\sigma(f_{\rm NL})$ from the inclusion of different probes. Here we have considered the cases of the blue and red clustering samples individually, the combination of both and the addition of external datasets (weak lensing and CMB data). For the blue and red samples, as well as their combination, we recover the same result obtained in [339]: the red sample alone does not yield competitive constraints given its small volume coverage ($\sigma(f_{\rm NL}|{\rm red}) \simeq 7$), while the higher number density and volume of the blue galaxies allows for a more interesting bound ($\sigma(f_{\rm NL}|{\rm blue}) \simeq 2$). The combination of both samples yields a slightly better constraint due to the multi-tracer effect, and the addition of external datasets improves it further $\sigma(f_{\rm NL}|{\rm all\,tracers}) \simeq 1.5$, mostly due to the improved measurement of the galaxy bias.

When switching on the lensing and GR effects we observe no significant improvement or degradation in $\sigma(f_{\rm NL})$. On the other hand we observe that GR effects cause a bias of $\sim 50\%$ for the combination of all tracers[4], corresponding to an effective value of $f_{\rm NL}^{\rm GR} \simeq -0.7$. This is in agreement with [382, 383, 343, 384]. Although this may not be a concern for the experimental setup considered here, other experiments targetting $f_{\rm NL}$ explicitly, such as SPHEREx [385], may need to account for these relativistic corrections. Magnification lensing, on the other hand, causes a much smaller effect, given its scale dependence. In the absence of CMB or cosmic shear measurements, we observe however a large bias on $f_{\rm NL}$ (of order 1σ) induced by magnification lensing. This is caused by the biased estimation of the galaxy bias parameters, which affect the amplitude of the correction due to $f_{\rm NL}$ if magnification is not taken into account (see also [386]).

4.3.4 Impact of magnification uncertainties

In the previous sections we have seen that the magnification term is important and can significantly bias cosmological parameter estimates if unaccounted for, as has also been previously shown by Refs. [346, 345]. Since the amplitude of the magnification term depends on the slope of the source number counts with apparent magnitude (see Eq. 4.2), an outstanding question is how well $s(z)$ needs to be measured in order to avoid a significant bias ($> 1\sigma$) from the magnification-related uncertainties alone. In order to test this, we have recomputed our forecasts for both the wCDM + $\Sigma\, m_\nu$ and Horndeski models, this time using a theoretical power spectrum that includes magnification bias with our fiducial model for $s(z)$, and an observed power spectrum in which we increase $s(z)$ by 10%. This then allows us to estimate the parameter bias associated with a 10% systematic uncertainty on $s(z)$ using the formalism described in Sec. 4.2. We find that the parameters of key relevance for galaxy clustering ($\sum m_\nu$, w_0, w_a, $c_{\rm B}$, $c_{\rm M}$ and $c_{\rm T}$) can be significantly biased by uncertainties of this order (e.g. 179% of σ for w_0).

These results can be used to quantify the level to which $s(z)$ must be known to avoid biasing individual parameters. Under the assumption that the parameter bias $\Delta\theta$ scales linearly with the relative systematic error on s, δs, we can estimate $\Delta\theta$ for any δs in terms of the bias computed

[4]Note that this value is found after marginalizing over all other cosmological and nuisance parameters. However, the result holds also under the assumption that all parameters other than $f_{\rm NL}$ are known.

in the 10% case $\Delta\theta = \rho\,\delta s$, where $\rho \equiv \Delta\theta/\delta s$ for $\delta s = 0.1$. Then, assuming that we can at most afford a bias $\Delta\theta = \epsilon\,\sigma(\theta)$, where $\sigma(\theta)$ is the 68% uncertainty on θ and $\epsilon \sim O(1)$, the corresponding maximum relative systematic error of s is given by

$$\delta s|_{\rm max} = \frac{\epsilon}{\rho}\sigma(\theta). \tag{4.21}$$

For $\epsilon = 1$, the allowed relative uncertainties for the different parameters are given in the last column of Table 4.1. We find that $s(z)$ must be correctly determined to the $\sim 5\%$ level in order to avoid significant biases on the dark energy parameters and the sum of neutrino masses. For the case of Horndeski parameters this requirement is relaxed to a $\sim 10\%$ systematic uncertainty, but we note that, given the degeneracy between the c_X and other standard cosmological parameters such as h, a systematic error on $s(z)$ could propagate into these as well. Consistency studies between different sets of probes will therefore be vital to detect these and other types of systematics.

4.4 Discussion

Accurate measurements of the large scale structure of the Universe are the next frontier of modern cosmology. Maps of the galaxy and diffuse gas distributions, of the CMB and of the gravitational potential via weak lensing will be used to place tight constraints on a plethora of cosmological parameters. In the past few years we have learnt of the importance of taking into account novel corrections to the observables of large scale structure, specifically through lensing magnification and GR effects. In this chapter, we have investigated how important these secondary corrections to the power spectrum of galaxy number counts are in terms of information content and potential biases to cosmological parameters. We have explored the relevance of these effects on three different families of cosmological parameters: extensions to the standard ΛCDM paradigm in the form of massive neutrinos and time-varying dark energy equation of state, Horndeski-like parametrizations of scalar-tensor theories, and the large-scale contribution of primordial non-Gaussianity to the galaxy power spectrum.

It is natural to split the secondary contributions mentioned above into two classes: the contribution from lensing magnification is relevant on small angular scales and is coherent over large redshift separations. This contribution is well known and has been used in the past in different scientific

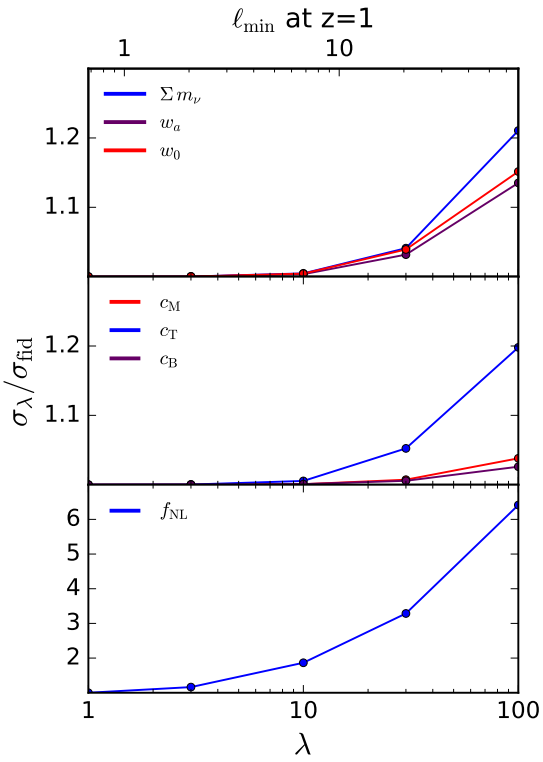

Figure 4.4: Relative degradation in the final constraints associated with removing all scales larger than a factor λ times the comoving horizon at the source redshift (the associated angular scales at $z = 1$ are shown in the upper twin x-axis). The results are shown for simple extensions to ΛCDM (upper panel), scalar-tensor theories (middle panel) and primordial non-Gaussianity (lower panel). Except in the case of $f_{\rm NL}$, the information content of the largest scales is heavily suppressed due to cosmic variance.

analyses. We group all other contributions under the umbrella term of "GR effects", given their relevance mostly on large scales, of the order of the horizon at the redshift of the source.

We have established, in agreement with previous studies [346, 345], that even though lensing magnification can be detected with high significance, it will not in general contribute strongly to improve the final constraints on any cosmological parameter. Although it may be relevant to constrain deviations from modified gravity (e.g. c_B in Section 4.3.2) using only clustering data, its information content is negligible when combined with cosmic shear and CMB observations. Nevertheless, using a Fisher approach we have shown that it will be necessary to model and account for this contribution to the galaxy power spectrum in order to avoid strong biases on dark-energy parameters and the sum of neutrino masses. The bias associated with neglecting the effects of magnification is most relevant when considering clustering alone as a cosmological probe, and gets reduced considerably after including shear and CMB. The reduced parameter uncertainties in the latter case imply that the associated biases are still significant, however. Our approach also allows us to quantify the level to which the number counts slope $s(z)$ must be known in order to avoid significantly biasing the most relevant late-time cosmological parameters. We find that $s(z)$ must be known at least the $\sim 5\%$ level, in rough agreement with [346]. An MCMC-based approach will be able to fully test the extent of these biases in a realistic scenario. On the other hand, and as expected given the scale dependence of the lensing contribution, this effect should not have a strong impact on the inferred value of $f_{\rm NL}$ given expected uncertainties.

The GR effects, on the other hand, are known to have a sub-dominant amplitude and, as expected, we find that they will have a negligible impact on both the uncertainty and bias on most cosmological parameters. The only exception to this is the level of primordial non-Gaussianity, given the similar scale dependence of these effects and the $\sim 1/k^2$ contribution of $f_{\rm NL}$. We find that the GR effects could induce a bias on this parameter of the order of $f_{\rm NL}^{\rm GR} \sim 0.7$, in agreement with previous estimate of the amplitude of these contributions. This is comparable to the uncertainty on $f_{\rm NL}$ expected from LSST, and will therefore be relevant for future experiments specifically targeting this science case. We emphasize though that systematic effects that may cause correlated fluctuations in the homogeneity of the galaxy sample (e.g. depth variations, dust extinction, star contamination) will need to be carefully treated in order to minimize their impact on the large-scale galaxy power spectrum, thus preserving this sensitivity of galaxy surveys to $f_{\rm NL}$. Since the amplitude of the

GR effects depends on the value of the magnification and evolution biases $s(z)$ and $f_{\rm evo}(z)$, the uncertainties on these quantities may hamper our ability to reach optimal constraints on $f_{\rm NL}$ or mitigate the associated bias on this parameter. This underpins the need to quantify the luminosity and time dependence of the background number density of sources for future Stage-IV surveys, already noted in the literature (e.g. [346]) in the context of the impact of lensing magnification on standard cosmological parameters.

It is also worth mentioning that, even though these GR effects are one of the few manifestly relativistic contributions to the power spectrum, and therefore may potentially contain valuable information to constrain departures from General Relativity, we find that their constraining power on modified gravity theories is negligible. This can be easily understood in terms of the scales involved: even if a given modified gravity theory could generate a significant difference in any of these GR terms, these effects are only relevant on horizon-size scales, and therefore their information content is heavily suppressed by cosmic variance. This can be explicitly verified by re-running these forecasts cutting out the largest scales and comparing the results with our fiducial predictions. To do so, for each redshift bin i with a median redshift z_i, we define a minimum scale $\ell_{\rm min}(z_i, \lambda)$ as the Fourier scale corresponding to the angular size of the horizon at that redshift divided by a factor λ:

$$\ell_{\rm min}(z_i, \lambda) = \lambda\, \chi(z_i) \frac{H(z_i)}{1+z_i} \tag{4.22}$$

Figure 4.4 shows the increment in the uncertainty of different cosmological parameters associated with the loss of these large scales as a function of λ. The results were obtained for the combination of LSST clustering, shear and CMB S4. We observe that, even removing scales that are 1% the size of the horizon, the degradation in the final constraints is at most $\sim 20\%$ for all cosmological parameters, with the exception of $f_{\rm NL}$.

On a different front, one might hope that the inclusion of the lensing magnification term in the number counts might mitigate some systematic uncertainties - specifically, it might help to pin down galaxy bias. And indeed, in the analysis of Horndeski theories, we have shown that including that term significantly changes the uncertainty in c_B by breaking some of its degeneracies with the galaxy bias parameters. While this is the case, it is not accompanied by a substantial reduction in the uncertainties in these parameters; the reduction in the uncertainty is of the order of a few percent.

One interesting aspect that we have not explored is the importance of the effects studied here in cross-correlations between the Integrated Sachs-Wolfe (ISW) effect and number counts [387]. This measurement could be particularly relevant to constrain modified gravity theories [388]. In principle the non-inclusion of the GR terms could bias estimates of cosmological parameters although this should strongly depend on the scales which are included in the standard analysis. We leave a systematic analysis of the ISW effect for future work.

Finally, it is worth stressing the fact that the results presented here are applicable to the combination of CMB and photometric galaxy samples assumed. Spectroscopic surveys, on the other hand, might be able to detect some of the GR effects studied here on intermediate scales as a local dipole in the cross-correlation function of different galaxy samples [389]. Although this is a challenging measurement [390, 391], it would be important to further understand its constraining power.

With this chapter we have assessed the importance of relativistic effects on cosmological parameter estimation with a particular emphasis on extensions of ΛCDM. Our understanding of the impact of these effects on the analysis of future data will allow us to reap the rewards of the next generation of cosmological surveys.

	all tracers				
Parameters	rel. improvement on σ from lensing	rel. bias from lensing	rel. improvement on σ from GR effects	rel. bias from GR effects	Max. error on $s(z)$
wCDM					
$\sum m_\nu$	$< 1\%$	320%	$< 1\%$	3%	9.8%
w_a	$< 1\%$	-203%	$< 1\%$	$< 1\%$	5.6%
w_0	$< 1\%$	261%	$< 1\%$	-3%	4.2%
Horndeski					
$c_{\rm M}$	$< 1\%$	175%	$< 1\%$	-7%	22%
$c_{\rm B}$	$< 1\%$	573%	$< 1\%$	1%	11%
$c_{\rm T}$	$< 1\%$	-237%	$< 1\%$	8%	23%
prim. non-Gaussianity					
$f_{\rm NL}$	-2%	17%	-3%	-45%	N.A.
	LSST galaxy clustering only				
wCDM					
$\sum m_\nu$	2%	255%	$< 1\%$	3%	N.A.
w_a	8%	125%	$< 1\%$	-2%	N.A.
w_0	2%	-269%	$< 1\%$	6%	N.A.
Horndeski					
$c_{\rm M}$	3%	139%	$< 1\%$	$< 1\%$	N.A.
$c_{\rm B}$	76%	104%	$< 1\%$	-5%	N.A.
$c_{\rm T}$	7%	-66%	$< 1\%$	$< 1\%$	N.A.
prim. non-Gaussianity					
$f_{\rm NL}$	-2%	168%	-6%	7%	N.A.

Table 4.1: Summary of results: improvement on the 1σ uncertainties, and parameter bias associated to the contributions of lensing magnification and GR effects to the number counts power spectrum. The upper set of columns corresponds to the combination of all tracers (LSST clustering, LSST shear and S4), while the lower columns correspond to LSST clustering only. Note that all results are shown as a relative improvement or bias, normalized by the fiducial 1σ uncertainties (which are different in these two cases). The three sets of rows correspond to the three parameter families studied here: wCDM+m_ν (top), Horndeski models (middle) and primordial non-Gaussianity (bottom). Note also that the constraints on $f_{\rm NL}$ and Horndeski models are also marginalized over Σm_ν. The last column shows, for all tracers jointly, the maximum systematic error on $s(z)$ that can be allowed to avoid a bias on each parameter larger than its 1σ uncertainty.

Chapter 5

Conclusions

In this section, we will describe open questions in cosmology, the challenges that will be faced while searching for their answers (Sec. 5.1), and how the findings of this thesis fit into the picture. We will describe the main results of this thesis and also describe how the work presented here could be extended (Sec. 5.2).

5.1 Open questions in modern cosmology

Here we will briefly describe several fields of active research in cosmology.

1. **What are the absolute neutrino masses?**

   As discussed in the previous chapters, the absolute neutrino masses are yet to be determined. Their value might shed light on how neutrino masses are generated. Both ground-based as well as cosmological experiments are ongoing. It is expected that the next generation of surveys, for example the Simons Observatory (SO), will narrow down the area where the sum of neutrino masses is expected. The projected sensitivity to the total neutrino mass is $\sigma(\Sigma m_\nu) = 31$ meV, when combining DESI BAO data and SO CMB power spectra and SO lensing potentials, assuming current measurements of the optical depth to reionization τ [121]. The sensitivity would improve if τ can be measured more precisely [52], for example with the LiteBIRD satellite [392]. In that case, a $3.5 - 5.9\sigma$ detection of the total neutrino mass is expected from this data combination, depending whether the neutrino mass hierarchy is normal or inverted [121]. Similar constraints of Σm_ν are expected from LSST [101], when combining cosmic shear with CMB data. However, cosmological neutrino mass constraints are model-dependent (see Chapter 2).

2. **Resolving current tensions**

Recently, cosmological parameter constraints inferred from high- and low-redshift probes seem to be in mild disagreement with each other [51] (see also Chapter 3). For example, there is a tension above 4σ between values of H_0 obtained from CMB data and local measurements of the expansion rate [51, 393, 394, 395, 396]. In addition, there is a tension between values of Ω_m-σ_8 determined by CMB and weak lensing datasets (see also Chapter 3). Numerous analyses have investigated whether the discrepancies might be explained with systematic errors in the analyses of these datasets [397, 398, 399, 277, 278, 279, 280, 281, 282], or whether new physics might be needed [293, 400, 401, 402, 403, 404, 405, 406, 407, 408, 283, 284, 272, 285, 286, 287, 288, 289, 290, 291] or whether our local Universe is different from the rest of the Universe [409, 410, 411, 412]. So far, the discrepancies persist, and the hope is that next generation experiments might shed new light on this puzzle, for example with gravitational wave observations [413, 414, 415, 416]. During the course of this DPhil, the first gravitational wave signal from the merger of a binary black hole was observed [417]. It is expected that while more gravitational wave signals are detected, the Hubble constant will be determined more precisely.

3. **What is the nature of dark energy?**

The nature of dark energy remains unknown. Models of dark energy include quintessence [418], k-essence [419, 420], coupled dark energy models [421] and modifications of gravity (see also [34, 422] for reviews). Future surveys, such as LSST, aim to measure the dark energy equation of state more precisely. Depending on the accuracy of future surveys to w and its time derivative, we might be able to distinguish between ΛCDM and dynamical dark energy models [423, 424, 425, 34].

4. **Testing gravity**

Another field of active research is the search for deviations from general relativity (see e.g. [426, 427, 10] for reviews). In particular, gravitational wave surveys offer the opportunity to search for deviations from general relativity [428], as already demonstrated by the discovery of a neutron binary star merger which ruled out many modified gravity scenarios [429, 430]. Galaxy surveys, such as Euclid, will search for deviations from general relativity as well [34].

5. **What is dark matter?** Many different candidates for dark matter have been proposed, for example weakly interacting massive particles (WIMPs) [431, 432], axions [433], fuzzy dark matter [434], sterile neutrinos [200] and primordial black holes [435, 436]. Currently planned next-decade surveys, such as LSST, aim to probe dark matter models by searching for deviations from the behaviour of standard cold, collisionless and non-interacting dark matter [437]. These probes include among others strong gravitational lensing, measurements of halo profiles and the abundance of compact objects.

6. **Testing inflation** Many inflation models predict primordial gravitational waves, which would generate B-mode polarization of the CMB. Efforts are ongoing to detect these B-modes by developing strategies for delensing of CMB polarization spectra [123, 124, 125]. Besides B-modes, many inflation models also predict primordial non-Gaussian fluctuations (see also Chapter 4). The last release of the Planck mission has found a value of $f_{\mathrm{NL,local}} = -0.9 \pm 5.1$ (68% C.L.) [438]. The determination of f_{NL} has the potential to distinguish between different inflation models.

Alongside new tests of theories, new data analysis techniques will be required in the future. Cosmological experiments have made very precise observations of our Universe, and upcoming experiments, such as CMB-S4 and Euclid, will improve the accuracy and reach of observations still further. New methods will be necessary in order to deal with very large datasets and to avoid systematic errors which become relevant because of the increased precision of upcoming experiments. This will require for example accurately modelling intrinsic alignments of galaxies [97, 98, 99], accurately describing baryonic effects on the matter power spectrum [91, 92, 93, 94, 95, 96] and obtaining accurate photometric redshifts for observed galaxies [63, 64, 65, 66, 67, 68]. In order to handle the large expected datasets from future surveys, machine learning methods are currently being developed [439, 440].

5.2 Summary of findings of this thesis and further remarks

Here will briefly recap the results of the previous chapters, and how they contribute to areas of active research discussed above. We will also briefly discuss how the work presented in this thesis

could be extended.

Time-varying dark energy and neutrinos

A detection of the neutrino mass from cosmology alone is one of the main aims of next-generation cosmological surveys. However, as shown by Ref. [52], the cosmological neutrino mass constraints would degrade in case of a time-varying dark energy equation of state. In Chapter 2 we showed that two specific parameterizations of time-varying dark energy (barotropic dark energy and early dark energy) exhibit degeneracies with neutrinos. This can affect cosmological constraints of the total neutrino mass sum Σm_ν and of the effective number of neutrinos, $N_{\rm eff}$. We showed how the combination of multiple probes across cosmic time, in particular CMB temperature, polarization and lensing and BAO can help to break some of these degeneracies. While current data is not yet powerful enough to distinguish completely between neutrinos and these dark energy models, we expect significant progress from future CMB S4 and DESI BAO data.

Ref. [441] further investigated how to break degeneracies between dark energy and neutrinos, focusing on the w_0-w_a parameterization of dark energy, and found that future galaxy clustering and cosmic shear data, for example from LSST, are projected to alleviate these degeneracies. They stated that the combination of CMB and LSS surveys is needed in order to achieve this aim, and that neither CMB nor LSS surveys alone will be able to measure the total neutrino mass.

Recently, Ref. [442] also forecasted the sensitivity to different CMB and LSS data combinations. In particular, they considered galaxy clustering, cosmic shear, intensity mapping and baryonic acoustic oscillations. The authors accounted for degeneracies of Σm_ν with $N_{\rm eff}$, and with a time-varying dark energy equation of state. Apart from that, they removed the information coming from non-linear scales in galaxy surveys. In all cases, they found that the neutrino mass will be measured with high precision. We note here that both Ref. [441] as well as Ref. [442] focused on the w_0-w_a parameterization of time-varying dark energy, and not on early dark energy and barotropic dark energy considered in Chapter 2.

Building on the work presented here, it would be interesting to study how the inclusion of further low-redshift data, such as cosmic shear and galaxy clustering, affects the constraints of early dark energy and barotropic dark energy models. In addition, the analysis could be extended by studying degeneracies between neutrinos and other cosmological scenarios. These include for

example curvature, modified gravity and inflationary parameters [443, 444].

Time-varying neutrino masses

In Chapter 3 we tested how the standard neutrino mass limit would change if neutrino masses were to be generated very late in the Universe [3]. Cosmology constrains the total neutrino mass sum to be lower than 120 meV assuming the Standard Model of cosmology or simple extensions [51]. However, the KATRIN experiment [193], a tritium β decay experiment which aims to detect the neutrino mass directly, has a lower sensitivity of 200 meV for the electron neutrino mass, making a direct detection of neutrino masses unlikely. We found that neutrino mass generation at low redshifts weakens the cosmological neutrino mass bound to $\Sigma m_\nu < 4.8$ eV (95% C.L.), opening new discovery regimes for KATRIN. These constraints were obtained from a combination of cosmic microwave background (CMB) data, CMB lensing, baryonic acoustic oscillations and supernovae data. The direct detection of neutrino masses with particle detectors would be a strong hint for such a model. Apart from that, we investigated if late generation of neutrino masses in the Universe could affect the current discrepancies between Ω_m-σ_8 measurements obtained from CMB, SZ and weak gravitational lensing experiments. Neutrinos had been discussed as a possible solution of these tensions before [292, 293]. We found no significant change in the discrepancies for the time-varying neutrino mass model compared to standard ΛCDM+Σm_ν.

The work presented in Chapter 3 could be extended in several ways. For example, it would be interesting to constrain the late neutrino mass generation model with additional datasets, for example with redshift space distortions, Lyman-alpha forest measurements and galaxy surveys. In addition, one could explore whether there is a deeper connection of neutrinos and dark energy. Neutrinos and dark energy have very similar energy scales today [294]. This raises the question whether neutrinos and dark energy are coupled with each other.

Relativistic effects in large scale structure

In Chapter 4, we investigated how important lensing magnification and other relativistic effects are for the estimation of cosmological parameters, for example for neutrino parameters and for parameters characterising modified gravity theories. The observed number density of galaxies at a particular redshift and solid angle in the sky differs from the true underlying number density

of galaxies because of these effects [336, 74, 73]. It has also been discussed in the literature whether relativistic effects might contain information about deviations from general relativity, and whether they could therefore be used to test modified gravity theories [445]. We found that lensing magnification needs to be modelled accurately in order to avoid a bias of the order of several standard deviations on cosmological parameters. By contrast, the other general relativistic corrections could be neglected in most cases, except when constraining primordial non-Gaussianity.

After our analysis about the impact of relativistic effects on cosmological parameter estimation in Chapter 4 was published, Ref. [446] also addressed the question how neglecting lensing magnification affects neutrino mass constraints and constraints of modified gravity parameters. The authors considered spectroscopic surveys as well, and looked at a different modified gravity parameterisation (Σ and μ) as compared to our analysis. Their analysis also found that neglecting lensing magnification can significantly bias cosmological parameter constraints. Similar results were also obtained by Ref. [447]. Here, the authors considered DE models with anisotropic stress and constant sound speed, and found that neglecting lensing can bias constraints of the galaxy bias, the Hubble constant and the dark energy equation of state.

Based on our results in Chapter 4, Ref. [448] further studied the lensing magnification effect when combining cosmic shear and galaxy clustering data. The authors found that the removal of the parts of the data vector that are most sensitive to magnification does not necessarily reduce the bias due to neglecting magnification. Therefore, future surveys, for which the lensing magnification effect is the most relevant, should correctly account for this effect in their analyses.

Another related result has been published recently by Ref. [449]. Here, the authors suggested that in the future kinematic SZ tomography could be used to detect general relativistic corrections in galaxy number counts. Similar to us, they also found that the GR effects should be taken into account here, as they can otherwise bias constraints of $f_{\rm NL}$.

Building on the work in Chapter 4, it would be interesting to study how the inclusion of lensing magnification might affect the results of current surveys. This effect if often neglected in current analyses, however it has been shown to be significant for galaxy clustering in our analysis and also for galaxy-galaxy lensing observations in Ref. [450].

Appendix A

Complete expressions for the corrections to the number counts of galaxies

The linear-order expression for the transfer function of number-count fluctuations in the i-th redshift bin, characterized by a radial selection function $W_i(z)$, is given as a sum over 10 different terms [370]:

$$\Delta_\ell^{\mathrm{D},i}(k) \equiv \int d\tau\, b\, \tilde{W}_i\, \delta_M(k,\tau)\, j_\ell(k\chi(\tau)), \qquad \Delta_\ell^{\mathrm{RSD},i}(k) \equiv \int d\tau\, (aH)^{-1} \tilde{W}_i(\tau)\, \theta(k,\tau)\, j_\ell''(k\chi(\tau)), \tag{A.1}$$

$$\Delta_\ell^{\mathrm{L},i}(k) \equiv \ell(\ell+1) \int d\tau, \tilde{W}_i^{\mathrm{L}}(\tau)\, (\Phi+\Psi)(k,\tau)\, j_\ell(k\chi(\tau)), \quad \Delta_\ell^{\mathrm{V1},i}(k) \equiv \int d\tau\, (f_{\mathrm{evo}} - 3)\, aH\, \tilde{W}_i(\tau)\, \frac{\theta(k,\tau)}{k^2}\, j_\ell(k\chi(\tau)), \tag{A.2}$$

$$\Delta_\ell^{\mathrm{V2},i}(k) \equiv \int d\tau, \left(1 + \frac{H'}{aH^2} + \frac{2-5s}{\chi\, aH} + 5s - f_{\mathrm{evo}}\right) \tilde{W}_i(\tau)\, \frac{\theta(k,\tau)}{k}\, j_\ell'(k\chi(\tau)), \tag{A.3}$$

$$\Delta_\ell^{\mathrm{P1},i}(k) \equiv \int dtau \left(2 + \frac{H'}{aH^2} + \frac{2-5s}{\chi\, aH} + 5s - f_{\mathrm{evo}}\right) \tilde{W}_i(\tau)\, \Psi(k,\tau)\, j_\ell(k\chi(\tau)), \tag{A.4}$$

$$\Delta_\ell^{\mathrm{P2},i}(k) \equiv \int d\tau\, (5s-2) \tilde{W}_i(\tau)\, \Phi(k,\tau)\, j_\ell(k\chi(\tau)), \quad \Delta_\ell^{\mathrm{P3},i}(k) \equiv \int d\tau\, (aH)^{-1} \tilde{W}_i(\tau)\, \Phi'(k,\tau)\, j_\ell(k\chi(\tau)), \tag{A.5}$$

$$\Delta_\ell^{\mathrm{P4},i}(k) \equiv \int d\tau\, \tilde{W}_i^{\mathrm{P4}}(\tau)\, (\Phi+\Psi)(k,\tau)\, j_\ell(k\chi(\tau)), \quad \Delta_\ell^{\mathrm{ISW},i}(k) \equiv \int d\tau\, \tilde{W}_i^{\mathrm{ISW}}(\tau)\, (\Phi+\Psi)'(k,\tau)\, j_\ell(k\chi(\tau)). \tag{A.6}$$

Here, $j_\ell(x)$ is the spherical Bessel function of order ℓ, and we have defined the window functions

$$\tilde{W}_i(\tau(z)) \equiv W_i(z) \left(\frac{d\tau}{dz}\right)^{-1}, \quad \tilde{W}_i^{\mathrm{L}}(\tau) \equiv \int_0^\tau d\tau' \tilde{W}_i(\tau') \frac{2-5s(\tau')}{2} \frac{\chi(\tau)-\chi(\tau')}{\chi(\tau)\chi(\tau)},$$
$$\tilde{W}_i^{\mathrm{P4}}(\tau) \equiv \int_0^\tau d\tau \tilde{W}_i(\tau') \frac{2-5s}{\chi}, \quad \tilde{W}_i^{\mathrm{ISW}}(\tau) \equiv \int_0^\tau d\tau \tilde{W}_i(\tau') \left(1 + \frac{H'}{aH^2} + \frac{2-5s}{\chi\, aH} + 5s - f_{\mathrm{evo}}\right)_{\tau'}.$$

The quantities δ_M, θ, Φ and Ψ above are transfer functions for density perturbations in the comoving synchronous gauge, for the velocity divergence in the conformal Newtonian gauge and for two metric

potentials in the same gauge[1].

Of the 10 terms in Eq. A.1 above, $\Delta^{\rm D}$, $\Delta^{\rm RSD}$ are the dominant density and redshift-space distortions terms respectively, $\Delta^{\rm L}$ is the contribution of lensing magnification and we have grouped the remaining 7 terms under a single "GR effects" contribution $\Delta^{\rm GR}$ in Eq. 4.1.

[1]The conformal Newtonian gauge is defined by the line element $ds^2 = a^2(\tau)\,[(1+2\Psi)d\tau^2 - (1-2\Phi)\delta_{ij}dx^i dx^j\,]$.

References

[1] Christiane S. Lorenz, Erminia Calabrese, and David Alonso, "Distinguishing between Neutrinos and time-varying Dark Energy through Cosmic Time," Phys. Rev. **D96**, 043510 (2017), arXiv:1706.00730 [astro-ph.CO] .

[2] Christiane S. Lorenz, Lena Funcke, Erminia Calabrese, and Steen Hannestad, "Time-varying neutrino mass from a supercooled phase transition: current cosmological constraints and impact on the Ω_m-σ_8 plane," Phys. Rev. **D99**, 023501 (2019), arXiv:1811.01991 [astro-ph.CO] .

[3] Gia Dvali and Lena Funcke, "Small neutrino masses from gravitational θ-term," Phys. Rev. **D93**, 113002 (2016), arXiv:1602.03191 [hep-ph] .

[4] Lena Funcke, "How gravity shapes the low-energy frontier of particle physics. Neutrino masses and domestic axions. A PhD thesis at the Department of Physics at Ludwig-Maximilians University Munich," (2018).

[5] Christiane S. Lorenz, David Alonso, and Pedro G. Ferreira, "Impact of relativistic effects on cosmological parameter estimation," Phys. Rev. **D97**, 023537 (2018), arXiv:1710.02477 [astro-ph.CO] .

[6] Albert Einstein, "Kosmologische Betrachtungen zur allgemeinen Relativitätstheorie," Sitzungsberichte der Königlich Preußischen Akademie der Wissenschaften (Berlin , 142–152 (1917).

[7] A. G. Riess, A. V. Filippenko, *et al.*, "Observational Evidence from Supernovae for an Accelerating Universe and a Cosmological Constant," Astron. J. **116**, 1009–1038 (1998), arXiv:astro-ph/9805201 .

[8] S. Perlmutter, G. Aldering, G. Goldhaber, R. A. Knop, P. Nugent, *et al.*, "Measurements of Ω and Λ from 42 High-Redshift Supernovae," The Astrophysical Journal **517**, 565–586 (1999), arXiv:astro-ph/9812133 .

[9] Alessandra Silvestri and Mark Trodden, "Approaches to Understanding Cosmic Acceleration," Rept. Prog. Phys. **72**, 096901 (2009), arXiv:0904.0024 [astro-ph.CO] .

[10] Timothy Clifton, Pedro G. Ferreira, Antonio Padilla, and Constantinos Skordis, "Modified Gravity and Cosmology," Phys. Rept. **513**, 1–189 (2012), arXiv:1106.2476 [astro-ph.CO] .

[11] Joel R. Primack and Michael A. K. Gross, "Hot dark matter in cosmology," , 287–308 (2000), arXiv:astro-ph/0007165 [astro-ph] .

[12] V. C. Rubin and W. K. Ford, Jr., "Rotation of the Andromeda Nebula from a Spectroscopic Survey of Emission Regions," The Astrophysical Journal **159**, 379 (1970).

[13] G. F. Smoot *et al.*, "Structure in the COBE differential microwave radiometer first-year maps," APJL **396**, L1–L5 (1992).

[14] N. Jarosik *et al.*, "Seven-year Wilkinson Microwave Anisotropy Probe (WMAP) Observations: Sky Maps, Systematic Errors, and Basic Results," APJS **192**, 14 (2011), arXiv:1001.4744 .

[15] J. A. Peacock, "The isotropic universe," in *Cosmological Physics* (Cambridge University Press, 1998) p. 65100.

[16] Daniel Baumann, "Inflation," in *Physics of the large and the small, TASI 09, proceedings of the Theoretical Advanced Study Institute in Elementary Particle Physics, Boulder, Colorado, USA, 1-26 June 2009* (2011) pp. 523–686, arXiv:0907.5424 [hep-th] .

[17] Andrei Linde, "Inflationary Cosmology after Planck 2013," in *Proceedings, 100th Les Houches Summer School: Post-Planck Cosmology: Les Houches, France, July 8 - August 2, 2013* (2015) pp. 231–316, arXiv:1402.0526 [hep-th] .

[18] G. Lemaître, "Expansion of the universe, A homogeneous universe of constant mass and increasing radius accounting for the radial velocity of extra-galactic nebulae," MNRAS **91**, 483–490 (1931).

[19] Phillip James Edwin Peebles, *The large-scale structure of the universe* (Princeton university press, 1980).

[20] Edward W. Kolb and Michael S. Turner, "The Early Universe," Front. Phys. **69**, 1–547 (1990).

[21] DA Kirzhnits, "Weinberg model and the "hot" Universe," Red **15**, 7–5 (1972).

[22] Steven Weinberg, "Gauge and global symmetries at high temperature," Physical Review D **9**, 3357 (1974).

[23] Louise Dolan and Roman Jackiw, "Symmetry behavior at finite temperature," Physical Review D **9**, 3320 (1974).

[24] Viatcheslav Mukhanov, *Physical Foundations of Cosmology* (Cambridge University Press, 2005).

[25] Julien Lesgourgues and Sergio Pastor, "Massive neutrinos and cosmology," Phys. Rept. **429**, 307–379 (2006), arXiv:astro-ph/0603494 [astro-ph] .

[26] P. J. E. Peebles, "Recombination of the Primeval Plasma," The Astrophysical Journal **153**, 1 (1968).

[27] Y. B. Zel'dovich, V. G. Kurt, and R. A. Syunyaev, "Recombination of Hydrogen in the Hot Model of the Universe," Soviet Journal of Experimental and Theoretical Physics **28**, 146 (1969).

[28] A. Friedman, "Über die Krümmung des Raumes," Zeitschrift für Physik **10**, 377–386 (1922).

[29] D. Baumann, Lecture notes for the Part Three Cosmology Course .

[30] A. Einstein, "Die Grundlage der allgemeinen Relativitätstheorie," Annalen der Physik **354**, 769–822 (1916).

[31] A. Einstein, "Die Feldgleichungen der Gravitation," Sitzungsberichte der Königlich Preußischen Akademie der Wissenschaften (Berlin), Seite 844-847. (1915).

[32] Scott Dodelson, *Modern Cosmology* (Academic Press, Amsterdam, 2003).

[33] Yun Wang and Peter M. Garnavich, "Measuring time dependence of dark energy density from type Ia supernova data," Astrophys. J. **552**, 445 (2001), arXiv:astro-ph/0101040 [astro-ph] .

[34] Luca Amendola *et al.*, "Cosmology and fundamental physics with the Euclid satellite," Living Rev. Rel. **21**, 2 (2018), arXiv:1606.00180 [astro-ph.CO] .

[35] Chung-Pei Ma and Edmund Bertschinger, "Cosmological perturbation theory in the synchronous and conformal Newtonian gauges," Astrophys. J. **455**, 7–25 (1995), arXiv:astro-ph/9506072 [astro-ph] .

[36] Antony Lewis and Sarah Bridle, "Cosmological parameters from CMB and other data: A Monte Carlo approach," Phys. Rev. **D66**, 103511 (2002), arXiv:astro-ph/0205436 [astro-ph] .

[37] J. Lesgourgues, "The Cosmic Linear Anisotropy Solving System (CLASS) I: Overview," ArXiv e-prints (2011), arXiv:1104.2932 [astro-ph.IM] .

[38] J. W. Fowler, M. D. Niemack, S. R. Dicker, A. M. Aboobaker, P. A. R. Ade, E. S. Battistelli, M. J. Devlin, R. P. Fisher, M. Halpern, P. C. Hargrave, A. D. Hincks, M. Kaul, J. Klein, J. M. Lau, M. Limon, T. A. Marriage, P. D. Mauskopf, L. Page, S. T. Staggs, D. S. Swetz, E. R. Switzer, R. J. Thornton, and C. E. Tucker, "Optical design of the Atacama Cosmology Telescope and the Millimeter Bolometric Array Camera," Applied Optics **46**, 3444–3454 (2007), astro-ph/0701020 .

[39] J. E. Carlstrom *et al.*, "The 10 Meter South Pole Telescope," Publications of the Astronomical Society of the Pacific **123**, 568 (2011), arXiv:0907.4445 [astro-ph.IM] .

[40] Planck Collaboration, Ade, P. A. R., *et al.*, "Planck early results. I. The Planck mission," A&A **536**, A1 (2011).

[41] Wayne Hu and Scott Dodelson, "Cosmic microwave background anisotropies," Ann. Rev. Astron. Astrophys. **40**, 171–216 (2002), arXiv:astro-ph/0110414 [astro-ph] .

[42] P. de Bernardis *et al.* (Boomerang), "A Flat universe from high resolution maps of the cosmic microwave background radiation," Nature **404**, 955–959 (2000), arXiv:astro-ph/0004404 [astro-ph] .

[43] S. Hanany *et al.*, "MAXIMA-1: A Measurement of the cosmic microwave background anisotropy on angular scales of 10 arcminutes to 5 degrees," Astrophys. J. **545**, L5 (2000), arXiv:astro-ph/0005123 [astro-ph] .

[44] C. L. Bennett, D. Larson, J. L. Weiland, N. Jarosik, G. Hinshaw, N. Odegard, K. M. Smith, R. S. Hill, B. Gold, M. Halpern, E. Komatsu, M. R. Nolta, L. Page, D. N. Spergel, E. Wollack, J. Dunkley, A. Kogut, M. Limon, S. S. Meyer, G. S. Tucker, and E. L. Wright, "Nine-year Wilkinson Microwave Anisotropy Probe (WMAP) Observations: Final Maps and Results," ApJS **208**, 20 (2013), arXiv:1212.5225 [astro-ph.CO] .

[45] Wayne Hu, "Lecture Notes on CMB Theory: From Nucleosynthesis to Recombination," (2008), arXiv:0802.3688 [astro-ph] .

[46] Matias Zaldarriaga, "The polarization of the cosmic microwave background," in *Measuring and modeling the universe. Proceedings, Symposium, Pasadena, USA, November 17-22, 2002* (2003) pp. 309–329, arXiv:astro-ph/0305272 [astro-ph] .

[47] Marc Kamionkowski, Arthur Kosowsky, and Albert Stebbins, "Statistics of cosmic microwave background polarization," Physical Review D **55**, 7368 (1997).

[48] Uros Seljak and Matias Zaldarriaga, "Signature of gravity waves in the polarization of the microwave background," Physical Review Letters **78**, 2054 (1997).

[49] Matias Zaldarriaga and Uroš Seljak, "All-sky analysis of polarization in the microwave background," Physical Review D **55**, 1830 (1997).

[50] David N Spergel and Matias Zaldarriaga, "Cosmic microwave background polarization as a direct test of inflation," Physical Review Letters **79**, 2180 (1997).

[51] N. Aghanim *et al.* (Planck), "Planck 2018 results. VI. Cosmological parameters," (2018), arXiv:1807.06209 [astro-ph.CO] .

[52] R. Allison, P. Caucal, E. Calabrese, J. Dunkley, and T. Louis, "Towards a cosmological neutrino mass detection," Phys. Rev. **D92**, 123535 (2015), arXiv:1509.07471 [astro-ph.CO] .

[53] Ariel Goobar and Bruno Leibundgut, "Supernova Cosmology: Legacy and Future," Annual Review of Nuclear and Particle Science **61**, 251–279 (2011), arXiv:1102.1431 [astro-ph.CO] .

[54] M. Betoule, J. Marriner, N. Regnault, J.-C. Cuillandre, P. Astier, J. Guy, C. Balland, P. El Hage, D. Hardin, R. Kessler, L. Le Guillou, J. Mosher, R. Pain, P.-F. Rocci, M. Sako, and K. Schahmaneche, "Improved photometric calibration of the SNLS and the SDSS supernova surveys," A&A **552**, A124 (2013), arXiv:1212.4864 [astro-ph.CO] .

[55] Masao Sako *et al.* (SDSS), "The Data Release of the Sloan Digital Sky Survey-II Supernova Survey," Publ. Astron. Soc. Pac. **130**, 064002 (2018), arXiv:1401.3317 [astro-ph.CO] .

[56] P. Astier, J. Guy, N. Regnault, R. Pain, E. Aubourg, D. Balam, S. Basa, R. G. Carlberg, S. Fabbro, D. Fouchez, I. M. Hook, D. A. Howell, H. Lafoux, J. D. Neill, N. Palanque-Delabrouille, K. Perrett, C. J. Pritchet, J. Rich, M. Sullivan, R. Taillet, G. Aldering, P. Antilogus, V. Arsenijevic, C. Balland, S. Baumont, J. Bronder, H. Courtois, R. S. Ellis, M. Filiol, A. C. Gonçalves, A. Goobar, D. Guide, D. Hardin, V. Lusset, C. Lidman, R. McMahon, M. Mouchet, A. Mourao, S. Perlmutter, P. Ripoche, C. Tao, and N. Walton, "The Supernova Legacy Survey: measurement of Ω_M, Ω and w from the first year data set," A&A **447**, 31–48 (2006), astro-ph/0510447 .

[57] Daniel J. Eisenstein and Wayne Hu, "Baryonic features in the matter transfer function," The Astrophysical Journal **496**, 605–614 (1998).

[58] David M. Goldberg and Michael A. Strauss, "Determination of the baryon density from large scale galaxy redshift surveys," Astrophys. J. **495**, 29 (1998), arXiv:astro-ph/9707209 [astro-ph] .

[59] A. Meiksin, Martin White, and J. A. Peacock, "Baryonic signatures in large-scale structure," Monthly Notices of the Royal Astronomical Society **304**, 851–864 (1999).

[60] Shaun Cole *et al.* (2dFGRS), "The 2dF Galaxy Redshift Survey: Power-spectrum analysis of the final dataset and cosmological implications," Mon. Not. Roy. Astron. Soc. **362**, 505–534 (2005), arXiv:astro-ph/0501174 [astro-ph] .

[61] Shadab Alam *et al.* (BOSS), "The clustering of galaxies in the completed SDSS-III Baryon Oscillation Spectroscopic Survey: cosmological analysis of the DR12 galaxy sample," Mon. Not. Roy. Astron. Soc. **470**, 2617–2652 (2017), arXiv:1607.03155 [astro-ph.CO] .

[62] Eyal A. Kazin *et al.*, "The WiggleZ Dark Energy Survey: improved distance measurements to z = 1 with reconstruction of the baryonic acoustic feature," Mon. Not. Roy. Astron. Soc. **441**, 3524–3542 (2014), arXiv:1401.0358 [astro-ph.CO] .

[63] E. D. Loh and E. J. Spillar, "Photometric redshifts of galaxies," Astrophysical Journal **303**, 154–161 (1986).

[64] M. J. Sawicki, H. Lin, and H. K. C. Yee, "Evolution of the Galaxy Population Based on Photometric Redshifts in the Hubble Deep Field," Astronomical Journal **113**, 1–12 (1997), astro-ph/9610100 .

[65] Narciso Benitez, "Bayesian Photometric Redshift Estimation," The Astrophysical Journal **536**, 571–583 (2000).

[66] Yun Wang, Neta Bahcall, and Edwin L. Turner, "A Catalog of Color-based Redshift Estimates for $z \lesssim 4$ Galaxies in the Hubble Deep Field," The Astronomical Journal **116**, 2081–2085 (1998).

[67] Andrew E. Firth, Ofer Lahav, and Rachel S. Somerville, "Estimating photometric redshifts with artificial neural networks," Monthly Notices of the Royal Astronomical Society **339**, 1195–1202 (2003).

[68] Adrian A. Collister and Ofer Lahav, "ANNz: Estimating photometric redshifts using artificial neural networks," Publ. Astron. Soc. Pac. **116**, 345–351 (2004), arXiv:astro-ph/0311058 [astro-ph] .

[69] Emiliano Sefusatti and Roman Scoccimarro, "Galaxy bias and halo-occupation numbers from large-scale clustering," Phys. Rev. **D71**, 063001 (2005), arXiv:astro-ph/0412626 [astro-ph] .

[70] E. Lifshitz, "Republication of: On the gravitational stability of the expanding universe," J. Phys.(USSR) **10**, 116 (1946), [Gen. Rel. Grav.49,no.2,18(2017)].

[71] Steven W. Allen, August E. Evrard, and Adam B. Mantz, "Cosmological Parameters from Observations of Galaxy Clusters," Annual Review of Astronomy and Astrophysics **49**, 409–470 (2011).

[72] Vincent Desjacques, Donghui Jeong, and Fabian Schmidt, "Large-Scale Galaxy Bias," Phys. Rept. **733**, 1–193 (2018), arXiv:1611.09787 [astro-ph.CO] .

[73] Anthony Challinor and Antony Lewis, "The linear power spectrum of observed source number counts," Phys. Rev. **D84**, 043516 (2011), arXiv:1105.5292 [astro-ph.CO] .

[74] Camille Bonvin and Ruth Durrer, "What galaxy surveys really measure," Phys. Rev. **D84**, 063505 (2011), arXiv:1105.5280 [astro-ph.CO] .

[75] A. J. S. Hamilton, "Linear redshift distortions: A Review," in *Ringberg Workshop on Large Scale Structure Ringberg, Germany, September 23-28, 1996* (1997) arXiv:astro-ph/9708102 [astro-ph] .

[76] Hee-Jong Seo and Daniel J. Eisenstein, "Probing dark energy with baryonic acoustic oscillations from future large galaxy redshift surveys," Astrophys. J. **598**, 720–740 (2003), arXiv:astro-ph/0307460 [astro-ph] .

[77] J. C. Jackson, "A Critique of Rees's Theory of Primordial Gravitational Radiation," Monthly Notices of the Royal Astronomical Society **156**, 1P–5P (1972).

[78] N. Kaiser, "Clustering in real space and in redshift space," MNRAS **227**, 1–21 (1987).

[79] Ofer Lahav, Per B. Lilje, Joel R. Primack, and Martin J. Rees, "Dynamical effects of the cosmological constant," Monthly Notices of the Royal Astronomical Society **251**, 128–136 (1991).

[80] W. L. W. Sargent and E. L. Turner, "A statistical method for determining the cosmological density parameter from the redshifts of a complete sample of galaxies." The Astrophysical Journal **212**, L3–L7 (1977).

[81] Andrew Johnson, Chris Blake, Jason Dossett, Jun Koda, David Parkinson, and Shahab Joudaki, "Searching for Modified Gravity: Scale and Redshift Dependent Constraints from Galaxy Peculiar Velocities," Mon. Not. Roy. Astron. Soc. **458**, 2725–2744 (2016), arXiv:1504.06885 [astro-ph.CO] .

[82] Matthias Bartelmann and Peter Schneider, "Weak gravitational lensing," Phys. Rept. **340**, 291–472 (2001), arXiv:astro-ph/9912508 [astro-ph] .

[83] Alexandre Refregier, "Weak gravitational lensing by large scale structure," Ann. Rev. Astron. Astrophys. **41**, 645–668 (2003), arXiv:astro-ph/0307212 [astro-ph] .

[84] Tommaso Treu, "Strong Lensing by Galaxies," Annual Review of Astronomy and Astrophysics **48**, 87–125 (2010), https://doi.org/10.1146/annurev-astro-081309-130924 .

[85] David J. Bacon, Alexandre R. Refregier, and Richard S. Ellis, "Detection of weak gravitational lensing by large-scale structure," Monthly Notices of the Royal Astronomical Society **318**, 625–640 (2000).

[86] Nick Kaiser, Gillian Wilson, and Gerard A. Luppino, "Large-Scale Cosmic Shear Measurements," arXiv e-prints (2000), arXiv:astro-ph/0003338 [astro-ph] .

[87] L. Van Waerbeke, Y. Mellier, T. Erben, J. C. Cuillandre, F. Bernardeau, R. Maoli, E. Bertin, H. J. McCracken, O. Le Fèvre, B. Fort, M. Dantel-Fort, B. Jain, and P. Schneider, "Detection of correlated galaxy ellipticities from CFHT data: first evidence for gravitational lensing by large-scale structures," A&A **358**, 30–44 (2000), astro-ph/0002500 .

[88] D. M. Wittman, J. A. Tyson, D. Kirkman, I. Dell'Antonio, and G. Bernstein, "Detection of weak gravitational lensing distortions of distant galaxies by cosmic dark matter at large scales," Nature **405**, 143–148 (2000), astro-ph/0003014 .

[89] Yannick Mellier, "Probing the universe with weak lensing," Ann. Rev. Astron. Astrophys. **37**, 127–189 (1999), arXiv:astro-ph/9812172 [astro-ph] .

[90] Nick Kaiser, "Weak Lensing and Cosmology," The Astrophysical Journal **498**, 26–42 (1998).

[91] Marcel P. van Daalen, Joop Schaye, C. M. Booth, and Claudio Dalla Vecchia, "The effects of galaxy formation on the matter power spectrum: a challenge for precision cosmology," MNRAS **415**, 3649–3665 (2011), arXiv:1104.1174 [astro-ph.CO] .

[92] Tim Eifler, Elisabeth Krause, Scott Dodelson, Andrew Zentner, Andrew Hearin, and Nickolay Gnedin, "Accounting for baryonic effects in cosmic shear tomography: Determining a minimal set of nuisance parameters using PCA," Mon. Not. Roy. Astron. Soc. **454**, 2451–2471 (2015), arXiv:1405.7423 [astro-ph.CO] .

[93] Nora Elisa Chisari, Mark L. A. Richardson, Julien Devriendt, Yohan Dubois, Aurel Schneider, M. C. Brun, Amandine Le, Ricarda S. Beckmann, Sebastien Peirani, Adrianne Slyz, and Christophe Pichon, "The impact of baryons on the matter power spectrum from the Horizon-AGN cosmological hydrodynamical simulation," (2018), 10.1093/mnras/sty2093, arXiv:1801.08559 [astro-ph.CO] .

[94] Peter L. Taylor, Thomas D. Kitching, and Jason D. McEwen, "Preparing for the Cosmic Shear Data Flood: Optimal Data Extraction and Simulation Requirements for Stage IV Dark Energy Experiments," Phys. Rev. **D98**, 043532 (2018), arXiv:1804.03667 [astro-ph.CO] .

[95] Hung-Jin Huang, Tim Eifler, Rachel Mandelbaum, and Scott Dodelson, "Modeling baryonic physics in future weak lensing surveys," (2018), arXiv:1809.01146 [astro-ph.CO] .

[96] Nora Elisa Chisari *et al.*, "Modelling baryonic feedback for survey cosmology," (2019), 10.21105/astro.1905.06082, arXiv:1905.06082 [astro-ph.CO] .

[97] Christopher M. Hirata and Uros Seljak, "Intrinsic alignment-lensing interference as a contaminant of cosmic shear," Phys. Rev. D **70**, 063526 (2004).

[98] Nora Elisa Chisari, Rachel Mandelbaum, Michael A. Strauss, Eric M. Huff, and Neta A. Bahcall, "Intrinsic alignments of group and cluster galaxies in photometric surveys," Monthly Notices of the Royal Astronomical Society **445**, 726–748 (2014).

[99] Nora Elisa Chisari, Sandrine Codis, Clotilde Laigle, Yohan Dubois, Christophe Pichon, Julien Devriendt, Adrianne Slyz, Lance Miller, Raphael Gavazzi, and Karim Benabed, "Intrinsic alignments of galaxies in the Horizon-AGN cosmological hydrodynamical simulation," Mon. Not. Roy. Astron. Soc. **454**, 2736–2753 (2015), arXiv:1507.07843 [astro-ph.CO] .

[100] Nora Elisa Chisari and Cora Dvorkin, "Cosmological Information in the Intrinsic Alignments of Luminous Red Galaxies," JCAP **1312**, 029 (2013), arXiv:1308.5972 [astro-ph.CO] .

[101] LSST Science Collaboration, P. A. Abell, J. Allison, S. F. Anderson, J. R. Andrew, J. R. P. Angel, L. Armus, D. Arnett, S. J. Asztalos, T. S. Axelrod, and et al., "LSST Science Book, Version 2.0," ArXiv e-prints (2009), arXiv:0912.0201 [astro-ph.IM] .

[102] M. Levi, C. Bebek, T. Beers, R. Blum, R. Cahn, D. Eisenstein, B. Flaugher, K. Honscheid, R. Kron, O. Lahav, P. McDonald, N. Roe, D. Schlegel, and representing the DESI collaboration, "The DESI Experiment, a whitepaper for Snowmass 2013," ArXiv e-prints (2013), arXiv:1308.0847 [astro-ph.CO] .

[103] R. Laureijs, J. Amiaux, S. Arduini, J. . Augueres, J. Brinchmann, R. Cole, M. Cropper, C. Dabin, L. Duvet, A. Ealet, and et al., "Euclid Definition Study Report," ArXiv e-prints (2011), arXiv:1110.3193 [astro-ph.CO] .

[104] R. A. Sunyaev and Y. B. Zeldovich, "The Observations of Relic Radiation as a Test of the Nature of X-Ray Radiation from the Clusters of Galaxies," Comments on Astrophysics and Space Physics **4**, 173 (1972).

[105] J. E. Carlstrom, G. P. Holder, and E. D. Reese, "Cosmology with the Sunyaev-Zel'dovich Effect," Annual Review of Astronomy and Astrophysics **40**, 643–680 (2002), astro-ph/0208192 .

[106] Julien Lesgourgues and Sergio Pastor, "Neutrino mass from Cosmology," Adv. High Energy Phys. **2012**, 608515 (2012), arXiv:1212.6154 [hep-ph] .

[107] Laura Salvati, Marian Douspis, and Nabila Aghanim, "Constraints from thermal Sunyaev-Zeldovich cluster counts and power spectrum combined with CMB," (2017), 10.1051/0004-6361/201731990, arXiv:1708.00697 [astro-ph.CO] .

[108] A. Gardini, E. Rasia, P. Mazzotta, G. Tormen, S. De Grandi, and L. Moscardini, "Simulating Chandra observations of galaxy clusters," Monthly Notices of the Royal Astronomical Society **351**, 505–514 (2004).

[109] Jean-Baptiste Melin and James G. Bartlett, "Measuring cluster masses with CMB lensing: a statistical approach," A&A **578**, A21 (2015), arXiv:1408.5633 [astro-ph.CO] .

[110] A. Blanchard and J. Schneider, "Gravitational lensing effect on the fluctuations of the cosmic background radiation," A&A **184**, 1–6 (1987).

[111] S. Cole and G. Efstathiou, "Gravitational lensing of fluctuations in the microwave background radiation," MNRAS **239**, 195–200 (1989).

[112] Uros Seljak, "Gravitational lensing effect on cosmic microwave background anisotropies: A Power spectrum approach," Astrophys. J. **463**, 1 (1996), arXiv:astro-ph/9505109 [astro-ph] .

[113] Antony Lewis and Anthony Challinor, "Weak gravitational lensing of the CMB," Phys. Rept. **429**, 1–65 (2006), arXiv:astro-ph/0601594 [astro-ph] .

[114] Uros Seljak and Matias Zaldarriaga, "Measuring Dark Matter Power Spectrum from Cosmic Microwave Background," Phys. Rev. Lett. **82**, 2636–2639 (1999).

[115] Marcel P. van Daalen, Joop Schaye, Ian G. McCarthy, C. M. Booth, and Claudio Dalla Vecchia, "The impact of baryonic processes on the two-point correlation functions of galaxies, subhaloes and matter," Mon. Not. Roy. Astron. Soc. **440**, 2997–3010 (2014), arXiv:1310.7571 [astro-ph.CO] .

[116] Sudeep Das, Blake D. Sherwin, *et al.*, "Detection of the Power Spectrum of Cosmic Microwave Background Lensing by the Atacama Cosmology Telescope," Phys. Rev. Letters **107**, 021301 (2011), arXiv:1103.2124 [astro-ph.CO] .

[117] R. Keisler, C. L. Reichardt, *et al.*, "A Measurement of the Damping Tail of the Cosmic Microwave Background Power Spectrum with the South Pole Telescope," The Astrophysical Journal **743**, 28 (2011), arXiv:1105.3182 [astro-ph.CO] .

[118] P. A. R. Ade *et al.* (Planck), "Planck 2013 results. XVII. Gravitational lensing by large-scale structure," Astron. Astrophys. **571**, A17 (2014), arXiv:1303.5077 [astro-ph.CO] .

[119] Matias Zaldarriaga and Uros Seljak, "Gravitational lensing effect on cosmic microwave background polarization," Phys. Rev. **D58**, 023003 (1998), arXiv:astro-ph/9803150 [astro-ph] .

[120] Marc Kamionkowski, Arthur Kosowsky, and Albert Stebbins, "A Probe of primordial gravity waves and vorticity," Phys. Rev. Lett. **78**, 2058–2061 (1997), arXiv:astro-ph/9609132 [astro-ph] .

[121] James Aguirre *et al.* (Simons Observatory), "The Simons Observatory: Science goals and forecasts," JCAP **1902**, 056 (2019), arXiv:1808.07445 [astro-ph.CO] .

[122] Y. Akrami *et al.* (Planck), "Planck 2018 results. X. Constraints on inflation," (2018), arXiv:1807.06211 [astro-ph.CO] .

[123] Uros Seljak and Christopher M. Hirata, "Gravitational lensing as a contaminant of the gravity wave signal in CMB," Phys. Rev. **D69**, 043005 (2004), arXiv:astro-ph/0310163 [astro-ph] .

[124] Blake D. Sherwin and Marcel Schmittfull, "Delensing the CMB with the Cosmic Infrared Background," Phys. Rev. **D92**, 043005 (2015), arXiv:1502.05356 [astro-ph.CO] .

[125] Kendrick M. Smith, Duncan Hanson, Marilena LoVerde, Christopher M. Hirata, and Oliver Zahn, "Delensing CMB polarization with external datasets," Journal of Cosmology and Astro-Particle Physics **2012**, 014 (2012), arXiv:1010.0048 [astro-ph.CO] .

[126] Andre de Gouvea, "TASI lectures on neutrino physics," (2004) pp. 197–258, arXiv:hep-ph/0411274 [hep-ph] .

[127] C. L. Cowan, F. Reines, F. B. Harrison, H. W. Kruse, and A. D. McGuire, "Detection of the free neutrino: a confirmation," Science **124**, 103–104 (1956).

[128] G. Danby, J-M. Gaillard, K. Goulianos, L. M. Lederman, N. Mistry, M. Schwartz, and J. Steinberger, "Observation of high-energy neutrino reactions and the existence of two kinds of neutrinos," Phys. Rev. Lett. **9**, 36–44 (1962).

[129] K. Kodama *et al.*, "Observation of tau neutrino interactions," Physics Letters B **504**, 218 – 224 (2001).

[130] The LEP Collaborations: ALEPH Collaboration, DELPHI Collaboration, L3 Collaboration, OPAL Collaboration, and the LEP Electroweak Working Group, "A Combination of Preliminary Electroweak Measurements and Constraints on the Standard Model," arXiv e-prints , hep-ex/0612034 (2006), arXiv:hep-ex/0612034 [hep-ex] .

[131] Gary Steigman, "Neutrinos And Big Bang Nucleosynthesis," Adv. High Energy Phys. **2012**, 268321 (2012), arXiv:1208.0032 [hep-ph] .

[132] T. Kajita, "Atmospheric neutrinos and discovery of neutrino oscillations," Proceedings of the Japan Academy, Series B Physical and Biological Sciences **86(4)**, 303–321 (2010).

[133] Edward Kearns, "Experimental measurements of atmospheric neutrinos," Nuclear Physics B - Proceedings Supplements **70**, 315 – 323 (1999), proceedings of the Fifth International Workshop on topics in Astroparticle and Underground Physics.

[134] John G. Learned (Super-Kamiokande), "The Atmospheric neutrino anomaly: Muon neutrino disappearance," , 89–130 (2000), arXiv:hep-ex/0007056 [hep-ex] .

[135] Y. Fukuda *et al.* (Super-Kamiokande Collaboration), "Evidence for oscillation of atmospheric neutrinos," Phys. Rev. Lett. **81**, 1562–1567 (1998).

[136] Bruce T. Cleveland, Timothy Daily, Jr. Raymond Davis, James R. Distel, Kenneth Lande, C. K. Lee, Paul S. Wildenhain, and Jack Ullman, "Measurement of the solar electron neutrino flux with the homestake chlorine detector," The Astrophysical Journal **496**, 505 (1998).

[137] K. S. Hirata, T. Kajita, T. Kifune, K. Kihara, M. Nakahata, K. Nakamura, S. Ohara, Y. Oyama, N. Sato, M. Takita, Y. Totsuka, Y. Yaginuma, M. Mori, A. Suzuki, K. Takahashi, T. Tanimori, M. Yamada, M. Koshiba, T. Suda, K. Miyano, H. Miyata, H. Takei, K. Kaneyuki,

H. Nagashima, Y. Suzuki, E. W. Beier, L. R. Feldscher, E. D. Frank, W. Frati, S. B. Kim, A. K. Mann, F. M. Newcomer, R. Van Berg, and W. Zhang, "Observation of ^{8}B solar neutrinos in the Kamiokande-II detector," Phys. Rev. Lett. **63**, 16–19 (1989).

[138] John N. Bahcall, Neta A. Bahcall, and Giora Shaviv, "Present status of the theoretical predictions for the ^{37}Cl solar-neutrino experiment," Phys. Rev. Lett. **20**, 1209–1212 (1968).

[139] W. C. Haxton, "The Solar Neutrino Problem," Annual Review of Astronomy and Astrophysics **33**, 459–504 (1995), hep-ph/9503430 .

[140] T J Bowles and V N Gavrin, "The status of the solar neutrino problem," Annual Review of Nuclear and Particle Science **43**, 117–164 (1993).

[141] Q. R. Ahmad and ohers (SNO Collaboration), "Direct evidence for neutrino flavor transformation from neutral-current interactions in the sudbury neutrino observatory," Phys. Rev. Lett. **89**, 011301 (2002).

[142] Ziro Maki, Masami Nakagawa, and Shoichi Sakata, "Remarks on the unified model of elementary particles," Progress of Theoretical Physics **28**, 870–880 (1962).

[143] B. Pontecorvo, "Neutrino Experiments and the Problem of Conservation of Leptonic Charge," Sov. Phys. JETP **26**, 984–988 (1968), [Zh. Eksp. Teor. Fiz.53,1717(1967)].

[144] M. Tanabashi *et al.* (Particle Data Group), "2018 Review of Particle Physics," Phys. Rev. **D 98**, 030001 (2018).

[145] S.M. Bilenky, J. Hoek, and S.T. Petcov, "On the oscillations of neutrinos with dirac and majorana masses," Physics Letters B **94**, 495 – 498 (1980).

[146] J. Schlechter and J. W. F. Valle, "Neutrinoless double-β decay in SU(2)xU(1) theories," Phys. Rev. **25**, 2951 (1982).

[147] M. Doi, T. Kotani, H. Nishiura, K. Okuda, and E. Takasugi, "CP violation in Majorana neutrinos," Physics Letters B **102**, 323 – 326 (1981).

[148] Q. R. Ahmad *et al.* (SNO Collaboration), "Measurement of the rate of $\nu_e + d \rightarrow p + p + e^-$ Interactions Produced by ^{8}B Solar Neutrinos at the Sudbury Neutrino Observatory," Phys. Rev. Lett. **87**, 071301 (2001).

[149] Peter Minkowski, "$\mu \rightarrow$eγ at a rate of one out of 109 muon decays?" Physics Letters B **67**, 421 – 428 (1977).

[150] Murray Gell-Mann, Pierre Ramond, and Richard Slansky, "Complex Spinors and Unified Theories," *Supergravity Workshop Stony Brook, New York, September 27-28, 1979*, Conf. Proc. **C790927**, 315–321 (1979), arXiv:1306.4669 [hep-th] .

[151] Tsutomu Yanagida, "Horizontal Symmetry and Masses of Neutrinos," Progress of Theoretical Physics **64**, 1103–1105 (1980).

[152] S. L. Glashow, "The future of elementary particle physics," in *Quarks and Leptons*, edited by Maurice Lévy, Jean-Louis Basdevant, David Speiser, Jacques Weyers, Raymond Gastmans, and Maurice Jacob (Springer US, Boston, MA, 1980) pp. 687–713.

[153] Rabindra N. Mohapatra and Goran Senjanović, "Neutrino mass and spontaneous parity nonconservation," Phys. Rev. Lett. **44**, 912–915 (1980).

[154] Mark Thomson, *Modern Particle Physics* (Cambridge University Press, 2013).

[155] Andre De Gouvea, "Neutrinos have mass: So what?" Mod. Phys. Lett. **A19**, 2799–2813 (2004), arXiv:hep-ph/0503086 [hep-ph] .

[156] Andr de Gouva, "Neutrino Mass Models," Annual Review of Nuclear and Particle Science **66**, 197–217 (2016).

[157] P. A. R. Ade *et al.* (Planck Collaboration), "Planck 2015 results. XIII. Cosmological parameters," A&A **594**, A13 (2016), arXiv:1502.01589 [astro-ph.CO] .

[158] K. Ichikawa, M. Fukugita, and M. Kawasaki, "Constraining neutrino masses by CMB experiments alone," Phys. Rev. D **71**, 043001 (2005), astro-ph/0409768 .

[159] D. A. Dicus, E. W. Kolb, A. M. Gleeson, E. C. G. Sudarshan, V. L. Teplitz, and M. S. Turner, "Primordial nucleosynthesis including radiative, Coulomb, and finite-temperature corrections to weak rate," Phys. Rev. D **26**, 2694 (1982).

[160] G. Mangano, G. Miele, S. Pastor, and M. Peloso, "A precision calculation of the effective number of cosmological neutrinos," Physics Letters B **534**, 8–16 (2002), astro-ph/0111408 .

[161] Pablo F. de Salas and Sergio Pastor, "Relic neutrino decoupling with flavour oscillations revisited," JCAP **1607**, 051 (2016), arXiv:1606.06986 [hep-ph] .

[162] Roberto Trotta and Steen H. Hansen, "Observing the helium abundance with CMB," Phys. Rev. **D69**, 023509 (2004), arXiv:astro-ph/0306588 [astro-ph] .

[163] S. Bashinsky and U. Seljak, "Signatures of relativistic neutrinos in CMB anisotropy and matter clustering," Phys. Rev. D **69**, 083002 (2004), astro-ph/0310198 .

[164] Kazuhide Ichikawa and Tomo Takahashi, "Revisiting the constraint on the helium abundance from CMB," Phys. Rev. **D73**, 063528 (2006), arXiv:astro-ph/0601099 [astro-ph] .

[165] Fabio Iocco, Gianpiero Mangano, Gennaro Miele, Ofelia Pisanti, and Pasquale D. Serpico, "Primordial Nucleosynthesis: from precision cosmology to fundamental physics," Phys. Rept. **472**, 1–76 (2009), arXiv:0809.0631 [astro-ph] .

[166] Z. Hou, R. Keisler, L. Knox, M. Millea, and C. Reichardt, "How massless neutrinos affect the cosmic microwave background damping tail," Phys. Rev. D **87**, 083008 (2013), arXiv:1104.2333 [astro-ph.CO] .

[167] M. Archidiacono, E. Calabrese, and A. Melchiorri, "Case for dark radiation," Phys. Rev. D **84**, 123008 (2011), arXiv:1109.2767 [astro-ph.CO] .

[168] G. Steigmann, "Neutrinos and Big Bang Nucleosynthesis," Adv. High Energy Physics **2012**, 268321 (2012), arXiv:1208.0032 [hep-ph] .

[169] Brent Follin, Lloyd Knox, Marius Millea, and Zhen Pan, "First Detection of the Acoustic Oscillation Phase Shift Expected from the Cosmic Neutrino Background," Phys. Rev. Lett. **115**, 091301 (2015), arXiv:1503.07863 [astro-ph.CO] .

[170] Daniel Green, Joel Meyers, and Alexander van Engelen, "CMB Delensing Beyond the B Modes," (2016), arXiv:1609.08143 [astro-ph.CO] .

[171] K. N. Abazajian *et al.* (Topical Conveners: K.N. Abazajian, J.E. Carlstrom, A.T. Lee), "Neutrino Physics from the Cosmic Microwave Background and Large Scale Structure," Astropart. Phys. **63**, 66–80 (2015), arXiv:1309.5383 [astro-ph.CO] .

[172] W. Hu, D. J. Eisenstein, and M. Tegmark, "Weighing neutrinos with galaxy surveys," Phys. Rev. Lett. **80**, 5255–5258 (1998), arXiv:astro-ph/9712057 [astro-ph] .

[173] A. Font-Ribera, P. McDonald, N. Mostek, B. A. Reid, H.-J. Seo, and A. Slosar, "DESI and other Dark Energy experiments in the era of neutrino mass measurements," JCAP **5**, 023 (2014), arXiv:1308.4164 .

[174] K. N. Abazajian *et al.*, "Cosmological and Astrophysical Neutrino Mass Measurements," Astropart. Phys. **35**, 177–184 (2011), arXiv:1103.5083 [astro-ph.CO] .

[175] A. Lewis and A. Challinor, "Weak gravitational lensing of the CMB," Phys. Rept. **429**, 1–65 (2006), astro-ph/0601594 .

[176] R. de Putter, O. Zahn, and E. V. Linder, "CMB lensing constraints on neutrinos and dark energy," Phys. Rev. D **79**, 065033 (2009), arXiv:0901.0916 [astro-ph.CO] .

[177] P. A. R. Ade *et al.* (Planck Collaboration), "Planck 2013 results. XVI. Cosmological parameters," A&A **571**, A16 (2014), arXiv:1303.5076 [astro-ph.CO] .

[178] B. D. Sherwin, A. van Engelen, N. Sehgal, M. Madhavacheril, *et al.*, "The Atacama Cosmology Telescope: Two-Season ACTPol Lensing Power Spectrum," ArXiv e-prints (2016), arXiv:1611.09753 .

[179] T. P. Walker, G. Steigman, D. N. Schramm, K. A. Olive, and H.-S. Kang, "Primordial nucleosynthesis redux," The Astrophysical Journal **376**, 51–69 (1991).

[180] "Primordial nucleosynthesis: From precision cosmology to fundamental physics," Physics Reports **472**, 1 – 76 (2009).

[181] Richard H. Cyburt, Brian D. Fields, Keith A. Olive, and Tsung-Han Yeh, "Big bang nucleosynthesis: Present status," Rev. Mod. Phys. **88**, 015004 (2016).

[182] Y. I. Izotov, T. X. Thuan, and N. G. Guseva, "A new determination of the primordial He abundance using the He i λ10830 emission line: cosmological implications," Mon. Not. Roy. Astron. Soc. **445**, 778–793 (2014), arXiv:1408.6953 [astro-ph.CO] .

[183] Francesco Capozzi, Eleonora Di Valentino, Eligio Lisi, Antonio Marrone, Alessandro Melchiorri, and Antonio Palazzo, "Global constraints on absolute neutrino masses and their ordering," Phys. Rev. D **95**, 096014 (2017).

[184] Kevork N. Abazajian *et al.* (CMB-S4), "CMB-S4 Science Book, First Edition," (2016), arXiv:1610.02743 [astro-ph.CO] .

[185] James Aguirre *et al.* (Simons Observatory), "The Simons Observatory: Science goals and forecasts," (2018), arXiv:1808.07445 [astro-ph.CO] .

[186] E. Calabrese, D. Alonso, and J. Dunkley, "Complementing the ground-based CMB Stage-4 experiment on large scales with the PIXIE satellite," ArXiv e-prints (2016), arXiv:1611.10269 [astro-ph.CO] .

[187] Thibaut Louis and David Alonso, "Calibrating Cluster Number Counts with CMB lensing," Phys. Rev. **D95**, 043517 (2017), arXiv:1609.03997 [astro-ph.CO] .

[188] E. Di Valentino, T. Brinckmann, M. Gerbino, V. Poulin, F. R. Bouchet, J. Lesgourgues, A. Melchiorri, and the CORE collaboration, "Exploring Cosmic Origins with CORE: Cosmological Parameters," ArXiv e-prints (2016), arXiv:1612.00021 [astro-ph.CO] .

[189] Gianpiero Mangano, Gennaro Miele, Sergio Pastor, Ofelia Pisanti, and Srdjan Sarikas, "Updated BBN bounds on the cosmological lepton asymmetry for non-zero θ_{13}," Phys. Lett. B **708**, 1 (2012), arXiv:1110.4335 [hep-ph] .

[190] V.M. Lobashev, "The search for the neutrino mass by direct method in the tritium beta-decay and perspectives of study it in the project katrin," Nuclear Physics A **719**, C153 – C160 (2003).

[191] Ch. Kraus *et al.*, "Final results from phase II of the Mainz neutrino mass search in tritium beta decay," Eur. Phys. J. **C40**, 447–468 (2005), arXiv:hep-ex/0412056 [hep-ex] .

[192] V. N. Aseev, A. I. Belesev, A. I. Berlev, E. V. Geraskin, A. A. Golubev, N. A. Likhovid, V. M. Lobashev, A. A. Nozik, V. S. Pantuev, V. I. Parfenov, A. K. Skasyrskaya, F. V. Tkachov, and S. V. Zadorozhny, "Upper limit on the electron antineutrino mass from the troitsk experiment," Phys. Rev. D **84**, 112003 (2011).

[193] G. Drexlin, V. Hannen, S. Mertens, and C. Weinheimer, "Current direct neutrino mass experiments," Adv. High Energy Phys. **2013**, 293986 (2013), arXiv:1307.0101 [physics.ins-det] .

[194] M. Aker *et al.* (KATRIN), "An improved upper limit on the neutrino mass from a direct kinematic method by KATRIN," (2019), arXiv:1909.06048 [hep-ex] .

[195] M. G. Betti *et al.* (PTOLEMY), "Neutrino physics with the PTOLEMY project: active neutrino properties and the light sterile case," JCAP **1907**, 047 (2019), arXiv:1902.05508 [astro-ph.CO] .

[196] A. Aguilar, L. B. Auerbach, R. L. Burman, D. O. Caldwell, E. D. Church, A. K. Cochran, J. B. Donahue, A. Fazely, G. T. Garvey, R. M. Gunasingha, R. Imlay, W. C. Louis, R. Majkic, A. Malik, W. Metcalf, G. B. Mills, V. Sandberg, D. Smith, I. Stancu, M. Sung, R. Tayloe, G. J. VanDalen, W. Vernon, N. Wadia, D. H. White, and S. Yellin (LSND Collaboration), "Evidence for neutrino oscillations from the observation of $\overline{\nu}_e$ appearance in a $\overline{\nu}_\mu$ beam," Phys. Rev. D **64**, 112007 (2001).

[197] A. A. Aguilar-Arevalo *et al.* (MiniBooNE), "Significant Excess of ElectronLike Events in the MiniBooNE Short-Baseline Neutrino Experiment," Phys. Rev. Lett. **121**, 221801 (2018), arXiv:1805.12028 [hep-ex] .

[198] Alessandro Mirizzi, Gianpiero Mangano, Ninetta Saviano, Enrico Borriello, Carlo Giunti, Gennaro Miele, and Ofelia Pisanti, "The strongest bounds on active-sterile neutrino mixing after planck data," Physics Letters B **726**, 8 – 14 (2013).

[199] Steen Hannestad, Rasmus Sloth Hansen, Thomas Tram, and Yvonne Y.Y. Wong, "Active-sterile neutrino oscillations in the early universe with full collision terms," Journal of Cosmology and Astroparticle Physics **2015**, 019–019 (2015).

[200] Kevork N. Abazajian, "Sterile neutrinos in cosmology," Phys. Rept. **711-712**, 1–28 (2017), arXiv:1705.01837 [hep-ph] .

[201] Scott Dodelson and Lawrence M. Widrow, "Sterile-neutrinos as dark matter," Phys. Rev. Lett. **72**, 17–20 (1994), arXiv:hep-ph/9303287 [hep-ph] .

[202] Uros Seljak, Alexey Makarov, Patrick McDonald, and Hy Trac, "Can sterile neutrinos be the dark matter?" Phys. Rev. Lett. **97**, 191303 (2006), arXiv:astro-ph/0602430 [astro-ph] .

[203] Esra Bulbul, Maxim Markevitch, Adam Foster, Randall K. Smith, Michael Loewenstein, and Scott W. Randall, "Detection of An Unidentified Emission Line in the Stacked X-ray spectrum of Galaxy Clusters," Astrophys. J. **789**, 13 (2014), arXiv:1402.2301 [astro-ph.CO] .

[204] Alexey Boyarsky, Oleg Ruchayskiy, Dmytro Iakubovskyi, and Jeroen Franse, "Unidentified Line in X-Ray Spectra of the Andromeda Galaxy and Perseus Galaxy Cluster," Phys. Rev. Lett. **113**, 251301 (2014), arXiv:1402.4119 [astro-ph.CO] .

[205] Kevork N. Abazajian, "Resonantly Produced 7 keV Sterile Neutrino Dark Matter Models and the Properties of Milky Way Satellites," Phys. Rev. Lett. **112**, 161303 (2014), arXiv:1403.0954 [astro-ph.CO] .

[206] O. Cremonesi and M. Pavan, "Challenges in Double Beta Decay," Adv. High Energy Phys. **2014**, 951432 (2014), arXiv:1310.4692 [physics.ins-det] .

[207] S. M. Bilenky, Amand Faessler, and F. Simkovic, "The Majorana neutrino masses, neutrinoless double beta decay and nuclear matrix elements," Phys. Rev. **D70**, 033003 (2004), arXiv:hep-ph/0402250 [hep-ph] .

[208] Markus A. Luty, "Baryogenesis via leptogenesis," Phys. Rev. D **45**, 455–465 (1992).

[209] E W Kolb and M S Turner, "Grand Unified Theories and the Origin of the Baryon Asymmetry," Annual Review of Nuclear and Particle Science **33**, 645–696 (1983).

[210] K. Abe *et al.* (T2K Collaboration), "Search for CP Violation in Neutrino and Antineutrino Oscillations by the T2K Experiment with 2.2×10^{21} Protons on Target," Phys. Rev. Lett. **121**, 171802 (2018).

[211] M. Agostini *et al.* (GERDA), "Results on Neutrinoless Double-β Decay of ^{76}Ge from Phase I of the GERDA Experiment," Phys. Rev. Lett. **111**, 122503 (2013), arXiv:1307.4720 [nucl-ex] .

[212] C. Alduino *et al.* (CUORE), "First Results from CUORE: A Search for Lepton Number Violation via $0\nu\beta\beta$ Decay of ^{130}Te," Phys. Rev. Lett. **120**, 132501 (2018), arXiv:1710.07988 [nucl-ex] .

[213] A. Gando *et al.* (KamLAND-Zen), "Search for Majorana Neutrinos near the Inverted Mass Hierarchy Region with KamLAND-Zen," Phys. Rev. Lett. **117**, 082503 (2016), [Addendum: Phys. Rev. Lett.117,no.10,109903(2016)], arXiv:1605.02889 [hep-ex] .

[214] S. Andringa *et al.* (SNO+), "Current Status and Future Prospects of the SNO+ Experiment," Adv. High Energy Phys. **2016**, 6194250 (2016), arXiv:1508.05759 [physics.ins-det] .

[215] Massimiliano Lattanzi and Martina Gerbino, "Status of neutrino properties and future prospects - Cosmological and astrophysical constraints," Front.in Phys. **5**, 70 (2018), arXiv:1712.07109 [astro-ph.CO] .

[216] Raul Jimenez, Thomas Kitching, Carlos Pena-Garay, and Licia Verde, "Can we measure the neutrino mass hierarchy in the sky?" JCAP **1005**, 035 (2010), arXiv:1003.5918 [astro-ph.CO] .

[217] Martina Gerbino, Massimiliano Lattanzi, Olga Mena, and Katherine Freese, "A novel approach to quantifying the sensitivity of current and future cosmological datasets to the neutrino mass ordering through Bayesian hierarchical modeling," Phys. Lett. **B775**, 239–250 (2017), arXiv:1611.07847 [astro-ph.CO] .

[218] Sunny Vagnozzi, Elena Giusarma, Olga Mena, Katherine Freese, Martina Gerbino, Shirley Ho, and Massimiliano Lattanzi, "Unveiling ν secrets with cosmological data: neutrino masses and mass hierarchy," Phys. Rev. **D96**, 123503 (2017), arXiv:1701.08172 [astro-ph.CO] .

[219] Steen Hannestad and Thomas Schwetz, "Cosmology and the neutrino mass ordering," JCAP **1611**, 035 (2016), arXiv:1606.04691 [astro-ph.CO] .

[220] Francesco Capozzi, Eleonora Di Valentino, Eligio Lisi, Antonio Marrone, Alessandro Melchiorri, and Antonio Palazzo, "Global constraints on absolute neutrino masses and their ordering," Phys. Rev. **D95**, 096014 (2017), arXiv:1703.04471 [hep-ph] .

[221] S. Gariazzo, M. Archidiacono, P. F. de Salas, O. Mena, C. A. Ternes, and M. Trtola, "Neutrino masses and their ordering: Global Data, Priors and Models," JCAP **1803**, 011 (2018), arXiv:1801.04946 [hep-ph] .

[222] Shouvik Roy Choudhury and Steen Hannestad, "Updated results on neutrino mass and mass hierarchy from cosmology," (2019), arXiv:1907.12598 [astro-ph.CO] .

[223] P. F. De Salas, S. Gariazzo, O. Mena, C. A. Ternes, and M. Trtola, "Neutrino Mass Ordering from Oscillations and Beyond: 2018 Status and Future Prospects," Front. Astron. Space Sci. **5**, 36 (2018), arXiv:1806.11051 [hep-ph] .

[224] L. Amendola and S. Tsujikawa, *Dark Energy : Theory and Observations by Luca Amendola and Shinji Tsujikawa. Cambridge University Press, 2010. ISBN: 9780521516006* (2010).

[225] Ronald A Fisher, "The logic of inductive inference," Journal of the royal statistical society **98**, 39–82 (1935).

[226] Harald Cramér, "A contribution to the theory of statistical estimation," Scandinavian Actuarial Journal **1946**, 85–94 (1946).

[227] C Radhakrishna Rao, "Information and the accuracy attainable in the estimation of statistical parameters," in *Breakthroughs in statistics* (Springer, 1992) pp. 235–247.

[228] Walter R Gilks, Sylvia Richardson, and David Spiegelhalter, *Markov chain Monte Carlo in practice* (Chapman and Hall/CRC, 1995).

[229] N. Metropolis, A. W. Rosenbluth, M. N. Rosenbluth, A. H. Teller, and E. Teller, "Equation of State Calculations by Fast Computing Machines," The Journal of Chemical Physics **21**, 1087–1092 (1953).

[230] RM Neal, "Technical report CRG-TR-93-1," Dept. of Computer Science, University of Toronto (1993).

[231] Andrew Gelman, Donald B Rubin, *et al.*, "Inference from iterative simulation using multiple sequences," Statistical science **7**, 457–472 (1992).

[232] Joanna Dunkley, Martin Bucher, Pedro G. Ferreira, Kavilan Moodley, and Constantinos Skordis, "Fast and reliable mcmc for cosmological parameter estimation," Mon. Not. Roy. Astron. Soc. **356**, 925–936 (2005), arXiv:astro-ph/0405462 [astro-ph] .

[233] B. D. Sherwin, J. Dunkley, S. Das, *et al.*, "Evidence for Dark Energy from the Cosmic Microwave Background Alone Using the Atacama Cosmology Telescope Lensing Measurements," Physical Review Letters **107**, 021302 (2011), arXiv:1105.0419 [astro-ph.CO] .

[234] E. J. Copeland, M. Sami, and S. Tsujikawa, "Dynamics of Dark Energy," International Journal of Modern Physics D **15**, 1753–1935 (2006), arXiv:hep-th/0603057 [hep-th] .

[235] P. A. R. Ade *et al.* (Planck Collaboration), "Planck 2015 results. XIV. Dark energy and modified gravity," A&A **594**, A14 (2016), arXiv:1502.01590 [astro-ph.CO] .

[236] E. Calabrese, R. de Putter, D. Huterer, E. V. Linder, and A. Melchiorri, "Future CMB constraints on early, cold, or stressed dark energy," Phys. Rev. D **83**, 023011 (2011), arXiv:1010.5612 [astro-ph.CO] .

[237] E. Calabrese, D. Huterer, E. V. Linder, A. Melchiorri, and L. Pagano, "Limits on dark radiation, early dark energy, and relativistic degrees of freedom," Phys. Rev. D **83**, 123504 (2011), arXiv:1103.4132 [astro-ph.CO] .

[238] M. Archidiacono, T. Brinckmann, J. Lesgourgues, and V. Poulin, "Physical effects involved in the measurements of neutrino masses with future cosmological data," JCAP **2**, 052 (2017), arXiv:1610.09852 .

[239] M. Doran and G. Robbers, "Early dark energy cosmologies," JCAP **6**, 026 (2006), astro-ph/0601544 .

[240] S. Hannestad, "Neutrino Masses and the Dark Energy Equation of State: Relaxing the Cosmological Neutrino Mass Bound," Physical Review Letters **95**, 221301 (2005), astro-ph/0505551 .

[241] Jan Hamann, Steen Hannestad, and Yvonne Y. Y. Wong, "Measuring neutrino masses with a future galaxy survey," JCAP **1211**, 052 (2012), arXiv:1209.1043 [astro-ph.CO] .

[242] A. Benoit-Lévy, K. M. Smith, and W. Hu, "Non-Gaussian structure of the lensed CMB power spectra covariance matrix," Phys. Rev. D **86**, 123008 (2012), arXiv:1205.0474 [astro-ph.CO] .

[243] Ruth Pearson and Oliver Zahn, "Cosmology from cross correlation of CMB lensing and galaxy surveys," Phys. Rev. **D89**, 043516 (2014), arXiv:1311.0905 [astro-ph.CO] .

[244] Sai Wang, Yi-Fan Wang, Dong-Mei Xia, and Xin Zhang, "Impacts of dark energy on weighing neutrinos: mass hierarchies considered," Phys. Rev. **D94**, 083519 (2016), arXiv:1608.00672 [astro-ph.CO] .

[245] Xin Zhang, "Weighing neutrinos in dynamical dark energy models," (2017), arXiv:1703.00651 [astro-ph.CO] .

[246] Weiqiang Yang, Rafael C. Nunes, Supriya Pan, and David F. Mota, "Effects of neutrino mass hierarchies on dynamical dark energy models," Phys. Rev. **D95**, 103522 (2017), arXiv:1703.02556 [astro-ph.CO] .

[247] Wayne Hu, "Structure formation with generalized dark matter," Astrophys. J. **506**, 485–494 (1998), arXiv:astro-ph/9801234 [astro-ph] .

[248] D. F. Mota, J. R. Kristiansen, T. Koivisto, and N. E. Groeneboom, "Constraining Dark Energy Anisotropic Stress," Mon. Not. Roy. Astron. Soc. **382**, 793–800 (2007), arXiv:0708.0830 [astro-ph] .

[249] E. V. Linder and R. J. Scherrer, "Aetherizing Lambda: Barotropic fluids as dark energy," Phys. Rev. D **80**, 023008 (2009), arXiv:0811.2797 .

[250] R. de Putter, D. Huterer, and E. V. Linder, "Measuring the speed of dark: Detecting dark energy perturbations," Phys. Rev. D **81**, 103513 (2010), arXiv:1002.1311 [astro-ph.CO] .

[251] C. L. Reichardt, R. de Putter, O. Zahn, and Z. Hou, "New Limits on Early Dark Energy from the South Pole Telescope," ApJL **749**, L9 (2012), arXiv:1110.5328 [astro-ph.CO] .

[252] V. Pettorino, L. Amendola, and C. Wetterich, "How early is early dark energy?" Phys. Rev. D **87**, 083009 (2013), arXiv:1301.5279 [astro-ph.CO] .

[253] E. Calabrese, M. Martinelli, S. Pandolfi, V. F. Cardone, C. J. A. P. Martins, S. Spiro, and P. E. Vielzeuf, "Dark energy coupling with electromagnetism as seen from future low-medium redshift probes," Phys. Rev. D **89**, 083509 (2014), arXiv:1311.5841 [astro-ph.CO] .

[254] P. G. Ferreira and M. Joyce, "Structure Formation with a Self-Tuning Scalar Field," Physical Review Letters **79**, 4740–4743 (1997), astro-ph/9707286 .

[255] D. Spergel, N. Gehrels, *et al.*, "Wide-Field InfraRed Survey Telescope-Astrophysics Focused Telescope Assets WFIRST-AFTA Final Report," ArXiv e-prints (2013), arXiv:1305.5422 [astro-ph.IM] .

[256] A. Lewis, A. Challinor, and A. Lasenby, "Efficient Computation of Cosmic Microwave Background Anisotropies in Closed Friedmann-Robertson-Walker Models," The Astrophysical Journal **538**, 473–476 (2000), astro-ph/9911177 .

[257] A. Lewis and S. Bridle, "Cosmological parameters from CMB and other data: A Monte Carlo approach," Phys. Rev. D **66**, 103511 (2002), astro-ph/0205436 .

[258] N. Aghanim *et al.* (Planck Collaboration), "Planck intermediate results. XLVI. Reduction of large-scale systematic effects in HFI polarization maps and estimation of the reionization optical depth," A&A **596**, A107 (2016), arXiv:1605.02985 [astro-ph.CO] .

[259] N. Aghanim *et al.* (Planck Collaboration), "Planck 2015 results. XI. CMB power spectra, likelihoods, and robustness of parameters," A&A **594**, A11 (2016), arXiv:1507.02704 [astro-ph.CO] .

[260] P. A. R. Ade *et al.* (Planck Collaboration), "Planck 2015 results. XV. Gravitational lensing," A&A **594**, A15 (2016), arXiv:1502.01591 [astro-ph.CO] .

[261] S. Alam *et al.* (Sloan Digital Sky Survey Collaboration), "The Eleventh and Twelfth Data Releases of the Sloan Digital Sky Survey: Final Data from SDSS-III," APJS **219**, 12 (2015), arXiv:1501.00963 [astro-ph.IM] .

[262] Ashley J. Ross, Lado Samushia, Cullan Howlett, Will J. Percival, Angela Burden, and Marc Manera, "The clustering of the SDSS DR7 main Galaxy sample I. A 4 percent distance measure at $z = 0.15$," Mon. Not. Roy. Astron. Soc. **449**, 835–847 (2015), arXiv:1409.3242 [astro-ph.CO] .

[263] F. Beutler, C. Blake, M. Colless, D. H. Jones, L. Staveley-Smith, L. Campbell, Q. Parker, W. Saunders, and F. Watson, "The 6dF Galaxy Survey: baryon acoustic oscillations and the local Hubble constant," Mon. Not. Roy. Astron. Soc. **416**, 3017–3032 (2011), arXiv:1106.3366 .

[264] Will J. Percival, Shaun Cole, Daniel J. Eisenstein, Robert C. Nichol, John A. Peacock, Adrian C. Pope, and Alexander S. Szalay, "Measuring the Baryon Acoustic Oscillation scale using the SDSS and 2dFGRS," Mon. Not. Roy. Astron. Soc. **381**, 1053–1066 (2007), arXiv:0705.3323 [astro-ph] .

[265] O. Pisanti, A. Cirillo, S. Esposito, F. Iocco, G. Mangano, G. Miele, and P. D. Serpico, "PArthENoPE: Public Algorithm Evaluating the Nucleosynthesis of Primordial Elements," Comput. Phys. Commun. **178**, 956–971 (2008), arXiv:0705.0290 [astro-ph] .

[266] David Alonso and Pedro G. Ferreira, "Constraining ultralarge-scale cosmology with multiple tracers in optical and radio surveys," Phys. Rev. **D92**, 063525 (2015), arXiv:1507.03550 [astro-ph.CO] .

[267] D. Baumann, D. Green, J. Meyers, and B. Wallisch, "Phases of new physics in the CMB," JCAP **1**, 007 (2016), arXiv:1508.06342 [astro-ph.CO] .

[268] Julien Lesgourgues, Gianpiero Mangano, Gennaro Miele, and Sergio Pastor, *Neutrino Cosmology* (Cambridge University Press, 2013).

[269] Niall MacCrann, Joe Zuntz, Sarah Bridle, Bhuvnesh Jain, and Matthew R. Becker, "Cosmic Discordance: Are Planck CMB and CFHTLenS weak lensing measurements out of tune?" Mon. Not. Roy. Astron. Soc. **451**, 2877–2888 (2015), arXiv:1408.4742 [astro-ph.CO] .

[270] Shahab Joudaki *et al.*, "CFHTLenS revisited: assessing concordance with Planck including astrophysical systematics," Mon. Not. Roy. Astron. Soc. **465**, 2033–2052 (2017), arXiv:1601.05786 [astro-ph.CO] .

[271] H. Hildebrandt *et al.*, "KiDS-450: Cosmological parameter constraints from tomographic weak gravitational lensing," Mon. Not. Roy. Astron. Soc. **465**, 1454 (2017), arXiv:1606.05338 [astro-ph.CO] .

[272] Shahab Joudaki *et al.*, "KiDS-450: Testing extensions to the standard cosmological model," Mon. Not. Roy. Astron. Soc. **471**, 1259–1279 (2017), arXiv:1610.04606 [astro-ph.CO] .

[273] Shahab Joudaki *et al.*, "KiDS-450 + 2dFLenS: Cosmological parameter constraints from weak gravitational lensing tomography and overlapping redshift-space galaxy clustering," Mon. Not. Roy. Astron. Soc. **474**, 4894–4924 (2018), arXiv:1707.06627 [astro-ph.CO] .

[274] M. A. Troxel *et al.* (DES), "Dark Energy Survey Year 1 Results: Cosmological Constraints from Cosmic Shear," (2017), arXiv:1708.01538 [astro-ph.CO] .

[275] P. A. R. Ade *et al.* (Planck), "Planck 2013 results. XX. Cosmology from SunyaevZeldovich cluster counts," Astron. Astrophys. **571**, A20 (2014), arXiv:1303.5080 [astro-ph.CO] .

[276] P. A. R. Ade *et al.* (Planck), "Planck 2015 results. XXIV. Cosmology from Sunyaev-Zeldovich cluster counts," Astron. Astrophys. **594**, A24 (2016), arXiv:1502.01597 [astro-ph.CO] .

[277] G. E. Addison, Y. Huang, D. J. Watts, C. L. Bennett, M. Halpern, G. Hinshaw, and J. L. Weiland, "Quantifying discordance in the 2015 Planck CMB spectrum," Astrophys. J. **818**, 132 (2016), arXiv:1511.00055 [astro-ph.CO] .

[278] George Efstathiou and Pablo Lemos, "Statistical Inconsistencies in the KiDS-450 Dataset," (2017), 10.1093/mnras/sty099, arXiv:1707.00483 [astro-ph.CO] .

[279] Elena Sellentin, Catherine Heymans, and Joachim Harnois-Draps, "The skewed weak lensing likelihood: why biases arise, despite data and theory being sound," (2017), 10.1093/mnras/sty988, arXiv:1712.04923 [astro-ph.CO] .

[280] M. A. Troxel *et al.* (DES), "Survey geometry and the internal consistency of recent cosmic shear measurements," (2018), arXiv:1804.10663 [astro-ph.CO] .

[281] Georges Obied, Cora Dvorkin, Chen Heinrich, Wayne Hu, and Vinicius Miranda, "Inflationary Features and Shifts in Cosmological Parameters from Planck 2015 Data," Phys. Rev. **D96**, 083526 (2017), arXiv:1706.09412 [astro-ph.CO] .

[282] Marika Asgari *et al.*, "Consistent cosmic shear in the face of systematics: a B-mode analysis of KiDS-450, DES-SV and CFHTLenS," (2018), arXiv:1810.02353 [astro-ph.CO] .

[283] Bruno J. Barros, Luca Amendola, Tiago Barreiro, and Nelson J. Nunes, "Coupled quintessence with a ΛCDM background: removing the σ_8 tension," (2018), arXiv:1802.09216 [astro-ph.CO] .

[284] Ian G. Mccarthy, Simeon Bird, Joop Schaye, Joachim Harnois-Deraps, Andreea S. Font, and Ludovic Van Waerbeke, "The BAHAMAS project: the CMB-large-scale structure tension and the roles of massive neutrinos and galaxy formation," (2017), arXiv:1712.02411 [astro-ph.CO] .

[285] Vivian Poulin, Kimberly K. Boddy, Simeon Bird, and Marc Kamionkowski, "Implications of an extended dark energy cosmology with massive neutrinos for cosmological tensions," Phys. Rev. **D97**, 123504 (2018), arXiv:1803.02474 [astro-ph.CO] .

[286] Simone Peirone, Matteo Martinelli, Marco Raveri, and Alessandra Silvestri, "Impact of theoretical priors in cosmological analyses: the case of single field quintessence," Phys. Rev. **D96**, 063524 (2017), arXiv:1702.06526 [astro-ph.CO] .

[287] Julien Lesgourgues, Gustavo Marques-Tavares, and Martin Schmaltz, "Evidence for dark matter interactions in cosmological precision data?" JCAP **1602**, 037 (2016), arXiv:1507.04351 [astro-ph.CO] .

[288] Vivian Poulin, Pasquale D. Serpico, and Julien Lesgourgues, "A fresh look at linear cosmological constraints on a decaying dark matter component," JCAP **1608**, 036 (2016), arXiv:1606.02073 [astro-ph.CO] .

[289] Manuel A. Buen-Abad, Martin Schmaltz, Julien Lesgourgues, and Thejs Brinckmann, "Interacting Dark Sector and Precision Cosmology," JCAP **1801**, 008 (2018), arXiv:1708.09406 [astro-ph.CO] .

[290] Eleonora Di Valentino, Alessandro Melchiorri, and Joseph Silk, "Cosmological hints of modified gravity?" Phys. Rev. **D93**, 023513 (2016), arXiv:1509.07501 [astro-ph.CO] .

[291] Adria Gomez-Valent and Joan Sola, "Relaxing the σ_8-tension through running vacuum in the Universe," EPL **120**, 39001 (2017), arXiv:1711.00692 [astro-ph.CO] .

[292] Richard A. Battye and Adam Moss, "Evidence for Massive Neutrinos from Cosmic Microwave Background and Lensing Observations," Phys. Rev. Lett. **112**, 051303 (2014), arXiv:1308.5870 [astro-ph.CO] .

[293] Mark Wyman, Douglas H. Rudd, R. Ali Vanderveld, and Wayne Hu, "Neutrinos Help Reconcile Planck Measurements with the Local Universe," Phys. Rev. Lett. **112**, 051302 (2014), arXiv:1307.7715 [astro-ph.CO] .

[294] Rob Fardon, Ann E. Nelson, and Neal Weiner, "Dark energy from mass varying neutrinos," JCAP **0410**, 005 (2004), arXiv:astro-ph/0309800 [astro-ph] .

[295] Niayesh Afshordi, Matias Zaldarriaga, and Kazunori Kohri, "On the stability of dark energy with mass-varying neutrinos," Phys. Rev. **D72**, 065024 (2005), arXiv:astro-ph/0506663 [astro-ph] .

[296] Urbano Franca, Massimiliano Lattanzi, Julien Lesgourgues, and Sergio Pastor, "Model independent constraints on mass-varying neutrino scenarios," Phys. Rev. **D80**, 083506 (2009), arXiv:0908.0534 [astro-ph.CO] .

[297] G. La Vacca and D. F. Mota, "Mass-varying neutrino in light of cosmic microwave background and weak lensing," A&A **560**, A53 (2013), arXiv:1205.6059 [astro-ph.CO] .

[298] A. W. Brookfield, Carsten van de Bruck, D. F. Mota, and D. Tocchini-Valentini, "Cosmology with massive neutrinos coupled to dark energy," Phys. Rev. Lett. **96**, 061301 (2006), arXiv:astro-ph/0503349 [astro-ph] .

[299] Anthony W. Brookfield, C. van de Bruck, D. F. Mota, and D. Tocchini-Valentini, "Cosmology of mass-varying neutrinos driven by quintessence: theory and observations," Phys. Rev. **D73**, 083515 (2006), [Erratum: Phys. Rev.D76,049901(2007)], arXiv:astro-ph/0512367 [astro-ph] .

[300] Ole Eggers Bjaelde, Anthony W. Brookfield, Carsten van de Bruck, Steen Hannestad, David F. Mota, Lily Schrempp, and Domenico Tocchini-Valentini, "Neutrino Dark Energy – Revisiting the Stability Issue," JCAP **0801**, 026 (2008), arXiv:0705.2018 [astro-ph] .

[301] Chao-Qiang Geng, Chung-Chi Lee, R. Myrzakulov, M. Sami, and Emmanuel N. Saridakis, "Observational constraints on varying neutrino-mass cosmology," JCAP **1601**, 049 (2016), arXiv:1504.08141 [astro-ph.CO] .

[302] S. M. Koksbang and S. Hannestad, "Constraining dynamical neutrino mass generation with cosmological data," JCAP **1709**, 014 (2017), arXiv:1707.02579 [astro-ph.CO] .

[303] S. Betts *et al.*, "Development of a Relic Neutrino Detection Experiment at PTOLEMY: Princeton Tritium Observatory for Light, Early-Universe, Massive-Neutrino Yield," in *Proceedings, 2013 Community Summer Study on the Future of U.S. Particle Physics: Snowmass on the Mississippi (CSS2013): Minneapolis, MN, USA, July 29-August 6, 2013* (2013) arXiv:1307.4738 [astro-ph.IM] .

[304] Gia Dvali and Lena Funcke, "Domestic Axion," (2016), arXiv:1608.08969 [hep-ph] .

[305] John F. Beacom, Nicole F. Bell, and Scott Dodelson, "Neutrinoless universe," Phys. Rev. Lett. **93**, 121302 (2004), arXiv:astro-ph/0404585 [astro-ph] .

[306] Steen Hannestad, "Structure formation with strongly interacting neutrinos - Implications for the cosmological neutrino mass bound," J. Cosmol. Astropart. Phys. **0502**, 11 (2005), arXiv:astro-ph/0411475 [astro-ph] .

[307] Lachlan Lancaster, Francis-Yan Cyr-Racine, Lloyd Knox, and Zhen Pan, "A tale of two modes: Neutrino free-streaming in the early universe," JCAP **1707**, 033 (2017), arXiv:1704.06657 [astro-ph.CO] .

[308] Brent Follin, Lloyd Knox, Marius Millea, and Zhen Pan, "First Detection of the Acoustic Oscillation Phase Shift Expected from the Cosmic Neutrino Background," Phys. Rev. Lett. **115**, 091301 (2015), arXiv:1503.07863 [astro-ph.CO] .

[309] D. J. Kapner, T. S. Cook, E. G. Adelberger, J. H. Gundlach, Blayne R. Heckel, C. D. Hoyle, and H. E. Swanson, "Tests of the gravitational inverse-square law below the dark-energy length scale," Phys. Rev. Lett. **98**, 021101 (2007), arXiv:hep-ph/0611184 [hep-ph] .

[310] Emanuele Castorina, Urbano Franca, Massimiliano Lattanzi, Julien Lesgourgues, Gianpiero Mangano, Alessandro Melchiorri, and Sergio Pastor, "Cosmological lepton asymmetry with a nonzero mixing angle θ_{13}," Phys. Rev. D **86**, 023517 (2012), arXiv:1204.2510 [astro-ph.CO] .

[311] Pierre Sikivie, "Axion Cosmology," *Axions: Theory, cosmology, and experimental searches. Proceedings, 1st Joint ILIAS-CERN-CAST axion training, Geneva, Switzerland, November 30-December 2, 2005*, Lect. Notes Phys. **741**, 19 (2008), arXiv:astro-ph/0610440 [astro-ph] .

[312] Paul Langacker, Gino Segre, and Sanjeev Soni, "Majorana Neutrinos, Nucleosynthesis, and the Lepton Asymmetry of the Universe," Phys. Rev. D **26**, 3425 (1982).

[313] Edward Witten, "Cosmological consequences of a light higgs boson," Nucl. Phys. B **177**, 477 – 488 (1981).

[314] Alan H. Guth, "Inflationary universe: A possible solution to the horizon and flatness problems," Phys. Rev. D **23**, 347–356 (1981).

[315] Daniel Yueker, Igor Mishustin, and Marcus Bleicher, "Modeling a delayed phase transition in the early universe," J. Phys. **G41**, 125005 (2014).

[316] Misha A. Stephanov, K. Rajagopal, and Edward V. Shuryak, "Signatures of the tricritical point in QCD," Phys. Rev. Lett. **81**, 4816–4819 (1998), arXiv:hep-ph/9806219 [hep-ph] .

[317] Tillmann Boeckel and Jürgen Schaffner-Bielich, "A little inflation in the early universe at the qcd phase transition," Phys. Rev. Lett. **105**, 041301 (2010), arXiv:0906.4520 [astro-ph.CO] .

[318] V. F. Mukhanov, *Physical Foundations of Cosmology* (Cambridge University Press, 2005).

[319] Antony Lewis, Anthony Challinor, and Anthony Lasenby, "Efficient computation of CMB anisotropies in closed FRW models," Astrophys. J. **538**, 473–476 (2000), arXiv:astro-ph/9911177 [astro-ph] .

[320] N. Aghanim *et al.* (Planck), "Planck 2015 results. XI. CMB power spectra, likelihoods, and robustness of parameters," Astron. Astrophys. **594**, A11 (2016), arXiv:1507.02704 [astro-ph.CO] .

[321] P. A. R. Ade *et al.* (Planck), "Planck 2015 results. XV. Gravitational lensing," Astron. Astrophys. **594**, A15 (2016), arXiv:1502.01591 [astro-ph.CO] .

[322] S. Alam, F. D. Albareti, C. Allende Prieto, F. Anders, S. F. Anderson, T. Anderton, B. H. Andrews, E. Armengaud, É. Aubourg, S. Bailey, and et al., "The Eleventh and Twelfth Data Releases of the Sloan Digital Sky Survey: Final Data from SDSS-III," ApJS **219**, 12 (2015), arXiv:1501.00963 [astro-ph.IM] .

[323] M. Betoule, J. Marriner, N. Regnault, J.-C. Cuillandre, P. Astier, J. Guy, C. Balland, P. El Hage, D. Hardin, R. Kessler, L. Le Guillou, J. Mosher, R. Pain, P.-F. Rocci, M. Sako, and K. Schahmaneche, "Improved photometric calibration of the snls and the sdss supernova surveys," A&A **552**, A124 (2013).

[324] Henk Hoekstra, Ricardo Herbonnet, Adam Muzzin, Arif Babul, Andisheh Mahdavi, Massimo Viola, and Marcello Cacciato, "The Canadian Cluster Comparison Project: detailed study of systematics and updated weak lensing masses," Mon. Not. Roy. Astron. Soc. **449**, 685–714 (2015), arXiv:1502.01883 [astro-ph.CO] .

[325] Andrew J. Long, Cecilia Lunardini, and Eray Sabancilar, "Detecting non-relativistic cosmic neutrinos by capture on tritium: phenomenology and physics potential," JCAP **1408**, 038 (2014), arXiv:1405.7654 [hep-ph] .

[326] S. Gariazzo, C. Giunti, M. Laveder, Y. F. Li, and E. M. Zavanin, "Light sterile neutrinos," J. Phys. **G43**, 033001 (2016), arXiv:1507.08204 [hep-ph] .

[327] Ue-Li Pen and Pengjie Zhang, "Observational Consequences of Dark Energy Decay," Phys. Rev. **D89**, 063009 (2014), arXiv:1202.0107 [astro-ph.CO] .

[328] Haim Goldberg, "Proposal for a constant cosmological constant," Phys. Lett. **B492**, 153–160 (2000), arXiv:hep-ph/0003197 [hep-ph] .

[329] Z. Chacko, Lawrence J. Hall, and Yasunori Nomura, "Acceleressence: dark energy from a phase transition at the seesaw scale," JCAP **0410**, 011 (2004), arXiv:astro-ph/0405596 [astro-ph] .

[330] Axel de la Macorra, "Interacting Dark Energy: Decay into Fermions," Astropart. Phys. **28**, 196–204 (2007), arXiv:astro-ph/0702239 [astro-ph] .

[331] Sourish Dutta, Stephen D. H. Hsu, David Reeb, and Robert J. Scherrer, "Dark radiation as a signature of dark energy," Phys. Rev. **D79**, 103504 (2009), arXiv:0902.4699 [astro-ph.CO] .

[332] Elcio Abdalla, L. L. Graef, and Bin Wang, "A Model for Dark Energy decay," Phys. Lett. **B726**, 786–790 (2013), arXiv:1202.0499 [gr-qc] .

[333] Lawrence M. Krauss and Andrew J. Long, "Metastability of the False Vacuum in a Higgs-Seesaw Model of Dark Energy," Phys. Rev. **D89**, 085023 (2014), arXiv:1310.5361 [hep-ph] .

[334] Ricardo G. Landim and Elcio Abdalla, "Metastable dark energy," Phys. Lett. **B764**, 271–276 (2017), arXiv:1611.00428 [hep-ph] .

[335] Camille Bonvin, Ruth Durrer, and M. Alice Gasparini, "Fluctuations of the luminosity distance," Phys. Rev. **D73**, 023523 (2006), [Erratum: Phys. Rev.D85,029901(2012)], arXiv:astro-ph/0511183 [astro-ph] .

[336] Jaiyul Yoo, "General Relativistic Description of the Observed Galaxy Power Spectrum: Do We Understand What We Measure?" Phys. Rev. **D82**, 083508 (2010), arXiv:1009.3021 [astro-ph.CO] .

[337] David Alonso, Philip Bull, Pedro G. Ferreira, Roy Maartens, and M. Santos, "Ultra large-scale cosmology in next-generation experiments with single tracers," Astrophys. J. **814**, 145 (2015), arXiv:1505.07596 [astro-ph.CO] .

[338] Uros Seljak, "Extracting primordial non-gaussianity without cosmic variance," Phys. Rev. Lett. **102**, 021302 (2009), arXiv:0807.1770 [astro-ph] .

[339] David Alonso and Pedro G. Ferreira, "Constraining ultralarge-scale cosmology with multiple tracers in optical and radio surveys," Phys. Rev. **D92**, 063525 (2015), arXiv:1507.03550 [astro-ph.CO] .

[340] José Fonseca, Stefano Camera, Mário Santos, and Roy Maartens, "Hunting down horizon-scale effects with multi-wavelength surveys," Astrophys. J. **812**, L22 (2015), arXiv:1507.04605 [astro-ph.CO] .

[341] Neal Dalal, Olivier Dore, Dragan Huterer, and Alexander Shirokov, "The imprints of primordial non-gaussianities on large-scale structure: scale dependent bias and abundance of virialized objects," Phys. Rev. **D77**, 123514 (2008), arXiv:0710.4560 [astro-ph] .

[342] Sabino Matarrese and Licia Verde, "The effect of primordial non-Gaussianity on halo bias," Astrophys. J. **677**, L77–L80 (2008), arXiv:0801.4826 [astro-ph] .

[343] M. Bruni, R. Crittenden, K. Koyama, *et al.*, "Disentangling non-Gaussianity, bias, and general relativistic effects in the galaxy distribution," Phys. Rev. D **85**, 041301 (2012), arXiv:1106.3999 [astro-ph.CO] .

[344] E. L. Turner, "The effect of undetected gravitational lenses on statistical measures of quasar evolution," "Astrophys. J. Lett." **242**, L135–L139 (1980).

[345] Wilmar Cardona, Ruth Durrer, Martin Kunz, and Francesco Montanari, "Lensing convergence and the neutrino mass scale in galaxy redshift surveys," Phys. Rev. **D94**, 043007 (2016), arXiv:1603.06481 [astro-ph.CO] .

[346] C. A. J. Duncan, B. Joachimi, A. F. Heavens, C. Heymans, and H. Hildebrandt, "On the complementarity of galaxy clustering with cosmic shear and flux magnification," MNRAS **437**, 2471–2487 (2014), arXiv:1306.6870 .

[347] R. K. Sachs and A. M. Wolfe, "Perturbations of a Cosmological Model and Angular Variations of the Microwave Background," The Astrophysical Journal **147**, 73 (1967).

[348] I. I. Shapiro, "Fourth Test of General Relativity," Physical Review Letters **13**, 789–791 (1964).

[349] Nick Kaiser, "Clustering in real space and in redshift space," MNRAS (1987), 10.1093/mnras/227.1.1.

[350] F. Beutler, H.-J. Seo, S. Saito, *et al.*, "The clustering of galaxies in the completed SDSS-III Baryon Oscillation Spectroscopic Survey: anisotropic galaxy clustering in Fourier space," MNRAS **466**, 2242–2260 (2017), arXiv:1607.03150 .

[351] M. Seldner and P. J. E. Peebles, "Statistical analysis of catalogs of extragalactic objects. XI - Evidence of correlation of QSOs and Lick galaxy counts," The Astrophysical Journal **227**, 30–36 (1979).

[352] E. Gaztañaga, "Correlation between Galaxies and Quasi-stellar Objects in the Sloan Digital Sky Survey: A Signal from Gravitational Lensing Magnification?" The Astrophysical Journal **589**, 82–99 (2003), astro-ph/0210311 .

[353] R. Scranton, B. Ménard, G. T. Richards, *et al.*, "Detection of Cosmic Magnification with the Sloan Digital Sky Survey," The Astrophysical Journal **633**, 589–602 (2005), astro-ph/0504510 .

[354] C. B. Morrison, R. Scranton, B. Ménard, S. J. Schmidt, J. A. Tyson, R. Ryan, A. Choi, and D. M. Wittman, "Tomographic magnification of Lyman-break galaxies in the Deep Lens Survey," MNRAS **426**, 2489–2499 (2012), arXiv:1204.2830 .

[355] I. Chiu, J. P. Dietrich, J. Mohr, *et al.*, "Detection of enhancement in number densities of background galaxies due to magnification by massive galaxy clusters," MNRAS **457**, 3050–3065 (2016), arXiv:1510.01745 .

[356] M. Garcia-Fernandez, E. Sánchez, I. Sevilla-Noarbe, *et al.*, "Weak lensing magnification in the Dark Energy Survey Science Verification Data," ArXiv e-prints (2016), arXiv:1611.10326 .

[357] Lam Hui, Enrique Gaztanaga, and Marilena LoVerde, "Anisotropic Magnification Distortion of the 3D Galaxy Correlation. 1. Real Space," Phys. Rev. **D76**, 103502 (2007), arXiv:0706.1071 [astro-ph] .

[358] M. Chevallier and D. Polarski, "Accelerating Universes with Scaling Dark Matter," International Journal of Modern Physics D **10**, 213–223 (2001), gr-qc/0009008 .

[359] N. Aghanim *et al.* (Planck), "Planck intermediate results. XLVI. Reduction of large-scale systematic effects in HFI polarization maps and estimation of the reionization optical depth," Astron. Astrophys. **596**, A107 (2016), arXiv:1605.02985 [astro-ph.CO] .

[360] Nathalie Palanque-Delabrouille *et al.*, "The one-dimensional Ly-alpha forest power spectrum from BOSS," Astron. Astrophys. **559**, A85 (2013), arXiv:1306.5896 [astro-ph.CO] .

[361] C. Patrignani *et al.* (Particle Data Group), "Review of particle physics," Chinese Physics C **40**, 100001 (2016).

[362] Eiichiro Komatsu and David N. Spergel, "Acoustic signatures in the primary microwave background bispectrum," Phys. Rev. **D63**, 063002 (2001), arXiv:astro-ph/0005036 [astro-ph] .

[363] P. A. R. Ade *et al.* (Planck), "Planck 2015 results. XVII. Constraints on primordial non-Gaussianity," Astron. Astrophys. **594**, A17 (2016), arXiv:1502.01592 [astro-ph.CO] .

[364] Licia Verde, Li-Min Wang, Alan Heavens, and Marc Kamionkowski, "Large scale structure, the cosmic microwave background, and primordial non-gaussianity," Mon. Not. Roy. Astron. Soc. **313**, L141–L147 (2000), arXiv:astro-ph/9906301 [astro-ph] .

[365] Gregory Walter Horndeski, "Second-order scalar-tensor field equations in a four-dimensional space," Int. J. Theor. Phys. **10**, 363 (1974).

[366] C. Deffayet, Gilles Esposito-Farese, and A. Vikman, "Covariant Galileon," Phys. Rev. **D79**, 084003 (2009), arXiv:0901.1314 [hep-th] .

[367] Emilio Bellini and Ignacy Sawicki, "Maximal freedom at minimum cost: linear large-scale structure in general modifications of gravity," JCAP **1407**, 050 (2014), arXiv:1404.3713 [astro-ph.CO] .

[368] Emilio Bellini, Antonio J. Cuesta, Raul Jimenez, and Licia Verde, "Constraints on deviations from CDM within Horndeski gravity," JCAP **1602**, 053 (2016), [Erratum: JCAP1606,no.06,E01(2016)], arXiv:1509.07816 [astro-ph.CO] .

[369] David Alonso, Emilio Bellini, Pedro G. Ferreira, and Miguel Zumalacrregui, "Observational future of cosmological scalar-tensor theories," Phys. Rev. **D95**, 063502 (2017), arXiv:1610.09290 [astro-ph.CO] .

[370] Enea Di Dio, Francesco Montanari, Julien Lesgourgues, and Ruth Durrer, "The CLASSgal code for Relativistic Cosmological Large Scale Structure," JCAP **1311**, 044 (2013), arXiv:1307.1459 [astro-ph.CO] .

[371] M. Zumalacárregui, E. Bellini, I. Sawicki, J. Lesgourgues, and P. G. Ferreira, "hi_class: Horndeski in the Cosmic Linear Anisotropy Solving System," JCAP **8**, 019 (2017), arXiv:1605.06102 .

[372] Dragan Huterer and Masahiro Takada, "Calibrating the nonlinear matter power spectrum: Requirements for future weak lensing surveys," Astropart. Phys. **23**, 369–376 (2005), arXiv:astro-ph/0412142 [astro-ph] .

[373] D. Huterer, M. Takada, G. Bernstein, and B. Jain, "Systematic errors in future weak-lensing surveys: requirements and prospects for self-calibration," MNRAS **366**, 101–114 (2006), astro-ph/0506030 .

[374] Adam Amara and Alexandre Refregier, "Systematic Bias in Cosmic Shear: Beyond the Fisher Matrix," Mon. Not. Roy. Astron. Soc. **391**, 228–236 (2008), arXiv:0710.5171 [astro-ph] .

[375] E. Calabrese, R. Hložek, N. Battaglia, *et al.*, "Precision epoch of reionization studies with next-generation CMB experiments," JCAP **8**, 010 (2014), arXiv:1406.4794 .

[376] B. A. Benson, P. A. R. Ade, Z. Ahmed, *et al.*, "SPT-3G: a next-generation cosmic microwave background polarization experiment on the South Pole telescope," in *Millimeter, Submillimeter, and Far-Infrared Detectors and Instrumentation for Astronomy VII*, Proceedings of the SPIE, Vol. 9153 (2014) p. 91531P, arXiv:1407.2973 [astro-ph.IM] .

[377] P. A. R. Ade *et al.* (BICEP2, Keck Array), "Improved Constraints on Cosmology and Foregrounds from BICEP2 and Keck Array Cosmic Microwave Background Data with Inclusion of 95 GHz Band," Phys. Rev. Lett. **116**, 031302 (2016), arXiv:1510.09217 [astro-ph.CO] .

[378] A. Suzuki, P. Ade, Y. Akiba, *et al.*, "The Polarbear-2 and the Simons Array Experiments," Journal of Low Temperature Physics **184**, 805–810 (2016), arXiv:1512.07299 [astro-ph.IM] .

[379] David Alonso, Pedro G. Ferreira, Matt J. Jarvis, and Kavilan Moodley, "Calibrating photometric redshifts with intensity mapping observations," Phys. Rev. **D96**, 043515 (2017), arXiv:1704.01941 [astro-ph.CO] .

[380] DES Collaboration, "Dark Energy Survey Year 1 Results: Cosmological Constraints from Galaxy Clustering and Weak Lensing," ArXiv e-prints (2017), arXiv:1708.01530 .

[381] J. Renk, M. Zumalacárregui, and F. Montanari, "Gravity at the horizon: on relativistic effects, CMB-LSS correlations and ultra-large scales in Horndeski's theory," JCAP **7**, 040 (2016), arXiv:1604.03487 .

[382] D. Bertacca, R. Maartens, A. Raccanelli, and C. Clarkson, "Beyond the plane-parallel and Newtonian approach: wide-angle redshift distortions and convergence in general relativity," JCAP **10**, 025 (2012), arXiv:1205.5221 .

[383] D. Jeong, F. Schmidt, and C. M. Hirata, "Large-scale clustering of galaxies in general relativity," Phys. Rev. D **85**, 023504 (2012), arXiv:1107.5427 .

[384] E. Di Dio, H. Perrier, R. Durrer, G. Marozzi, A. Moradinezhad Dizgah, J. Noreña, and A. Riotto, "Non-Gaussianities due to relativistic corrections to the observed galaxy bispectrum," JCAP **3**, 006 (2017), arXiv:1611.03720 .

[385] O. Doré, M. W. Werner, M. Ashby, *et al.*, "Science Impacts of the SPHEREx All-Sky Optical to Near-Infrared Spectral Survey: Report of a Community Workshop Examining Extragalactic, Galactic, Stellar and Planetary Science," ArXiv e-prints (2016), arXiv:1606.07039 .

[386] T. Namikawa, T. Okamura, and A. Taruya, "Magnification effect on the detection of primordial non-Gaussianity from photometric surveys," Phys. Rev. D **83**, 123514 (2011), arXiv:1103.1118 .

[387] R. G. Crittenden and N. Turok, "Looking for a Cosmological Constant with the Rees-Sciama Effect," Physical Review Letters **76**, 575–578 (1996), astro-ph/9510072 .

[388] J. Renk, M. Zumalacárregui, F. Montanari, and A. Barreira, "Galileon Gravity in Light of ISW, CMB, BAO and H_0 data," ArXiv e-prints (2017), arXiv:1707.02263 .

[389] C. Bonvin, L. Hui, and E. Gaztañaga, "Asymmetric galaxy correlation functions," Phys. Rev. D **89**, 083535 (2014), arXiv:1309.1321 .

[390] E. Gaztanaga, C. Bonvin, and L. Hui, "Measurement of the dipole in the cross-correlation function of galaxies," JCAP **1**, 032 (2017), arXiv:1512.03918 .

[391] S. Alam, H. Zhu, R. A. C. Croft, S. Ho, E. Giusarma, and D. P. Schneider, "Relativistic distortions in the large-scale clustering of SDSS-III BOSS CMASS galaxies," MNRAS **470**, 2822–2833 (2017), arXiv:1709.07855 .

[392] M. Hazumi *et al.*, "LiteBIRD: a small satellite for the study of B-mode polarization and inflation from cosmic background radiation detection," *SPIE Astronomical Telescopes + Instrumentation 2012 Amsterdam, Netherlands, July 1-6, 2012*, Proc. SPIE Int. Soc. Opt. Eng. **8442**, 844219 (2012).

[393] Adam G. Riess, Stefano Casertano, Wenlong Yuan, Lucas M. Macri, and Dan Scolnic, "Large Magellanic Cloud Cepheid Standards Provide a 1% Foundation for the Determination of the Hubble Constant and Stronger Evidence for Physics Beyond LambdaCDM," Astrophys. J. **876**, 85 (2019), arXiv:1903.07603 [astro-ph.CO] .

[394] Kenneth C. Wong *et al.*, "H0LiCOW XIII. A 2.4% measurement of H_0 from lensed quasars: 5.3σ tension between early and late-Universe probes," (2019), arXiv:1907.04869 [astro-ph.CO] .

[395] Wendy L. Freedman, Barry F. Madore, Dylan Hatt, Taylor J. Hoyt, In-Sung Jang, *et al.*, "The Carnegie-Chicago Hubble Program. VIII. An Independent Determination of the Hubble Constant Based on the Tip of the Red Giant Branch," (2019), arXiv:1907.05922 [astro-ph.CO] .

[396] S. Joudaki *et al.*, "KiDS+VIKING-450 and DES-Y1 combined: Cosmology with cosmic shear," (2019), arXiv:1906.09262 [astro-ph.CO] .

[397] George Efstathiou, "H0 Revisited," Mon. Not. Roy. Astron. Soc. **440**, 1138–1152 (2014), arXiv:1311.3461 [astro-ph.CO] .

[398] David N. Spergel, Raphael Flauger, and Rene Hloek, "Planck Data Reconsidered," Phys. Rev. **D91**, 023518 (2015), arXiv:1312.3313 [astro-ph.CO] .

[399] Wenlong Yuan, Adam G. Riess, Lucas M. Macri, Stefano Casertano, and Dan Scolnic, "Consistent Calibration of the Tip of the Red Giant Branch in the Large Magellanic Cloud on the Hubble Space Telescope Photometric System and Implications for the Determination of the Hubble Constant," (2019), arXiv:1908.00993 [astro-ph.GA] .

[400] Jose Luis Bernal, Licia Verde, and Adam G. Riess, "The trouble with H_0," JCAP **1610**, 019 (2016), arXiv:1607.05617 [astro-ph.CO] .

[401] Tanvi Karwal and Marc Kamionkowski, "Dark energy at early times, the Hubble parameter, and the string axiverse," Phys. Rev. **D94**, 103523 (2016), arXiv:1608.01309 [astro-ph.CO] .

[402] Eleonora Di Valentino, Cline Behm, Eric Hivon, and Franois R. Bouchet, "Reducing the H_0 and σ_8 tensions with Dark Matter-neutrino interactions," Phys. Rev. **D97**, 043513 (2018), arXiv:1710.02559 [astro-ph.CO] .

[403] Vivian Poulin, Tristan L. Smith, Tanvi Karwal, and Marc Kamionkowski, "Early Dark Energy Can Resolve The Hubble Tension," Phys. Rev. Lett. **122**, 221301 (2019), arXiv:1811.04083 [astro-ph.CO] .

[404] Christina D. Kreisch, Francis-Yan Cyr-Racine, and Olivier Dor, "The Neutrino Puzzle: Anomalies, Interactions, and Cosmological Tensions," (2019), arXiv:1902.00534 [astro-ph.CO] .

[405] Supriya Pan, Weiqiang Yang, Eleonora Di Valentino, Arman Shafieloo, and Subenoy Chakraborty, "Reconciling H_0 tension in a six parameter space?" (2019), arXiv:1907.12551 [astro-ph.CO] .

[406] Kevin Aylor, Mackenzie Joy, Lloyd Knox, Marius Millea, Srinivasan Raghunathan, and W. L. Kimmy Wu, "Sounds Discordant: Classical Distance Ladder and λCDM-based Determinations of the Cosmological Sound Horizon," The Astrophysical Journal **874**, 4 (2019).

[407] Prateek Agrawal, Francis-Yan Cyr-Racine, David Pinner, and Lisa Randall, "Rock 'n' Roll Solutions to the Hubble Tension," (2019), arXiv:1904.01016 [astro-ph.CO] .

[408] Lloyd Knox and Marius Millea, "The Hubble Hunter's Guide," (2019), arXiv:1908.03663 [astro-ph.CO] .

[409] Hans Boehringer, Gayoung Chon, and Chris A. Collins, "Observational evidence for a local underdensity in the Universe and its effect on the measurement of the Hubble Constant," (2019), arXiv:1907.12402 [astro-ph.CO] .

[410] Harry Desmond, Bhuvnesh Jain, and Jeremy Sakstein, "Local resolution of the Hubble tension: The impact of screened fifth forces on the cosmic distance ladder," Phys. Rev. **D100**, 043537 (2019), arXiv:1907.03778 [astro-ph.CO] .

[411] Lucas Lombriser, "Consistency of the local Hubble constant with the cosmic microwave background," (2019), arXiv:1906.12347 [astro-ph.CO] .

[412] W. D'Arcy Kenworthy, Dan Scolnic, and Adam Riess, "The Local Perspective on the Hubble Tension: Local Structure Does Not Impact Measurement of the Hubble Constant," Astrophys. J. **875**, 145 (2019), arXiv:1901.08681 [astro-ph.CO] .

[413] B. P. Abbott *et al.* (LIGO Scientific, Virgo, 1M2H, Dark Energy Camera GW-E, DES, DLT40, Las Cumbres Observatory, VINROUGE, MASTER), "A gravitational-wave standard siren measurement of the Hubble constant," Nature **551**, 85–88 (2017), arXiv:1710.05835 [astro-ph.CO] .

[414] Stephen M. Feeney, Hiranya V. Peiris, Andrew R. Williamson, Samaya M. Nissanke, Daniel J. Mortlock, Justin Alsing, and Dan Scolnic, "Prospects for resolving the Hubble constant tension with standard sirens," Phys. Rev. Lett. **122**, 061105 (2019), arXiv:1802.03404 [astro-ph.CO] .

[415] Daniel J. Mortlock, Stephen M. Feeney, Hiranya V. Peiris, Andrew R. Williamson, and Samaya M. Nissanke, "Unbiased Hubble constant estimation from binary neutron star mergers," (2018), arXiv:1811.11723 [astro-ph.CO] .

[416] Carlos A. P. Bengaly, Chris Clarkson, and Roy Maartens, "The Hubble constant tension with next generation galaxy surveys," (2019), arXiv:1908.04619 [astro-ph.CO] .

[417] B. P. Abbott *et al.* (LIGO Scientific Collaboration and Virgo Collaboration), "Observation of gravitational waves from a binary black hole merger," Phys. Rev. Lett. **116**, 061102 (2016).

[418] R. R. Caldwell, Rahul Dave, and Paul J. Steinhardt, "Cosmological imprint of an energy component with general equation of state," Phys. Rev. Lett. **80**, 1582–1585 (1998), arXiv:astro-ph/9708069 [astro-ph] .

[419] C. Armendariz-Picon, Viatcheslav F. Mukhanov, and Paul J. Steinhardt, "A Dynamical solution to the problem of a small cosmological constant and late time cosmic acceleration," Phys. Rev. Lett. **85**, 4438–4441 (2000), arXiv:astro-ph/0004134 [astro-ph] .

[420] C. Armendariz-Picon, Viatcheslav F. Mukhanov, and Paul J. Steinhardt, "Essentials of k essence," Phys. Rev. **D63**, 103510 (2001), arXiv:astro-ph/0006373 [astro-ph] .

[421] Christof Wetterich, "The Cosmon model for an asymptotically vanishing time dependent cosmological 'constant'," Astron. Astrophys. **301**, 321–328 (1995), arXiv:hep-th/9408025 [hep-th] .

[422] Jaewon Yoo and Yuki Watanabe, "Theoretical Models of Dark Energy," International Journal of Modern Physics D **21**, 1230002 (2012), arXiv:1212.4726 [astro-ph.CO] .

[423] R. R. Caldwell and Eric V. Linder, "The Limits of quintessence," Phys. Rev. Lett. **95**, 141301 (2005), arXiv:astro-ph/0505494 [astro-ph] .

[424] Amol Upadhye, Mustapha Ishak, and Paul J. Steinhardt, "Dynamical dark energy: Current constraints and forecasts," Phys. Rev. **D72**, 063501 (2005), arXiv:astro-ph/0411803 [astro-ph] .

[425] David J. E. Marsh, Philip Bull, Pedro G. Ferreira, and Andrew Pontzen, "Quintessence in a quandary: Prior dependence in dark energy models," Phys. Rev. **D90**, 105023 (2014), arXiv:1406.2301 [astro-ph.CO] .

[426] Pedro G. Ferreira, "Cosmological Tests of Gravity," (2019), 10.1146/annurev-astro-091918-104423, arXiv:1902.10503 [astro-ph.CO] .

[427] Tessa Baker *et al.*, "The Novel Probes Project – Tests of Gravity on Astrophysical Scales," (2019), arXiv:1908.03430 [astro-ph.CO] .

[428] Jose Mara Ezquiaga and Miguel Zumalacrregui, "Dark Energy in light of Multi-Messenger Gravitational-Wave astronomy," Front. Astron. Space Sci. **5**, 44 (2018), arXiv:1807.09241 [astro-ph.CO] .

[429] T. Baker, E. Bellini, P. G. Ferreira, M. Lagos, J. Noller, and I. Sawicki, "Strong constraints on cosmological gravity from GW170817 and GRB 170817A," Phys. Rev. Lett. **119**, 251301 (2017), arXiv:1710.06394 [astro-ph.CO] .

[430] Jose Mara Ezquiaga and Miguel Zumalacrregui, "Dark Energy After GW170817: Dead Ends and the Road Ahead," Phys. Rev. Lett. **119**, 251304 (2017), arXiv:1710.05901 [astro-ph.CO] .

[431] Gianfranco Bertone, Dan Hooper, and Joseph Silk, "Particle dark matter: Evidence, candidates and constraints," Phys. Rept. **405**, 279–390 (2005), arXiv:hep-ph/0404175 [hep-ph] .

[432] Gerard Jungman, Marc Kamionkowski, and Kim Griest, "Supersymmetric dark matter," Physics Reports **267**, 195 – 373 (1996).

[433] David J. E. Marsh, "Axion Cosmology," Phys. Rept. **643**, 1–79 (2016), arXiv:1510.07633 [astro-ph.CO] .

[434] Wayne Hu, Rennan Barkana, and Andrei Gruzinov, "Cold and fuzzy dark matter," Phys. Rev. Lett. **85**, 1158–1161 (2000), arXiv:astro-ph/0003365 [astro-ph] .

[435] J. García-Bellido, "Massive Primordial Black Holes as Dark Matter and their detection with Gravitational Waves," in *Journal of Physics Conference Series*, Journal of Physics Conference Series, Vol. 840 (2017) p. 012032, arXiv:1702.08275 .

[436] Miguel Zumalacarregui and Uros Seljak, "Limits on stellar-mass compact objects as dark matter from gravitational lensing of type Ia supernovae," Phys. Rev. Lett. **121**, 141101 (2018), arXiv:1712.02240 [astro-ph.CO] .

[437] Alex Drlica-Wagner *et al.* (LSST Dark Matter Group), "Probing the Fundamental Nature of Dark Matter with the Large Synoptic Survey Telescope," (2019), arXiv:1902.01055 [astro-ph.CO] .

[438] Y. Akrami *et al.* (Planck), "Planck 2018 results. IX. Constraints on primordial non-Gaussianity," (2019), arXiv:1905.05697 [astro-ph.CO] .

[439] Janis Fluri, Tomasz Kacprzak, Aurelien Lucchi, Alexandre Refregier, Adam Amara, Thomas Hofmann, and Aurel Schneider, "Cosmological constraints with deep learning from KiDS-450 weak lensing maps," Phys. Rev. **D100**, 063514 (2019), arXiv:1906.03156 [astro-ph.CO] .

[440] Emille E. O. Ishida, "Machine learning and the future of supernova cosmology," Nature Astronomy **3**, 680–682 (2019), arXiv:1908.02315 [astro-ph.IM] .

[441] Siddharth Mishra-Sharma, David Alonso, and Joanna Dunkley, "Neutrino masses and beyond-CDM cosmology with LSST and future CMB experiments," Phys. Rev. **D97**, 123544 (2018), arXiv:1803.07561 [astro-ph.CO] .

[442] Thejs Brinckmann, Deanna C. Hooper, Maria Archidiacono, Julien Lesgourgues, and Tim Sprenger, "The promising future of a robust cosmological neutrino mass measurement," JCAP **1901**, 059 (2019), arXiv:1808.05955 [astro-ph.CO] .

[443] Steffen Hagstotz, Max Gronke, David Mota, and Marco Baldi, "Breaking cosmic degeneracies: Disentangling neutrinos and modified gravity with kinematic information," Astron. Astrophys. **629**, A46 (2019), arXiv:1902.01868 [astro-ph.CO] .

[444] Martina Gerbino, Katherine Freese, Sunny Vagnozzi, Massimiliano Lattanzi, Olga Mena, Elena Giusarma, and Shirley Ho, "Impact of neutrino properties on the estimation of inflationary parameters from current and future observations," Phys. Rev. **D95**, 043512 (2017), arXiv:1610.08830 [astro-ph.CO] .

[445] Janina Renk, Miguel Zumalacarregui, and Francesco Montanari, "Gravity at the horizon: on relativistic effects, CMB-LSS correlations and ultra-large scales in Horndeski's theory," JCAP **1607**, 040 (2016), arXiv:1604.03487 [astro-ph.CO] .

[446] Eleonora Villa, Enea Di Dio, and Francesca Lepori, "Lensing convergence in galaxy clustering in CDM and beyond," JCAP **1804**, 033 (2018), arXiv:1711.07466 [astro-ph.CO] .

[447] Wilmar Cardona, Rubn Arjona, and Savvas Nesseris, "Lensing convergence and anisotropic dark energy in galaxy redshift surveys," (2019), arXiv:1907.10130 [astro-ph.CO] .

[448] Leander Thiele, Christopher A. J. Duncan, and David Alonso, "Disentangling magnification in combined shear-clustering analyses," (2019), arXiv:1907.13205 [astro-ph.CO] .

[449] Dagoberto Contreras, Matthew C. Johnson, and James B. Mertens, "Towards detection of relativistic effects in galaxy number counts using kSZ Tomography," (2019), arXiv:1904.10033 [astro-ph.CO] .

[450] Basundhara Ghosh, Ruth Durrer, and Elena Sellentin, "General Relativistic corrections in density-shear correlations," JCAP **1806**, 008 (2018), arXiv:1801.02518 [astro-ph.CO] .